NASA TECHNICAL NOTE

NASA TN D-7943

NASA TN D-7943

AEROTHERMAL PERFORMANCE AND STRUCTURAL INTEGRITY OF A RENÉ 41 THERMAL PROTECTION SYSTEM AT MACH 6.6

William D. Deveikis, Robert Miserentino, Irving Weinstein, and John L. Shideler

Langley Research Center
Hampton, Va. 23665

NATIONAL AERONAUTICS AND SPACE ADMINISTRATION • WASHINGTON, D. C. • NOVEMBER 1975

1. Report No. NASA TN D-7943	2. Government Accession No.	3. Recipient's Catalog No.
4. Title and Subtitle AEROTHERMAL PERFORMANCE AND STRUCTURAL INTEGRITY OF A RENÉ 41 THERMAL PROTECTION SYSTEM AT MACH 6.6		5. Report Date November 1975 6. Performing Organization Code
7. Author(s) William D. Deveikis, Robert Miserentino, Irving Weinstein, and John L. Shideler		8. Performing Organization Report No. L-9945
9. Performing Organization Name and Address NASA Langley Research Center Hampton, Va. 23665		10. Work Unit No. 506-17-22-01 11. Contract or Grant No.
12. Sponsoring Agency Name and Address National Aeronautics and Space Administration Washington, D.C. 20546		13. Type of Report and Period Covered Technical Note 14. Sponsoring Agency Code
15. Supplementary Notes		

16. Abstract

A flightweight (10.6 kg/m^2 (2.18 lb/ft^2)) 106.7 by 148.3 cm (42.0 by 58.4 in.) panel based on a metallic thermal-protection-system concept for hypersonic and reentry vehicles was subjected repeatedly to thermal cycling by quartz-lamp radiant heating using a thermal history representative of a reentry heat pulse and to aerodynamic heating at heating rates required to sustain a surface temperature of 1089 K (1960° R). The panel consisted of a corrugated heat shield and support members of 0.05-cm (0.02-in.) thick René 41 of riveted construction and 5.08-cm (2-in.) thick silica fibrous insulation packages covered by René 41 foil and inconel screening. All tests were conducted in the Langley 8-foot high-temperature structures tunnel with the heat-shield corrugations alined in the stream direction. Nominal free-stream Mach number was 6.6, and free-stream unit Reynolds number was 5.118×10^6 per meter (1.56×10^6 per foot). Local Mach numbers were from 6.2 to 4.4; surface pressures were from 3.5 to 11.7 kPa (0.5 to 1.7 psia); and local dynamic pressures were from 97 to 158 kPa (14 to 23 psi). The panel sustained 5.33 hr of intermittent radiant heating and 6.5 min of intermittent aerodynamic heating of up to 1-min duration for differential pressures up to 6.2 kPa (0.9 psi) with no apparent degradation of thermal or structural integrity, as indicated by temperature distributions and results from load-deflection tests and vibration surveys of natural frequencies.

17. Key Words (Suggested by Author(s))	18. Distribution Statement
Thermal protection system Hypersonic Corrugated surface Turbulent heat transfer	Unclassified – Unlimited Subject Category 18

19. Security Classif. (of this report)	20. Security Classif. (of this page)	21. No. of Pages	22. Price*
Unclassified	Unclassified	98	$4.75

*For sale by the National Technical Information Service, Springfield, Virginia 22161

CONTENTS

AEROTHERMAL PERFORMANCE AND STRUCTURAL INTEGRITY OF A RENÉ 41 THERMAL PROTECTION SYSTEM AT MACH 6.6

William D. Deveikis, Robert Miserentino, Irving Weinstein,
and John L. Shideler
Langley Research Center

SUMMARY

A flightweight (10.6 kg/m^2 (2.18 lb/ft^2)) 106.7 by 148.3 cm (42.0 by 58.4 in.) panel of a corrugated René 41 thermal-protection-system concept for hypersonic and reentry vehicles was subjected to both radiant and aerodynamic heating in order to evaluate its thermal performance and structural integrity. The panel consisted of 0.05-cm (0.02-in.) thick heat shield and support members of riveted construction and 5.08-cm (2-in.) thick silica fibrous insulation packages covered with René 41 foil and inconel screening. It was designed to carry a uniform pressure of 20.7 kPa (3 psia) at a surface temperature of 1089 K (1960° R). Test goal was to protect a stainless-steel substructure from temperatures above 422 K (760° R) for 28 min. All tests were conducted in the Langley 8-foot high-temperature structures tunnel with the heat-shield corrugations alined in the stream direction. Nominal free-stream Mach number was 6.6, and free-stream unit Reynolds number was 5.118×10^6 per meter (1.56×10^6 per foot). Angle of attack was varied to produce local Mach numbers from 6.2 to 4.4, surface pressures from 3.5 to 11.7 kPa (0.5 to 1.7 psia), and local dynamic pressures from 97 to 158 kPa (14 to 23 psi). The panel sustained 5.33 hr of intermittent radiant heating and 6.5 min of intermittent aerodynamic heating of up to 1-min duration for differential pressures up to 6.2 kPa (0.9 psi) following radiant preheating. In addition, the panel endured tunnel start and shutdown acoustic loading of up to 157 dB for about 30 sec per test.

The panel suffered no apparent degradation of thermal or structural integrity and was tolerant of abuses from electrical arcing, water impingement on the hot surface, and accelerations up to 12g. The largest measured change in panel natural frequency was 6 Hz (3.5 percent). During radiant heating, the substructure temperature limit occurred 26 min after heating started, and panel thermal performance was predictable with reasonable accuracy. During aerodynamic heating, temperature-rise rates on support members approximated those obtained under radiant heating. However, as expected, thermal performance degraded when hot gases from the boundary layer were unrealistically forced through the panel interior. For the heating and loading conditions of the tests, analysis indicated stress concentrations within yield-stress limits but higher than the proportional

limit. The stress concentrations were located in the angles formed by the juncture of pairs of legs on the truss-shaped support members. Results of the investigation identified areas for improving panel design to enhance concept suitability for flight application.

INTRODUCTION

Hypersonic cruise and reentry vehicles (such as Space Shuttle) will require lightweight thermal protection systems that should endure many flights before requiring refurbishment. However, as reported in references 1 and 2, these systems present critical technological deficiencies in terms of materials, reuse potential, and, hence, economical refurbishment. Consequently, NASA has initiated a major effort to develop the necessary design technology for suitable thermal protection systems. As part of this effort, the Langley Research Center, through experiment and analysis, is evaluating several full-scale, flightweight panels of metallic and nonmetalic concepts. (See, for example, ref. 3.) Experimentally, thermal performance and structural integrity are assessed from repeated exposures to two types of heating. One type is radiant heating from quartz lamps for exposure times up to approximately 1/2 hr using a surface-temperature history representative of a reentry heat pulse from Earth orbit. The other type is aerodynamic heating with associated pressure loading for exposure times up to 1-min duration in the hypersonic stream of the Langley 8-foot high-temperature structures tunnel. Analytical tools employed are a finite-difference computer program (ref. 4) for thermal analysis and a finite-element computer program (ref. 5) for stress analysis.

The present investigation was the first of the series conducted and, therefore, served the twofold purpose of evaluating a metallic (René 41) thermal protection system and of verifying the test techniques (ref. 6) that were developed for the present evaluation program. The panel used was a corrugated heat shield with insulation packages. It was designed for service on a reentry surface where temperatures reach approximately 1089 K (1960° R), as depicted in figure 1, and to protect the load-carrying substructure from temperatures above 422 K (760° R). The metallic heat-shield design was based on a multisupported concept reported in reference 7. Its configuration is convenient for covering large areas uninterrupted by longitudinal (streamwise) panel-to-panel joints. Hence, the number of places requiring sealing against inflow of hot boundary-layer gases is minimized. Therefore, for the present investigation, the prime requirements were (1) to design and fabricate a panel which covered the largest area that could be accepted by the test fixture and (2) to test only for thermal and structural response. The resulting panel had no transverse (spanwise) thermal expansion joints, and problems of sealing the edges and the representation of a thermally realistic substructure were not addressed.

Prior to thermal testing, the structural characteristics of the panel were determined from static load-deflection tests and vibration surveys. Upon completion of these

tests, the panel was subjected to the radiant-heating and aerodynamic-heating tests which were to be conducted alternately. Occasionally, panel structural integrity was checked by additional vibration surveys. For the aerodynamic-heating tests, nominal free-stream conditions were: Mach number, 6.6; total temperature, 1722 K (3100° R); and unit Reynolds number, 5.1×10^6 per meter (1.56×10^6 per foot). Surface temperatures, temperature distributions through the panel, surface deformations, natural frequencies, and results from thermal and stress analyses are presented herein. The test and analytical results are used to assess the thermal and structural performance of the thermal protection system and to identify potential areas for improving its design.

SYMBOLS

Values are given both in SI Units and in U.S. Customary Units. The measurements and calculations were made in U.S. Customary Units.

a — panel length between supports in x-direction (streamwise)

D_x — panel bending stiffness in x-direction (fig. 7)

F — reaction force, N (lb)

f — frequency, Hz

$K_d = \frac{k_d a^3}{D_x}, K_r = \frac{k_r a}{D_x}, K_t = \frac{k_t a}{D_x}$ — nondimensional deflection, rotational, and torsional spring constants, respectively

k_d, k_r, k_t — deflectional, rotational, and torsional spring constants, respectively, per unit length

l — panel length, cm (in.)

M — Mach number

m — number of half-waves in x-direction (streamwise, fig. 7) between adjacent supports

n — number of half-waves in y-direction (transverse to stream, fig. 7) over width of panel

p	pressure, Pa (psia)
q	dynamic pressure, Pa (psi)
R	Reynolds number
T	temperature, K (^{o}R)
t	time, sec
w	panel width, cm (in.)
x,y,z	panel coordinates (see fig. 7), cm (in.)
α	angle of attack, deg
β	compressibility parameter, $\sqrt{M^2 - 1}$
Δp	differential-pressure load on panel, Pa (psi)
δ	deflection, cm (in.)
σ	stress, Pa (psi)

Subscripts:

b	base of panel holder
l	local condition at edge of boundary layer
max	maximum
t	total condition in combustor
tu	tensile ultimate
ty	tensile yield
∞	free stream

PANEL, PANEL HOLDER, AND INSTRUMENTATION

Thermal-Protection-System Panel

Description and design. - The thermal-protection-system panel used in the present investigation is shown attached to a substructure of stainless-steel hat-section members in figure 2. The panel consisted of the following components: A rectangular René 41 sheet-metal heat shield with 60° circular-arc corrugations that ran longitudinally (streamwise); four continuous René 41 transverse support members that were alined laterally (spanwise); 14 René 41 V-shaped center support members that were oriented longitudinally; and a set of insulation packages placed at the bottom of the support members. Heat shield and support members were joined by rivets. The support members were arranged so that they divided the heat shield into bays of approximately equal length. Stainless-steel screening was placed across the hat-section members to take the place of a substructure wall and thus to support the insulation packages. For the present installation, the packages were tied to the screening with nickel chromium (Nichrome) wire. The support members were bolted directly to the hat-section members through holes cut in the screening. Combined unit mass of the heat shield and support members was approximately 6.4 kg/m^2 (1.30 lb/ft^2). Total unit mass of the thermal protection system was 10.6 kg/m^2 (2.18 lb/ft^2). Masses of panel elements are itemized in table I.

The simplicity of the heat-shield design and its low mass are attractive features of this system. Its configuration absorbs lateral thermal displacements and therefore obviates the need for heavy, built-up transverse beams. Thus, the corrugations in the heat shield allow free lateral thermal expansion, and flexible bents at the top and bottom of the transverse support members allow nearly unrestrained longitudinal thermal growth. The center supports carry the aerodynamic drag loads. In designing the heat shield, corrugation radius was governed by the stiffness needed to beam the loading produced by aerodynamic surface pressures to the support members. The support members were sized to carry a uniform pressure of 20.7 kPa (3 psia) at a temperature of 1089 K (1960° R) without buckling as columns and without yielding. Design calculations were based on temperature-dependent material properties given in appendix A.

Fabrication details. - The panel was fabricated from materials on hand. René 41 components were cut and die-formed from 0.05-cm (0.02-in.) thick sheet that, as a result of uncertainties in material properties, had been re-solution treated for 2 hours in air at 1339 K (2410° R). Cutting and forming operations were performed without difficulty. The components were then aged 4 hr in air at 1172 K (2110° R) and air cooled. Formed configurations did not distort during the aging process. Inasmuch as the properties of the René 41 material can be adversely affected by reactions with elements in other materials, including body chemicals (see ref. 8), the heat shield and support members were both

freon and ultrasonically cleansed before aging and after assembly; degreased tools and rivets were used in assembling the components; and surgical rubber gloves were worn when components were handled.

Heat-shield details and dimensions are sketched in figure 3. The heat shield was 148.3 cm (58.4 in.) long and 106.7 cm (42.0 in.) wide. It contained 13 corrugations separated by narrow flat sections spaced at 8.01-cm (3.154-in.) intervals. Corrugation radius and height were 5.9 cm (2.32 in.) and 0.8 cm (0.31 in.), respectively. Inasmuch as there was no single sheet on hand large enough for the heat shield, two pieces of sheet were required to make up its width. The two pieces were overlapped along a flat section and were joined by two staggered rows of spotwelds spaced 1.27 cm (0.5 in.) apart. The spotwelds in each row were 0.64 cm (0.25 in.) apart. Five holes were drilled and dimpled through the heat shield along the center line of each flat at intervals of 35.56 cm (14 in.) to provide 70 attachment points for the support members. Each attachment point was reinforced by a 0.05-cm (0.02-in.) thick René 41 doubler approximately 2.03 cm (0.8 in.) square. Each doubler was spotwelded in four places to the underside of the heat shield.

The support members are sketched in figure 3(b) and are shown photographically in figure 4. The transverse support members were reinforced by 0.05-cm (0.02-in.) thick René 41 right-angle elements riveted at every attachment as illustrated in figure 3(b) and shown in figure 4(a). These elements prevented the introduction of eccentric loads at the top of the column-type supports and provided the desired stiffness in bending at the bottom. The center support members were assembled to give the box configuration shown in figure 4(b) for torsional stiffness in taking out the aerodynamic drag loads. The box configuration was obtained by overlapping and spotwelding top and bottom flanges of individual center support sections together at four places. All support members were attached to the heat shield with 0.40-cm (0.16-in.) diameter, A-286 stainless-steel countersunk blind rivets. The right-angle reinforcing elements were attached with brazier head rivets. This type of rivet was used in order to observe effects of aerodynamic heating on protruding rivet heads. Anchor nuts were fastened to the bottom flanges on all support members for convenient attachment to the hat-section substructure members. The hat sections were formed from 0.13-cm (0.05-in.) thick, type 347 stainless steel. Anchor nuts were fastened to the flanges of the hat sections for convenient attachment to the test fixture.

Insulation package.- In order to satisfy the requirement limiting substructure temperature to 422 K (760° R) after an exposure time of approximately 1/2 hr at a surface temperature of 1089 K (1960° R), a 5.08-cm (2-in.) thickness of layered silica fibrous (Micro-Quartz) insulation having a density of 67 kg/m^3 (4.2 lb/ft^3) was used in packages tailored to fit snugly between support members, as shown in figure 5. Rectangular packages were used between transverse support members, but the center packages were

notched to fit around the center support members. A ship lap joint was also provided on the center packages as a means of interrupting a direct radiation path to the panel interior. Small packages were constructed to fit inside the box of the center support members. Photographs of insulation packages are shown in figure 6. The insulation material was enclosed in envelopes constructed of 200-mesh screen made of Inconel 650 on the sides and undersurface and a 0.005-cm (0.002-in.) thick René 41 foil reflector surface on the top as shown in figure 5 and in the photograph of figure 6(b). The screening provided soft corners and sides to fit around the legs of support members and also permitted package venting during the rapid pressure changes of the wind-tunnel start and shutdown periods. The envelopes were assembled by spotwelding. Each package was made up of 12 layers of insulation. Wafers of a single layer of insulation were inserted between the layers along two rows on approximately 12.7 cm (5 in.) centers as shown in the photograph of figure 6(a). These wafers provided "hard" points for attaching the package to the substructure screening (fig. 2(b)) and aided in maintaining overall package thickness. The "hard" points were capped at the top and bottom by 0.005-cm (0.002-in.) thick René 41 foil wafers that were held together with 0.05-cm (0.018-in.) diameter (26-gage) nickel chromium (Nichrome) wire looped through the package. Package weight was 4.3 kg/m^2 (0.88 lb/ft^2). A photograph of the fitted center packages is shown in figure 6(c).

Panel Holder

Description.- The panel was tested using the panel holder illustrated in figure 7. Details on the development of this test fixture are given in reference 9. The panel holder is rectangular in planform, 141 cm (55.4 in.) wide by 300 cm (118 in.) long, and is 30.5 cm (12 in.) deep. Its lower surface is bevelled 20^o from the sharp leading edge. Exterior surfaces are covered with 2.54-cm (1-in.) thick Glasrock foam tiles which protect the internal structure from the aerodynamic heating environment produced in the wind tunnel. For wind-tunnel testing, the panel holder is sting mounted at its base. Test panels are mounted within a rectangular cavity 108 cm (42.5 in.) wide by 152 cm (60 in.) long located 102 cm (40 in.) downstream from the leading edge. Aerodynamic fences along the sides of the panel holder provide two-dimensional flow over the test area, and a boundary-layer trip of 0.24-cm (0.094-in.) diameter stainless-steel spheres near the leading edge generates turbulent flow over the panel surface. Surface pressures and aerodynamic heating rates are varied by pitching the panel holder. Differential-pressure loading of the panel is controlled by regulating the cavity pressure under the panel by means of spring-loaded vent doors in the boxes shown at the base of the panel holder. Details of the differential-pressure control system are described in the section entitled "Differential-Pressure Control" and in reference 6.

Panel installation.- The panel and hat-section substructure assembly was bolted through six 7.62-cm (3-in.) steel channel beams that, in turn, were bolted to the leading- and trailing-edge walls of the cavity in the panel holder. Spacing of the beams was as shown in figure 7(a). The panel was inclined 0.3° to the panel-holder surface. It was mounted so that the crests of corrugations intersected the Glasrock surface at the leading edge and the flats between corrugations intersected the Glasrock surface at the trailing edge. Thus, the corrugations provided rearward-facing steps at the trailing edge, as shown in figure 7(b). Panel inclination was accomplished by using hat sections of different heights (see fig. 3). This orientation was chosen because it presented fewer aerodynamic problems, especially with respect to interference heating at the leading and trailing edges.

No attempt was made to close the open corrugations at the trailing edge. Thus, the openings provided a natural interior venting capability in the event that the differential-pressure control system would not perform as expected. (The differential-pressure control system was to be proof tested in the present test program.) Total vent area of the open corrugations was 41.3 cm^2 (6.4 in^2). Panel side edges and the ends of the flat surfaces at the trailing edge rested on a frame formed by the flanges of René 41 closeouts configured as shown in figure 8. The closeouts (fig. 8(a)) were 0.05 cm (0.02 in.) thick and were bolted to the side and trailing-edge walls of the cavity. The leading edge of the heat shield was covered by the seal and fairing unit shown in figure 8(b). The flat sections between the corrugation closeouts ramped down from the Glasrock to the flats on the heat shield. In order to avoid separation of the leading-edge fairing from the heat-shield surface by thermal distortion, the crests of the fairing and the heat shield were clamped by a round-head rivet. As illustrated in figure 8(c), relative motion from thermal expansion between the fairing and heat-shield leading edge was allowed by slots cut in the crests of the fairing. A view of the panel and panel holder in the test chamber of the wing tunnel is shown in figure 9.

Instrumentation

Panel temperatures were sensed by eighty-two 30-gage, chromel-alumel thermocouples. Forty-six thermocouples were distributed over the back surface of the heat shield as shown in the sketch of figure 10; 30 were spaced at 2.54-cm (1-in.) intervals down the legs of the seven support members indicated in figure 10 by letter designations; four were placed inside the insulation package near the center of the panel – one each near the upper and lower surfaces and two at half depth; and two were used for sensing the air temperature within the cavity under the hat sections. Where temperatures were expected to be very hot, as on the heat shield and support members, stainless-steel-sheathed thermocouple assemblies were used. A typical thermocouple installation on the heat shield can be seen in the photograph of figure 4(a). The ends of the thermocouple

wires were alined normal to the flow direction and were spotwelded to the heat shield to form the junction. The wires were slacked to allow for thermal growth of the heat shield and passed through a two-hole ceramic bead to maintain separation of the wires. The sheathing was strapped to the heat shield with small strips of stainless-steel foil that were spotwelded to the heat shield. It was then routed down the legs of support members and joined to glass-cloth-covered thermocouple extension wiring below the insulation package where temperatures were expected to be cooler. The thermocouple installation technique on the legs of support members was similar to that on the heat shield. Glass-cloth-covered thermocouple wires were used in the insulation packages. For that installation, individual thermocouple wires were spotwelded to 0.94 by 5.08 cm (0.37 by 2.0 in.) strips of 0.04-cm (0.016-in.) thick René 41 sheet. These strips were then placed between layers of insulation at the desired depth.

In addition to the use of thermocouples, detailed coverage of surface temperatures during aerodynamic heating was obtained remotely by means of infrared radiometry. The radiometer was located outside the test stream about 183 cm (72 in.) above the center of the heat shield and scanned a 76.2 cm (30 in.) square, as shown in figure 10. This area was surveyed by 150 scanlines every 5 sec. Details of the radiometer are reported in reference 6.

Six high-temperature (922 K (1660° R)) deflectometers that operated on the inductive principle were distributed under the heat shield, as shown by the circle symbols in figure 10, to sense static deflections and dynamic response of the heat shield. The deflectometers were mounted in stainless-steel holders that were bolted to the channel beams supporting the panel. The deflectometer face was set at a distance of 0.09 cm (0.035 in.) from the back surface of the heat shield. Deflectometer power supply units were housed in two nitrogen-gas-cooled containers located between the pairs of channel beams.

Surface pressures were measured at four orifices spaced around the periphery of the panel-holder cavity and one orifice in the Glasrock 8.57 cm (3.38 in.) upstream of the cavity leading edge. Also measured were the differential pressure between the surface and the airspace under the heat shield, the cavity static pressure under the hat sections, the panel-holder base pressure, and pitot pressure at the trailing edge of the heat shield. All these measurements were obtained from strain-gage pressure transducers connected to 0.15-cm (0.060-in.) inside diameter stainless-steel orifice tubing. The transducers were located in the cavity under the hat sections. Panel accelerations were measured with an accelerometer mounted under the panel near its center of gravity.

High-speed motion-picture cameras were used for photographing the heat shield during wind-tunnel tests, and still photography was used for recording panel surface appearance throughout the test series.

APPARATUS AND TESTS

Test Facility

The present tests were conducted in the Langley 8-foot high-temperature structures tunnel shown schematically in figure 11. This facility is a hypersonic blowdown wind tunnel that operates at a nominal Mach number of 7, at total pressures between 4.1 and 24.1 MPa (600 and 3500 psia), and at nominal total temperatures between 1389 and 2000 K (2500° and 3600° R). Corresponding free-stream unit Reynolds numbers are between 1×10^6 and 10×10^6 per meter (0.3×10^6 and 3.0×10^6 per foot). Within the operating envelope bounded by these conditions, the aerodynamic pressures and heating rates encountered in flight at Mach 7 in the altitude range between 25 and 40 km (80 000 and 130 000 ft) are obtained.

The high-energy test medium is the products of combustion of a mixture of methane and air which is burned within a pressurized combustion chamber. The combustion products are then expanded to the test-section Mach number through an axisymmetric contoured nozzle having an exit diameter of 2.4 m (8 ft). In the test section, the stream is a free jet with a usable test core approximately 1.2 m (4 ft) in diameter over a length of 4.3 m (14 ft) that is diffused and pumped to the atmosphere by means of a single-stage annular air ejector. Total temperature is controlled by regulating the fuel-to-air ratio. Air storage capacity is sufficient for run times up to 2 min. The combustion products are considered to be in chemical equilibrium and are oxidizing. Partial pressure of free oxygen is calculated to be 70 Pa (0.01 psia) over the range of stream conditions.

Test models are protected from adverse tunnel startup and shutdown transient loads by storing them in a pod below the test stream until the desired hypersonic flow conditions are established. The model is then inserted rapidly into the stream on a hydraulically actuated elevator having a mass of 13 608 kg (30 000 lbm) and can travel vertically over a distance of 2.1 m (7 ft) to the stream center line in 1 sec. A model pitch system provides a range of angles of attack up to ±20°. Prior to tunnel shutdown, the model is withdrawn from the stream. Other details on this test facility are reported in reference 9.

Radiant Heaters

The present test program required the installation of two retractable, hydraulically actuated quartz-lamp radiators for thermal cycling and preheating the panel in the pod beneath the tunnel test chamber (ref. 6). Preheating was necessary because the relatively short aerodynamic exposure times available precluded obtaining desired temperature distributions through the panel. The radiators parted above the heat-shield longitudinal center line, retracted spanwise in opposite directions, as in the sketch of figure 12, and were transported on a steel framework carriage mounted on rails. Full travel time in

each direction was 1 sec. Each radiator was made up of 10 gold-plated, water-cooled reflector units containing 16 tungsten filament quartz lamps rated at 2000 W. Lamp distance above the model surface was 10.2 cm (4 in.). This distance was dictated both by the height of the aerodynamic fences on the sides of the panel holder and by what was believed to be the minimum allowable clearance that would preclude arcing to the heat shield at the reduced pressures during wind-tunnel operations.

Both radiators were divided into three zones. Voltage to the outer zones was ratioed to the center zones to give the desired surface temperature distribution. An ignitron tube power supply controlled by a closed loop servosystem continuously compared the output from a heat-shield thermocouple and the desired temperature input which was plotted on a time-based curve. Three-phase electrical power was distributed to the lamps through a system of rubber-covered copper cables that were wrapped in glass tape behind the reflector units. Maximum power capacity available was 1 mW.

Acoustic and Buffet Protection

A pair of retractable baffles shown in figure 13 was mounted to the carriage of the quartz-lamp radiators to shield the panel from potentially damaging acoustic pressures that occur during tunnel startup and shutdown and from severe buffeting associated with abnormal shutdowns. Under the baffles, the acoustic energy is attenuated approximately from 168 dB to 157 dB over the range of combustor pressures for which the flow is subsonic. Other details on the baffles are given in reference 6.

Differential-Pressure Control

Provision for varying the differential-pressure loading normal to the panel surface was built into the panel holder both as a means of protecting the panel during tunnel startup and shutdown and of extending the range of test variables. The differential-pressure control system consists of spring-loaded vent and fill doors at the base of the panel holder, as shown in figures 7 and 14, and a supply of nitrogen gas. On tunnel start, the vent doors allow the pressure within the cavity to follow the test-chamber evacuation rate of 41.4 kPa (6.0 psia) per second. On tunnel shutdown, the fill doors allow the pressure in the cavity to follow the test-chamber compression rate of up to 1 atmosphere per second. With this system, either positive (inward acting) or negative (outward acting) differential-pressure loading can be applied when the panel is in the stream. Positive differential pressures as high as 17.2 kPa (2.5 psi) are achievable by varying angle of attack up to -18° and venting cavity pressure to panel-holder base pressure. Differential pressure can also be varied between positive and negative values independently of angle of attack by locking the vent doors closed and pumping nitrogen gas into the cavity. The door locks are pneumatically actuated pins.

Tests

Panel evaluation test program.- The present investigation focused on panel structural and thermal response during repeated exposures to both radiant and aerodynamic heating to observe cumulative effects of cyclic heating. Structural response was evaluated by comparing structural static and dynamic characteristics of the panel before and after the heating tests. These characteristics were determined from static load-deflection tests and vibration surveys of natural frequencies. Panel structural integrity was monitored during the heating test series by means of visual inspections, surface mapping, and vibration surveys. Details of the procedures, apparatus, and results from the characterization tests are presented in appendix B.

In the heating tests, the panel was subjected to the three types of surface heating profiles shown in figure 15. The profile of figure 15(a) illustrates a radiant heating thermal cycle. This profile approximated the surface temperature encountered during a reentry heat pulse from Earth orbit (ref. 10). The profile of figure 15(b) illustrates a combined radiant preheating and aerodynamic-heating (aerothermal) test. These two types of tests were interspersed throughout the test series. The profile of figure 15(c) illustrates an aerothermal shock test in which the panel was not preheated. This type of test was conducted to observe panel response to the most severe test that could be applied. A summary of all of the tests is presented in table II.

Thermal cycle.- For thermal cycling events (fig. 15(a)), the radiant heaters were programed to allow heatup and cooldown of the heat shield at a rate of 2.8 K/sec (5° R/sec) to 1089 K (1960° R) and to maintain a constant surface temperature for periods up to 28 min. However, surface cooldown was to commence when the substructure temperature reached 422 K (760° R). The programed cooldown rate was maintained by the radiant heaters until a surface temperature was reached below which natural (uncontrolled) cooling dominated.

Radiant-preheat—aerothermal test.- In the radiant-preheat—aerothermal test (fig. 15(b)), the heat shield was preheated at a rate of 2.8 K/sec (5° R/sec) to 1089 K (1960° R) and was maintained at that temperature until one of two desired temperature distributions through the panel was present. These were indicated when the substructure temperature reached either 311 K (560° R) or 422 K (760° R) and corresponded to distributions that occur early and late, respectively, in reentry. The panel was then exposed to the tunnel stream for as long as possible at conditions that would sustain the preheat surface temperature of 1089 K (1960° R). Surface cooldown following aerodynamic exposure was uncontrolled because arcing problems precluded use of the radiant heaters in the low-pressure environment of the tunnel prior to shutdown.

For these tests, the tunnel was started when the desired substructure temperature was reached. If nominal flow conditions could not be achieved, radiant heating was con-

tinued as in a thermal cycle. When the correct flow conditions were established, the procedure, as illustrated in figure 16, was to de-energize the quartz lamps, retract the radiators and acoustic baffles, and insert and simultaneously pitch the panel holder so that it attained the desired angle of attack on reaching the stream center line. At the end of aerodynamic exposure the procedure was reversed, and tunnel shutdown was initiated after the radiators and acoustic baffles covered the panel. The desired interval between radiator retraction and panel insertion was 5 sec for minimum interruption of panel heating. On insertion, the panel entered the edge of the stream 1 sec after the elevator began lifting and reached the stream center line after an additional second. Panel acceleration during insertion and withdrawal was usually approximately 6g.

A maximum duration tunnel run required operating at high total conditions. Consequently, the average combustor-chamber pressure was 18.2 MPa (2641 psia), and the average total temperature was 1762 K (3173° R). (Two tests, 4 and 11, table II, were inadvertently conducted at an average combustion pressure of 6.9 MPa (1005 psia).) Average free-stream Mach number was 6.6, and average free-stream unit Reynolds number was 5.1×10^6 per meter (1.56×10^6 per foot). For most tests, panel-holder angle of attack was -9°; its selection was based on the turbulent calibration data of reference 9 and an estimate of the heating rate required for the preheat surface temperature. However, during three tests (tests 26, 31, and 34, table II), panel-holder angle of attack was varied between -3° and -12° to obtain data on the variation of positive differential pressure with angle of attack. These tests resulted in local Mach numbers at the panel from 6.2 to 4.4, surface pressures from 3.5 to 11.7 kPa (0.5 to 1.7 psia), and local dynamic pressures from 97 to 158 kPa (14 to 23 psi). In tests 26 and 31, the cavity pressure was vented to panel-holder base pressure. In test 34, the vent doors were closed and the cavity was pressurized to maintain an unloaded panel at various angles of attack.

Aerothermal shock test.- In the aerothermal shock test (fig. 15(c)), the panel was not preheated prior to its insertion into the tunnel stream. The test was conducted to evaluate panel response to transient aerodynamic heating. In addition, panel-holder angle of attack was increased in steps to approximately -12° to obtain data on the variation of positive differential-pressure loading with angle of attack with the vent doors closed and then was decreased to -9° for the remainder of aerodynamic exposure. Surface cooling after withdrawal was uncontrolled. The radiant heaters and acoustic baffles covered the panel during tunnel transient periods, and free-stream conditions were the same as for the radiant-preheat-aerothermal test.

Data Acquisition

During thermal cycles and preheat events, thermocouple output was recorded at a sampling rate of once every 2 sec. When the wind tunnel was operating, thermocouple and pressure-transducer outputs were recorded at a sampling rate of 20 per second.

Outputs from the infrared radiometer and deflectometers were recorded on FM tape. All data were reduced to engineering quantities at the Langley central digital data recording facility. Analytical quantities reported herein for the wind-tunnel tests are based on the thermal, transport, and flow properties of the combustion products test medium as determined from reference 11. Free-stream conditions in the test section were determined from reference measurements in the combustion chamber by using results from tunnel stream survey tests such as reported in reference 9. Local Mach number was obtained from oblique-shock relations.

RESULTS AND DISCUSSION

Summary of Panel Test Experience

The panel was tested in the sequence given in table II. As indicated, a positive differential pressure of 6.9 kPa (1 psi) was applied statically to the panel at the beginning and at the conclusion of the test series. In addition, the panel was vibrated to obtain up to nine natural frequencies on 17 occasions throughout the test series. (Results from these structural characterization tests are presented in appendix B.) The panel was also subjected to 12 thermal cycles at a surface temperature of 1089 K (1960° R), 10 radiant-preheat—aerothermal tests, and one aerothermal shock test. However, in attempting radiant-preheat—aerothermal tests, there were 21 false starts of the wind tunnel during which the panel did not enter the test stream but which resulted in 14 additional thermal cycles. For those events, the panel was simultaneously subjected to the effects of rapid test-chamber evacuation to near-vacuum conditions of 0.7 and 2.1 kPa (0.1 and 0.3 psia) and to tunnel start and shutdown acoustics under the baffles for about 30 sec per test.

Heat-shield and substructure temperature histories from all the heating tests are presented in sequential order in figure 17. The interrupted histories from tests 2 and 5 reflect intermittent electrical power failures to the quartz-lamp radiators, whereas the interrupted history from test 33 was deliberate in order to photograph the radiantly heated heat-shield surface. Environmental conditions and panel exposure times are summarized in table III for each type of heating test. Thus, the panel endured the following: 5.33 hr at a surface temperature of 1089 K (1960° R); 6.5 min in a Mach 6.6 stream that loaded the panel externally to differential pressures of up to 6.2 kPa (0.9 psi) while maintaining a surface temperature of 1089 K (1960° R); 12.9 min at low pressures resulting from 22 rapid test-chamber evacuations during preheating; and 81 excursions on the elevator that produced panel accelerations of up to 12g on a few occasions. (The high accelerations that exceeded the nominal value of 6g were inadvertent and occurred during calibration of the elevator control system.) Moreover, the heat shield was struck by electrical arcing from the quartz-lamp radiators during nearly every evacuation of the test chamber. On at least two insertions, a cloud of steam wiped along the hot surface

as the panel entered the stream boundary layer and momentarily decreased heat-shield temperatures by about 22 K (40° R). In those instances, water leaking from the tunnel nozzle cooling system sprayed onto the Glasrock surface upstream of the panel prior to insertion. The panel survived the foregoing with no apparent degradation of structural integrity. Therefore, these tests revealed an attribute inherent in this rather simple, lightweight thermal-protection-system concept – namely, ruggedness.

Panel Thermal Performance

Thermal cycle.- Panel thermal performance under radiant heating is demonstrated in figure 18 by thermocouple data obtained near the center of the panel during test 17 (table III). Variations of temperature with time are shown in figure 18 for the heat shield at flat 8 (fig. 10) from thermocouple 11 located 18 cm (7 in.) upstream of the center of the panel, for center support A (fig. 10), for the substructure, for the air in the cavity under the substructure, and for the insulation package. Calculated temperatures of support A obtained from a thermal analysis of this panel (presented in appendix C) are superimposed for comparison with the experimental values (fig. 18). The calculations were based on the output of heat-shield thermocouple 11 which was used as the surface heating input to the computer program. The very good agreement obtained between experiment and calculation indicates that a complex structural configuration can be modeled to predict interior temperatures resulting from heat conduction through the depth of the structure with reasonable accuracy.

During surface heatup at 2.8 K/sec (5° R/sec), 265 sec elapsed before the substructure temperature began increasing. In the constant-temperature period, temperatures on center support A were about 56 K (100° R) lower than in the insulation package (compare temperatures at locations 3 and 4 in fig. 18), indicating that excessive heat was not conducted down the support member. At 1268 sec into the constant-temperature period, the substructure temperature limit of 422 K (760° R) was reached, and surface cooldown was initiated at a rate of 2.8 K/sec (5° R/sec). At that time, average heat-shield temperature was 1089 K (1960° R) within a spread of ±35 K (±63° R). At 185 sec into the cooldown period, the substructure temperature peaked at 429 K (773° R), and cooldown using the quartz-lamp radiators terminated because the programed cooldown rate exceeded the natural surface cooldown rate. Panel heating and cooling processes are illustrated in figure 19 by temperature distributions on center support member A. During the constant surface-temperature period (fig. 19(a)), the temperatures on the support member increased to the approximately linear distributions of different slope above and below the top of the insulation package, as shown by the data at the end of that period. During panel cooldown (fig. 19(b)), the maximum temperature moved toward the substructure. The shaded band in figure 19(a) indicates the spread in temperatures obtained down all instrumented support members at the end of the constant surface-temperature period. The

width of the band reflects thermal response to variations in heat-shield temperature, to the heat-sink effect of the cavity walls, and to variations in the amount of radiation blockage provided by the insulation packages at the support members. The cooler edge of the shaded band is the distribution obtained from support member E (fig. 10) at the heat-shield edge. The dashed curve in figure 19(a) was obtained from calculated values based on an assumed surface-temperature history similar to the output of heat-shield thermocouple 11. These values fall within the shaded band and were used in a stress analysis of the panel which is presented in appendix D.

Thermal growth during the thermal cycle was indicated by scratches on the trailing-edge closeout where the trailing edge of the heat shield had rubbed and by a change in color of the oxidized coating where the heat-shield leading edge was covered by the leading-edge fairing. The length of the scratches and of the discoloration as measured with a ruler showed that the heat shield grew longitudinally about 0.80 cm (0.31 in.) in either direction from the center support members. This result agrees with the calculated thermal displacement reported in appendix D.

The time at which the substructure temperature limit occurred fell 2 min short of the desired 28 min. However, the use of a more realistic substructure of aluminum alloy with its greater thermal capacity would have extended this protection time. Inasmuch as the current Space Shuttle guideline limits the substructure temperature to 450 K (810° R) after 28 min of heating, the thermal performance of the present thermal protection system in a radiant heating environment is considered excellent.

Radiant-preheat—aerothermal test.- The effect of aerodynamic heating on panel thermal performance following a radiant preheat is shown in figure 20 by thermocouple data plotted as a function of time. Calculated temperatures from the thermal analysis presented in appendix C are also included. As a companion to this figure, figure 21 is presented to show the thermal response during aerodynamic exposure on an expanded time scale. The data were obtained during test 19 (table III). In that test, the panel was preheated for 648 sec, at which time the substructure temperature was 318 K (573° R), and panel exposure time in the stream was the longest of the test series (61 sec). (Aerodynamic exposure times varied as a result of anomalies in test facility operation.) Panel-holder angle of attack was -9°, and the cavity pressure was vented to base pressure in order to apply maximum positive differential pressure on the panel.

The thermal response to this type of test is characterized as follows (figs. 20 and 21): panel cooling by aspiration during test-chamber evacuation on tunnel startup near the end of the radiant preheat; additional cooling at reduced ambient pressure (2.1 kPa (0.3 psia)) for a 5-sec interval between quartz-lamp radiator retraction and panel entry into the stream; substantially greater temperature rise rates throughout the interior after entry into the stream; heat-shield temperature recovery by aerodynamic

heating; and uncontrolled cooldown after withdrawal from the stream. After approximately 16 sec in the stream, the heat-shield temperature (fig. 21) recovered from the 5-sec cooldown prior to insertion to an average value of 1089 K (1960° R) within a spread of ±28 K (±50° R). Thus, the preselected panel-holder angle of attack of -9° was approximately correct for the stream conditions of these tests. Positive differential pressure was 4.8 kPa (0.7 psi). At 220 sec into the cooldown period, the substructure temperature peaked at 382 K (688° R). The calculated curves in figure 20 show very good agreement with measured temperatures during radiant preheating, but the thermal modeling does not account for variations caused by the flow of hot gases through the interior of the panel during aerodynamic heating. Consequently, in the aerodynamic portion of the test, the calculated temperature at locations 3 and 4 on the support member and on the substructure underpredicted the corresponding measured temperature by about 83 K (150° R) and 44 K (80° R), respectively.

Although support-member temperatures increased after insertion, insulation temperatures appeared not to be affected by the insertion event (fig. 20(b)). The increase in heating along the support members after entry into the stream resulted from an unrealistic situation in which hot gases were drawn from the boundary layer by differential pressure between the surface and the cavity, through the gaps between the insulation packages, and out the vent doors at the base of the panel holder. (See fig. 7.) From the slope of the curve for the substructure temperature given in figure 20(a), it appears that if the time in the stream could have been extended, the substructure temperature limit would have occurred at a time far short of the desired 28 min. In fact, as demonstrated by the temperature distributions on the support member in figure 22, the distribution obtained after only 58 sec in the stream – following a relatively short radiant preheat – approximated that obtained after 1563 sec of radiant heating in the thermal cycle of test 17 (fig. 19(a)). However, the circulation of hot gases to the cavity under the hat sections can be retarded by keeping the vent doors closed. In that event, the cavity pressure primarily vents through the open corrugations at the heat-shield trailing edge with the result that the temperature rise rate on the lower part of the support member (location 4) is substantially less than when the vent doors are open, as indicated in figure 23. The data for this figure were obtained during test 31 (table III) in which the vent doors were closed for approximately 9 sec and then were opened while the panel holder was at $\alpha = -9^{\circ}$. This effect is further illustrated in figure 24, where slopes of the thermocouple output at location 4 are plotted as a function of time for 4-sec periods taken just before airflow began and before and after the vent doors opened. These results show the following: (1) when the vent doors were closed, the variation of temperature rise rate with time at the bottom of the support member (location 4) was the same both before airflow began near the end of the radiant preheat period and after panel insertion into the stream, and (2) when the vent doors were opened, the temperature rise rate increased markedly. At that time, the

pressure under the open corrugations at the heat-shield trailing edge decreased by about 0.8 kPa (0.12 psia), and positive differential pressure loading of the panel increased by the same amount. This result indicated a diversion of some of the interior flow from the open corrugations to the base of the panel holder. Therefore, in a more realistic test setup, the present concept shows excellent potential for protecting a substructure from a severe aerodynamic-heating environment. In the present test series, no attempt was made to seal the side edges positively against boundary-layer inflow. Future development tests of this thermal-protection-system concept should address this problem.

Aerothermal shock test.- In order to observe panel response under transient aerodynamic heating, the panel was subjected to aerothermal shock by inserting it into the stream without preheating (test 35, table III). In this test, the vent doors were locked closed to minimize internal flow of hot gases and thus maximize thermal gradient. Exposure time in the stream was 46 sec. Positive differential pressures up to 6.2 kPa (0.9 psi) were obtained for panel-holder angles of attack up to approximately -12°. Maximum cold-wall heating rate to the surface was 158 kW/m^2 (14 Btu/ft^2-sec) as determined from heat-shield thermocouple data for $\alpha = -9^{\circ}$. This result is within 5 percent of the flat-plate turbulent cold-wall value determined from the calibration data of reference 9 for a panel angle of attack of -9.3°.

The thermal response of the panel to these conditions is shown in figure 25 by thermocouple data plotted as a function of time. As indicated, heat-shield temperature increased very rapidly from the initial room-temperature value on insertion into the stream. Just prior to withdrawal from the stream, the average heat-shield temperature was 1096 K (1972° R) within a spread of ±29 K ($\pm 53^{\circ}$ R). The distribution of heat-shield temperatures at that time was similar to that obtained in test 19 (table III) in which the panel was preheated. The longer exposure time with the vent doors closed, relative to test 31 (previously discussed), afforded a better opportunity in test 35 to observe panel performance under conditions that would not force hot boundary-layer gases down the support member. That this, indeed, was the case is indicated by the relatively high temperatures on the portion of the support member located above the insulation package (locations 1 and 2) with respect to the very low temperatures <367 K (<660° R) on the lower portion of the support member (locations 3 and 4) adjacent to the insulation package. The temperature of the substructure and of the air under the substructure did not vary during the aerodynamic exposure period. These results indicate that the thermal performance of the present thermal-protection-system concept in a severe aerothermal shock environment is excellent.

Calculated support-member temperatures based on two different heat-shield temperature histories as input are also shown in figure 25. In addition to the calculations based on a measured heat-shield temperature history from thermocouple 11, calculations

were performed using a heat-shield temperature history based on heat-transfer coefficient and adiabatic wall temperature as determined from tunnel stream conditions corresponding to the various angles of attack. The latter calculations were independent of any measured heat-shield temperature response and reflected the accuracy with which the heat-transfer coefficient and adiabatic wall temperature were determined. The calculated temperatures based on the measured heat-shield temperature history as input (dashed curves) considerably underpredicted temperatures on the upper half of the support member (locations 1 and 2). The calculations based on the heat-shield temperature history determined from flow conditions (dash-dot curves) showed good agreement at location 1 and better agreement at location 2 than was obtained by the former calculations. However, the latter calculations overpredicted the measured heat-shield temperature, and therefore, higher calculated support-member temperatures would be expected. The agreement obtained by both methods with experiment was much better at locations 3 and 4 and was excellent on the substructure. These calculated results indicate the need for better definition of the convective heat-transfer process that was obviously present to some extent under the heat shield even when the vent doors were closed.

Surface temperatures.- As indicated earlier, thermocouple data showed that aerodynamic heating tended to smooth out the heat-shield temperature distribution obtained by radiant preheating from a spread of ±35 K (±63° R) to ±28 K (±50° R). Digitized traces of scanlines obtained from the infrared radiometer in test 19 in figure 26 showed a much smaller spread in the heat-shield surface temperatures during aerodynamic exposure than did the thermocouple data – only ±8.3 K (±15° R). In this figure, the scanlines were obtained along the flat sections and along the crests of corrugations over approximately one-half of the infrared viewing area between the center-line corrugation 7 and corrugation 11. The data were taken after approximately 55 sec of aerodynamic exposure. Temperatures along corrugations appeared uniformly distributed, whereas the protruding brazier-head rivets produced peaks in the distributions along flat sections. The peaks indicated rivet temperatures that averaged at least 30 K (54° R) higher than the average surface temperature. Inasmuch as the size of the resolution element scanning the surface was larger than the rivet head, actual rivet temperatures were probably somewhat higher than indicated. As shown in figures 26(b), 26(d), and 26(e), good agreement was obtained between temperatures given by infrared radiometry and by thermocouples.

Spanwise surface-temperature distributions at various longitudinal stations are presented in figure 27. The data for this figure are cross plots of digitized data traces spaced at approximately 0.6-cm (0.25-in.) intervals. Between support members $x/l = 0.381$ and $x/l = 0.657$ (figs. 27(d) and 27(b)), the distributions appeared flat within a spread of ±8.3 K (±15° R) and show good agreement with thermocouple data. At $x/l = 0.281$ and $x/l = 0.736$ (figs. 27(e) and 27(a)), the effect of the hotter, protruding

brazier-head rivets is clearly indicated. These results are pictorially represented in figure 28. A plot of the temperatures across the center-line corrugation 7 is presented in figure 29. Data from four thermocouples and from 14 infrared scans show that the temperatures were within ±5.6 K (±10° R) over the corrugation. Interestingly, the data from both systems reflected the same trends and indicated a small increase in temperature near the corners joining the corrugations and flat sections.

Under transient aerodynamic-heating conditions, rivets and support members are initially heat sinks; consequently, their temperatures lag those of the surrounding surface. This effect is seen as downward pointing spikes on scanlines of surface temperature obtained from the infrared radiometer during test 35 (table III), as shown in figure 30. The digitized trace shown in this figure was obtained 15 sec after panel insertion in the stream. The agreement of infrared and thermocouple data is within 28 K (50° R).

Panel Integrity

Thermal.- Panel thermal integrity can be evaluated from figure 31 by comparing the variations of temperature with time obtained from thermocouples on the heat shield and on center-support member A during thermal cycles conducted early and late in the test series (tests 13 and 33, table III). In figure 31, only the first heatup in test 33 (fig. 17) is plotted. Test 13 was the earliest thermal cycle of sufficient duration to allow adequate response at the bottom of the support member (location 4) for comparison with a subsequent test. Test 33 was the last thermal cycle that was free of radiant-heater output anomalies. Through test 13, the panel had been subjected to nine thermal cycles, of which six resulted from abortive tunnel runs, and to four radiant-preheat—aerothermal tests for approximately 1 hr of radiant heating at 1089 K (1960° R) and 2.3 min of aerodynamic heating. After the panel endured 14 additional thermal cycles, of which seven resulted from abortive tunnel runs, and five radiant-preheat—aerothermal tests for an additional 4.3 hr of radiant heating at 1089 K (1960° R) and 2.6 min of aerodynamic heating, no degradation in thermal response was evident during test 33. The similarity of the temperature histories along the support member indicates excellent thermal integrity for this panel.

Structural.- Panel structural integrity during the present test series can be assessed by comparing the natural frequencies obtained from vibration surveys taken between heating tests; these frequencies are presented in table IV. Details of the procedures for the vibration surveys are given in appendix B. Experimental and calculated natural frequencies and mode shapes obtained from the static characterization tests conducted prior to the heating tests are also given in appendix B. The tabulated frequencies are for one half-wave (m = 1) in the stream direction between support members and 1, 2, 6, and 9 half-waves in the cross-stream direction. The number of accumulated test events between vibration surveys is also given in table IV. The largest observed change in

panel natural frequency between vibration surveys was 6 Hz, and changes in the natural frequency appeared to be independent of the type of event or the number of events between vibration surveys, which was as high as seven (between tests 29 and 32, table II). The maximum change in natural frequency throughout the test series was about 3.5 percent. Although some scatter and drifting in frequencies occurred, first downward and then upward, no indications of serious structural degradation were detectable from results of the vibration surveys. During aerodynamic exposures, no evidence of panel flutter by the heat shield was indicated, as might be expected for highly orthotropic panels where the flow is alined with the major stiffness. An estimate of the flutter parameter from reference 12 showed that the heat shield should flutter at a value of q/β above 5033 kPa (730 psi), whereas the maximum wind-tunnel test value was only approximately 34 kPa (5 psi). However, as reported in reference 13, the flutter parameter for highly orthotropic panels can reduce more than an order of magnitude for small angles of yaw. Thus in a flight application, this heat-shield concept may be flutter prone if the corrugations are not alined with the flow direction.

Surface deformation.- A contour map of the changes in heat-shield surface deformation made at the end of the test series is plotted in figure 32. Each contour represents a deviation of 0.025 cm (0.010 in.) with respect to pretest values. In general, variations in the surface were within only one or two skin thicknesses as a result of an outward warp along the trailing edge toward the left corner, looking upstream. The largest change in surface shape was a depression approximately 0.23 cm (0.09 in.) deep shown on the center-line crest in the leading-edge bay. This depression extended to the adjacent flat sections and is believed to have occurred during test 6 (table III); further discussion of this test follows in the next section. Data on static loads and deflections given in appendix B indicated no detectable changes in stiffness of the support members from the beginning to the end of the test series.

Posttest condition of panel.- Except for the appearance of the heat-shield surface, which became increasingly discolored and pitted as the tests progressed, the panel was in excellent structural condition at the conclusion of the test series. Photographs of the heat-shield surface taken prior to testing and after the final test are shown in figure 33. The large, lighter areas shown in figure 33(b) reflect a pattern produced by the quartz-lamp radiators during preheating and thermal cycling events. Temperatures from thermocouples in these areas during radiant heating were approximately 44 K (80° R) higher than in the darker areas. Rainbow-like color variations appeared at random intervals along the side edges of the panel from effects of burnt silicone rubber sealant used on the walls of the rectangular cutout in the panel holder. Other contaminants marked the surface with white, powdery deposits, which may have resulted from an occasional broken quartz lamp, and with dried streaks from liquid deposits – perhaps drops of hydraulic fluid. Extensive pitting and scratching resulted from electrical arcing, as in the photo-

graph of figure 34, and from impacts by particles in the tunnel test stream. The particles were produced by flaking of a coating of plasma-sprayed alumina used for thermal protection on the combustor liner of the wind tunnel. All upstream surfaces of protruding rivet heads and the leading edge of some flush rivet heads were eroded, as shown in the photographs of figure 35.

At the back of the panel, most of the bolted connections between the support members and the stainless-steel substructure hat-section members had seized slightly so that an audible snap occurred as they were loosened using a ratchet wrench for disassembly. The heavy stainless-steel wire screen, the back surface of the Inconel 650 screen envelope covering the insulation material, the back surface of the heat shield, and the support members resembled their pretest appearance. The finish of the René 41 foil on the upper surface of the insulation packages, shown in figure 36, was oxidized to hues of blue and purple from repeated exposures to the test temperatures.

A careful visual inspection of the heat shield and support members showed no stretched or twisted support members, dimensional changes, or cracks other than a hairline crack around two (out of 112) spotweld craters at the top of the two outboard center support members. The origin of the cracks is not known, and it cannot be stated with certainty that they were not present prior to testing. Nevertheless, they were not structurally degrading. However, inasmuch as the cracks were located in both outboard center support members, they may have developed during testing from the unrealistic panel edge condition provided by the side-edge closeouts (fig. 8). These relatively rigid components impeded vertical motion of the heat-shield side edges induced by the thermal expansion of the outboard corrugations, acoustics, buffeting, and surface pressures encountered during aerodynamic testing. Such vertical motion would have occurred for an edge condition more representative of a heat-shield to heat-shield longitudinal joint in a reentry application. The only obvious indication of some structural change that could be attributed to an effect of testing was that all of the center support members could rotate freely about the countersunk rivets that fastened them to the heat shield. All other riveted connections appeared tight. It is believed that the rivets may have loosened during test 6 (table III). In that test, 12 thermocouples and six deflectometer probes were destroyed by heat-shield impact when the panel was subjected to combustor noise of at least 154 dB for at least 1 min during an aborted attempt to run the tunnel when the ejector failed to operate and tunnel shutdown was unusually severe.

Heat-shield and support-member stresses. - A stress analysis of the heat shield and support members using the SNAP (Structural Network Analysis Program of ref. 5) finite-element digital computer program is presented in appendix D. The analysis was based on material properties given in appendix A. The results indicated that for the loading and heating conditions of the present tests (excluding aerothermal shock), stresses in the heat shield were low and that the support members offered little resistance to ther-

mal growth. However, in the transverse support members, maximum compressive inplane stresses of 552 MPa (80 ksi) were concentrated in the angles formed by the intersection of each pair of legs at the bottom of the support member. Tensile stresses of 241 MPa (35 ksi) were concentrated in the angles at the top of the support member. Although these stresses were well within yield-stress limits, they exceeded the proportional limit. An assessment of their severity in terms of life degradation is beyond the scope of the present investigation and would require a nonlinear analysis using a finer grid of finite elements. Nevertheless, further development work to reduce stress concentrations in the transverse support members is indicated.

Recommended Improvements in Design

The results from the present panel evaluation substantiated the viability of the René 41 thermal protection concept and also indicated where improvements in detail design would enhance its practicality for service on hypersonic vehicles. Thus, the transverse support member should be designed so that stress levels in the formed angles are reduced. As indicated in appendix D, design changes might include (1) dimpling the angle to allow thermal growth or (2) riveting separate legs together to form the truss-shaped support. Inasmuch as the heat shield was lightly loaded, its thickness could be reduced to save mass. Further development work should also concentrate on making this type of heat shield flutter free. Toward this end, consideration should be given to placing the insulation in contact with the heat shield so that it can assist in damping heat-shield vibrations. Placing the insulation against the heat shield should also eliminate the need to totally envelop the insulation in screening or foil and, thus, might result in further savings in mass.

CONCLUDING REMARKS

A large, flightweight panel for a metallic thermal-protection-system concept for reentry- and hypersonic-vehicle application was tested in the Langley 8-foot high-temperature structures tunnel to evaluate its aerothermal performance and its structural integrity. The panel consisted of a 106.7 by 148.3 cm (42.0 by 58.4 in.) corrugation-stiffened heat shield riveted to support members made of 0.05-cm (0.02-in.) thick heat treated and aged René 41 sheet material and 5.08-cm (2-in.) thick silica fibrous insulation packages that were covered with René 41 foil and Inconel 650 screening. The insulation packages were located at the bottom of the support members. The system was designed to protect the substructure from temperatures above 422 K (760° R) for 28 min and to carry a uniform pressure of 20.7 kPa (3 psi) at a surface temperature of 1089 K (1960° R). Total mass of the system was 10.6 kg/m^2 (2.18 lb/ft^2). The panel was subjected to the following tests: 12 thermal cycles by radiant heating at atmospheric pres-

sure to a surface temperature of 1089 K (1960° R) for constant-temperature exposure times up to 21 min; 14 thermal cycles by radiant heating with intermittent pressure and acoustic pulses (rapid reduction in ambient pressure to 0.7 kPa (0.1 psia) and acoustic pressures to 162 dB); 10 radiant preheats followed by aerodynamic exposures that produced differential-pressure loading up to 6.2 kPa (0.9 psi), local Mach numbers from 6.2 to 4.4, local dynamic pressures from 97 to 158 kPa (14 to 23 psi), and aerodynamic heating rates that maintained a surface temperature of 1089 K (1960° R); and one aerothermal shock test at a cold-wall turbulent heating rate of 158 kW/m^2 (14 Btu/ft^2-sec). Aerodynamic exposure times were up to 1 min at a nominal free-stream Mach number of 6.6 and a nominal free-stream unit Reynolds number of 5.118×10^6 per meter (1.56×10^6 per foot). Heat-shield corrugations were alined with the stream.

During these tests, the panel sustained 5.33 hr at a surface temperature of 1089 K (1960° R), 6.5 min in the aerothermal environment, and accelerations of up to 12g without apparent degradation of thermal or structural integrity. The panel demonstrated that under radiant heating it can protect the substructure from temperatures above 422 K (760° R) for 26 min with a surface-heating history corresponding to a typical reentry heat pulse from Earth orbit. This is well within the current shuttle guideline that limits the substructure temperature to 450 K (810° R) after 28 min of heating. The panel also demonstrated excellent potential for thermal protection in a severe aerodynamic-heating environment by temperature rise rates on support members that approximated those obtained under radiant heating. However, as would be expected, panel thermal performance degraded when hot gases from the boundary layer were forced through the panel interior.

Thermal analysis demonstrated that this thermal-protection-system concept can be modeled to predict thermal response with reasonable accuracy. Stress analysis, based on the test pressures and heating rates, indicated stress concentrations in the angles formed by the intersection of support-member legs within yield-stress limits but greater than the proportional limit by as much as 30 percent. In view of these calculated stresses, further development work should consider redesigning support members to reduce the level of stress concentration. Design changes might include (1) dimpling the angle to allow thermal growth or (2) riveting separate legs together to form the truss-shaped support. Inasmuch as the stress analysis also showed that the heat shield was lightly loaded, mass can be saved by reducing the heat-shield thickness.

Although no evidence of panel flutter was indicated during the aerodynamic exposures, this heat-shield concept may be flutter prone at small angles of yaw, according to analysis. Therefore, further development work should also focus on making the heat shield flutter free. As a step toward this end, placing the insulation against the heat shield would aid in damping heat-shield vibrations. This action would eliminate the need for totally enveloping the insulation in screening or foil, which might also result in further mass saving.

Langley Research Center
National Aeronautics and Space Administration
Hampton, Va. 23665
July 18, 1975

APPENDIX A

MATERIAL PROPERTIES

This appendix presents the material properties which were used in the thermal and stress analyses of the test panel. Table V contains temperature-independent values of emittance and density which were determined by tests or were obtained from standard material handbooks. Figure 37 gives temperature-dependent properties, most of which were taken from reference 14. Values of thermal conductivity and specific heat in figures 37(a) and 37(b) are connected by straight lines since linear interpolation between known values is used in the program.

APPENDIX B

PANEL CHARACTERIZATION

Static Load-Deflection Tests and Results

Tests.- Panel static load-deflection data were obtained experimentally before and after the heating test series. A differential-pressure loading technique was employed, using the setup as shown in figure 38. With this technique, the heat shield was covered with a sheet of vinyl, and the edges of the vinyl were sealed to the Glasrock surface of the panel holder. A vacuum pump reduced the pressure within the cavity under the panel and thus induced a uniform load over the heat shield. Cavity pressure was reduced in increments of 1.4 kPa (0.2 psi) to a maximum differential pressure of 6.9 kPa (1 psi) and then was increased by the same increments. Panel deflections were recorded at each pressure level from the output of a deflectometer system mounted on a traversing trolley and bridge mechanism that can survey the entire heat-shield surface. The mechanism was operated so that the deflectometer was transported in the spanwise direction on the bridge which traversed the heat-shield length on rails. For these tests, the traversing mechanism surveyed heat-shield surface deflections along the length of only one flat and the crest of one corrugation near the longitudinal center line. Output of the deflectometer probe was recorded on an x-y plotter. Deflections were also recorded from the outputs of the six deflectometers mounted under the heat shield (fig. 10) and from readings of 12 dial micrometer gages on the surface; these gages were used to check symmetry of deflections.

Static loads and panel deflections.- Panel deflections measured along a flat nearest the center line are presented in figure 39 as a function of length. Inasmuch as the deflections varied linearly with loading, they were normalized with respect to the maximum loading of 6.9 kPa (1.0 psia) which totaled 10.9 kN (2453 lb). Support-member locations are indicated by a center line and dashed lines. The results obtained at the beginning and at the conclusion of the test series were virtually the same and so are shown as a single curve. The repeatability of results indicates that heat-shield and support stiffnesses did not change.

The raw data were corrected by the amount of the deflections of the heavy channel beams to which the hat-section substructure members were mounted. The correction was determined by using simple beam theory and was verified by the data from the fixed deflectometers. Deflections were symmetrical about the center support which deflected the least of the supports, i.e., about one-half the heat-shield thickness. Deflections of the transverse supports adjacent to the center support were approximately 63 percent greater than the deflection of the center support, whereas the deflections of the transverse

supports adjacent to the leading and trailing edges were only about 27 percent greater than those of the center support.

Maximum deflections of the heat shield between supports, excluding support-member deflections, occurred in the leading- and trailing-edge bays and were approximately three times those that occurred in the interior bays. Maximum deflection of the heat shield in these outer bays amounted to a little more than one skin thickness.

Vibration Modes and Frequency Surveys

Tests.- Panel vibration modes and frequencies were obtained before and after the heating tests and intermittently during the test program. The surveys were conducted using the portable setup shown in the photograph of figure 40. The panel was excited by an electrodynamic shaker mounted above the heat shield. In order to define mode shapes, the entire surface was surveyed using the traversing trolley and bridge mechanism as was done during the static load-deflection tests. Resonant frequencies were indicated by the peak amplitude response shown on an oscilloscope, and modal frequencies were surveyed in the range between 50 and 500 Hz by using a frequency sweep technique. The natural frequencies thus obtained provided a convenient means of detecting panel structural degradation after a thermal cycle or a wind-tunnel test, as indicated by significant changes in natural frequency.

Panel vibration modes and frequencies.- Some of the experimentally observed nodal patterns and frequencies determined from vibration surveys of the panel that were conducted at the beginning of the test series are presented in figure 41. Up to two heat-shield bays were surveyed. Although the interplay of heat-shield and support-member responses often precluded clear definition of the mode shapes, sufficient information was generated to indicate that mode shapes are complex, a characteristic that was identified in reference 15 for a corrugated panel constructed of René 41 similar to the present panel.

Experimental and calculated natural frequencies (calculations based on theory of ref. 13) of the panel are given in table VI and are plotted in figure 42 as a function of the mode number n up to 10 modes. The measured natural frequencies varied between 222 and 376 Hz, and their agreement with calculated values is fairly good (within 5.5 percent) through the mode $n = 7$. After the seventh mode, the agreement between experiment and calculation diverges. The boundary conditions assumed in the calculations were that the streamwise edges of the heat shield were simply supported and that the other two edges were supported by deflectional, rotational, and torsional springs of equal stiffness, respectively. The approach used in obtaining calculated frequencies was to identify the deflectional spring constant K_d from the deflection data determined by the static load tests as shown in figure 43. In that figure, calculated and measured heat-shield and

support-member deflections in half of an interior bay bounded by a center support member are compared and show good agreement; although the other half of the bay would be different since, on the panel, the leading- and trailing-edge supports are unequal. Rotational and torsional constraints were then adjusted for a "best fit" of the vibration data. The calculated frequencies were obtained using $K_d = 75.5$, $K_r = 10$, and $K_t = 5$. The technique used is described in reference 16.

APPENDIX C

THERMAL ANALYSIS OF RENÉ 41 THERMAL PROTECTION SYSTEM

A thermal analysis was made to predict the temperatures on the surface and through the depth of a metallic thermal protection system for comparison with the experimental results. The program used for the analysis was MITAS (Martin Interactive Thermal Analysis System) which is described in reference 4. The panel is divided into a network of nodes where each node is considered to be a constant temperature region. The network solution is obtained by using a finite differencing technique. The region modeled for the thermal analysis was a symmetrical section in the center of the panel (see fig. 10) over a length of 17.8 cm (7.0 in.) and width of 4.0 cm (1.6 in.) and included a center support member and a node containing a surface thermocouple.

A schematic for the section modeled is shown in figure 44. The modeling included a node representing the rivet that attached the support member to the heat shield and a node representing the bolt that attached the support member to the hat section. The insulation blanket was divided into a number of nodes through the thickness.

Figure 45 shows a section through the panel identifying the various components and the modes of heat transfer considered in the analysis. The preheating tests allowed the quartz lamps to radiate to the heat-shield surface to maintain a controlled surface temperature. The modeling allowed for a radiation interchange between the heat-shield surface, the support members, and the insulation package as indicated in the figure. Conduction was considered to have occurred along all surface and support nodes, through the insulation package, and along the hat sections. A radiation heat loss was allowed from the lower surface of the thermal protection system.

Temperature-dependent thermal properties for the materials used as components in the thermal-protection system are presented in figure 37. The material density and the constant-value emittance of these materials are given in table V.

The following assumptions were made for the analysis: (1) The initial starting temperature for all nodes was taken as the local ambient condition, (2) The emittance values used for radiation were taken as a constant value for each material involved, (3) There was no thermal interchange considered between the support nodes and the ends of the insulation nodes since the temperature at adjacent locations were nearly the same, and (4) An aluminum plate 1.3 cm (0.5 in.) thick was placed below the system to represent an equivalent structure to which heat radiated (this plate represented the mesh screens on the lower surface of the insulation package, the instrumentation wiring, and the cavity walls of the panel holder). Calculated temperatures are compared with thermocouple measurements through the depth of the panel in the main text.

APPENDIX D

STRESS ANALYSIS OF RENÉ 41 THERMAL PROTECTION SYSTEM

A stress analysis of the René 41 heat shield was performed by using the SNAP (Structural Network Analysis Program of ref. 5) finite-element digital computer program. The length of the portion modeled by finite elements (see fig. 10) represents the aft 20.96 cm (8.25 in.) of the total heat-shield length of approximately 147.32 cm (58 in.). Lengthwise (x-direction) rigid body displacements of the entire heat shield are prevented by the center supports, and thermal growth of the heat shield occurs from the center supports. The transverse supports, located every 35.56 cm (14 in.) from the center supports, prevent lateral (y-direction) displacements, carry pressure loads, and flex to accommodate thermal growth of the heat shield. The end portion of the heat shield was selected for modeling since the greatest displacement due to thermal growth occurs at the end.

The grid used for modeling is shown in figure 46. The 4-node elements contain both membrane and bending stiffness and, consequently, the stresses calculated are the sum of membrane and bending stresses. All elements were 0.05 cm (0.020 in.) thick except that the elements around support attachments (nodes 59 and 112) were 0.10 cm (0.040 in.) to include doublers at these locations. A beam 0.10 cm (0.040 in.) long with extremely high stiffness properties connected nodes 45 and 112 to represent the attachment of the heat shield to the support. The right-angle reinforcing elements were added after the stress analysis was performed (compare fig. 46 with fig. 3) and so were not modeled. Conditions of symmetry were used at the nodes along cut edges to represent the remainder of the heat shield and support member. Node 59 was completely restrained from motion to represent a riveted attachment to the substructure. An initial longitudinal displacement (x-direction) was assigned to nodes 1 to 5 to represent the thermal growth of the portion of the heat shield upstream of that location. Temperature-dependent values of material modulus of elasticity, coefficient of thermal expansion, and Poisson's ratio used in this analysis are given in figure 37.

Loading and heating conditions applied to the structure were a 3.5-kPa (0.5-psi) differential pressure pushing the heat shield inward, a uniform surface temperature of 1089 K (1960° R), and a temperature gradient of 1089 K (1960° R) at the top of the support to 450 K (810° R) at the bottom of the support member. An assumed surface-temperature history was used with the MITAS program described in appendix C to calculate the temperature distribution shown by the dashed line in figure 19(a). An initial temperature of 294 K (530° R) was assumed for the temperature history followed by a 2.8 K/sec (5° R/sec) rise to 1089 K (1960° R). The surface temperature was held constant for approximately 1300 sec and then was reduced to 294 K (530° R) at a rate of

2.8 K/sec (5° R/sec). The temperature distribution shown in figure 19(a) (dashed line) was calculated at a time corresponding to the end of the constant-temperature period. These loading conditions were selected because a 3.5-kPa (0.5-psi) differential pressure load was expected during wind-tunnel tests and because maximum thermal expansion of the support was expected at the end of the constant-temperature period of the surface-temperature history. The agreement of the calculated temperature gradient with the experimental scatter band from test 17 (table III) indicates that the calculated results represent a reasonable temperature distribution.

The resulting longitudinal displacement and reaction forces of the support members at the trailing edge are given in figure 47. The displacement of 0.85 cm (0.335 in.) agrees closely with the measured value of 0.80 cm (0.313 in.). The small reaction force, 3.58 N (0.803 lb), which results entirely from thermal growth of the heat shield, indicates that the support members are highly flexible in the length direction.

Inplane stress contours showing the summation of membrane and bending stress are plotted on the developed surface of the support member in figure 48 and show that the maximum stress is compressive and occurs in the angle formed by the intersection of each pair of support-member legs at the bottom of the support (see 552-MPa (80-ksi) contour). The stress appears to be primarily a result of constrained thermal expansion rather than a result of the temperature gradient. The stress level in the upper angle formed by the intersection of each pair of support-member legs exceeds 345-MPa (50-ksi) tension and appears to be caused, at least in part, by the temperature gradient down the top portion of the support. The right-angle reinforcing element, which was not modeled, was attached near this location of maximum stress. However, this element should have had negligible effect on the thermal stresses in this region since the element was attached by a single rivet. These stresses fall well within yield-stress limits (see appendix A) but exceed the proportional limit. Although these stresses may not be critical for short duration tests (no evidence of failure was found as a result of the tests reported herein), their level is such that a nonlinear analysis and a finer grid of finite elements in the regions of maximum stress would be required to assess their severity accurately. For example, such a detailed study might be necessary if a heat-shield support of the design considered herein were to be used for a specific life application. Furthermore, any additional development of this type of support should probably consider design changes to reduce stress levels in the formed angles. Such changes might include (1) dimpling the angle to allow thermal growth or (2) riveting separate legs together to form the truss-shaped support.

APPENDIX D

Heat-shield stresses, plotted on the developed surface of the heat shield, are shown in figure 49. They are relatively low compared with the stresses in the support members because the high flexibility of the support allowed essentially unrestrained thermal growth. The maximum shear stresses for the heat shield and the support were small and are not shown. In each case they were about one-tenth the value of the previously mentioned maximum stresses.

REFERENCES

1. Anderson, Roger A.; Brooks, William A., Jr.; Leonard, Robert W.; and Maltz, Joseph: Structures – A Technology Overview. Astronaut. & Aeronaut., vol. 9, no. 2, Feb. 1971, pp. 38-47.

2. Stein, Bland A.; Bohon, Herman L.; and Rummler, Donald R.: An Assessment of Radiative Metallic Thermal Protection Systems for Space Shuttle. NASA Space Shuttle Technology Conference – Dynamics and Aeroelasticity; Structures and Materials, NASA TM X-2570, 1972, pp. 267-302.

3. Hunt, L. Roane; and Bohon, Herman L.: Performance of LI-1542 Reusable Surface Insulation System in a Hypersonic Stream. NASA TM X-71955, 1974.

4. Martin Interactive Thermal Analyzer System – Version 1.0. User's Manual. MDS-SPLPD-71-FD238 (REV 3), Martin Marietta Corp., Mar. 1972.

5. Whetstone, W. D.: Structural Network Analysis Program – User's Manual. Static Analysis Version V70E. LMSC-HREC D162812. Lockheed Missiles & Space Co., Dec. 14, 1970.

6. Deveikis, William D.; Bruce, Walter E., Jr.; and Karns, John R.: Techniques for Aerothermal Tests of Large, Flightweight Thermal Protection Panels in a Mach 7 Wind Tunnel. NASA TM X-71983, 1974.

7. Plank P. P.; Sakata, I. F.; Davis, G. W.; and Richie, C. C.: Hypersonic Cruise Vehicle Wing Structure Evaluation. NASA CR-1568, 1970.

8. Lyman, T., ed.: Metals Handbook. Volume 2.- Heat Treating, Cleaning and Finishing. 8th ed. American Soc. Metals, c.1964.

9. Deveikis, William D.; and Hunt, L. Roane: Loading and Heating of a Large Flat Plate at Mach 7 in the Langley 8-Foot High-Temperature Structures Tunnel. NASA TN D-7275, 1973.

10. Eidinoff, H. L.; and Rose, L.: Thermal-Structural Evaluation of TD Ni-20Cr Thermal Protection System Panels. NASA CR-132487, 1974.

11. Leyhe, E. W.; and Howell, R. R.: Calculation Procedure for Thermodynamic, Transport, and Flow Properties of the Combustion Products of a Hydrocarbon Fuel Mixture Burned in Air With Results for Ethylene-Air and Methane-Air Mixtures. NASA TN D-914, 1962.

12. Erickson, Larry L.: Supersonic Flutter of Flat Rectangular Orthotropic Panels Elastically Restrained Against Edge Rotation. NASA TN D-3500, 1966.

13. Sawyer, James Wayne: Flutter of Elastically Supported Orthotropic Panels Including the Effects of Flow Angle. NASA TN D-7491, 1974.

14. Mechanical Properties Data Center, Belfour Stulen, Inc.: Aerospace Structural Metals Handbook – 1974 Publication. AFML-TR-68-115, U.S. Air Force, c.1974.

15. Carden, Huey D.; Durling, Barbara J.; and Walton, William C., Jr.: Space Shuttle TPS Panel Vibration Studies. NASA Space Shuttle Technology Conference, Volume III – Dynamics and Aeroelasticity, NASA TM X-2274, 1971, pp. 27-48.

16. Heard, Walter L., Jr.; and Bohon, Herman L.: Natural Vibration and Flutter of Elastically Supported Corrugation-Stiffened Panels – Experiment and Theory. NASA TN D-5986, 1970.

TABLE I.- MASS OF PANEL ELEMENTS

Item	Mass		Unit mass		Thickness	
	kg	lb	kg/m^2	lb/ft^2	cm	in.
Corrugated René 41 heat shield with 70 doublers	7.60	16.76	4.81	0.98	(a)	(a)
4 René 41 transverse support members	.86	1.90	----	---	0.05	0.020
14 René 41 upper reinforcing elements	[b].04	[b].09	----	---	.05	.020
13 René 41 lower reinforcing elements	[b].05	[b].11	----	---	.05	.020
14 René 41 center support members	1.17	2.58	----	---	.05	.020
52 floating anchor nuts	.08	.18	----	---	----	----
14 rigid anchor nuts	.01	.02	----	---	----	----
70 countersunk rivets	.06	.13	----	---	----	----
156 brazier head rivets	.18	.40	----	---	----	----
Heat shield and support assembly	10.05	22.17	6.36	1.30	10.6	4.16
Insulation packages	7.12	15.69	4.26	.88	5.1	2.00
Thermal protection system	17.17	37.86	10.62	2.18	10.6	4.16

[a]Corrugated heat shield, 0.05 cm (0.020 in.); doublers, 0.05 cm (0.020 in.).
[b]Calculated.

TABLE II.- SUMMARY OF TESTS

Test	Type of test	Remarks
	Static load deflection	Four tests conducted at Δp = 6.9 kPa (1 psi); natural vibration modes and frequencies obtained; panel surface deformations mapped at zero load
1	Thermal cycle	
2	Thermal cycle	Vibration survey followed this test
3	Thermal cycle from aborted tunnel run[a]	Vibration survey followed this test
4	Radiant preheat and aerothermal	Low total pressure
5	Thermal cycle from aborted tunnel run	
6	Thermal cycle from aborted tunnel run	Hard shutdown destroyed 12 thermocouples and 6 deflectometers; vibration survey followed this test
7	Thermal cycle from aborted tunnel run	
8	Thermal cycle from aborted tunnel run	Vibration survey followed this test
9	Thermal cycle from aborted tunnel run	
10	Radiant preheat and aerothermal	Vibration survey followed this test
11	Radiant preheat and aerothermal	Low total pressure
12	Radiant preheat and aerothermal	Vibration survey followed this test
13	Thermal cycle	
14	Thermal cycle from aborted tunnel run	
15	Thermal cycle from two aborted tunnel runs	Hard shutdown; vibration survey and surface mapping followed this test
16	Thermal cycle from three aborted tunnel runs	
17	Thermal cycle	
18	Thermal cycle from two aborted tunnel runs	Vibration survey and surface mapping followed this test

[a]False tunnel start resulted in no aerodynamic exposure but subjected the panel to rapid test-section evacuation and recompression; also to acoustic loading of 157 dB.

TABLE II.- SUMMARY OF TESTS – Concluded

Test	Type of test	Remarks
19	Radiant preheat and aerothermal	Vibration survey followed this test
20	Radiant preheat and aerothermal	Test aborted after 2 sec in tunnel stream
21	Thermal cycle	Vibration survey followed this test
22	Thermal cycle	
23	Thermal cycle	
24	Radiant preheat and aerothermal	
25	Thermal cycle	Vibration survey followed this test
26	Radiant preheat and aerothermal	Pitch angle varied
27	Thermal cycle	
28	Thermal cycle	Vibration survey followed this test
29	Thermal cycle from three aborted tunnel runs	Vibration survey followed this test
30	Thermal cycle from aborted tunnel run	
31	Radiant preheat and aerothermal	False tunnel start preceded aerodynamic exposure; pitch angle varied; vent doors closed initially, then opened
32	Thermal cycle from two aborted tunnel runs	Vibration survey followed this test
33	Thermal cycle	
34	Radiant preheat and aerothermal	Pitch angle varied; vent door closed; cavity pressurized
35	Aerothermal shock	Pitch angle varied; vent doors closed; vibration survey followed
36	Thermal cycle	
	Static load deflection	Two tests conducted at $\Delta p = 6.9$ kPa (1 psi); natural vibration modes and frequencies obtained; panel surface deformations mapped at zero load

TABLE III.- TEST CONDITIONS

(a) Thermal cycles[a]

Test	Time at 1089 K (1960° R), sec	Peak substructure temperature	
		K	°R
1	60	---	---
2	272	---	---
13	930	---	---
17	1268	429	773
21	1227	428	770
22	1225	433	779
23	1198	443	798
25	1033	438	788
27	1204	433	780
28	1138	446	803
33	815	---	---
36	593	409	737

[a]2.8 K/sec (5° R/sec) heatup and cooldown with a constant surface temperature period at 1089 K (1960° R).

TABLE III. - TEST CONDITIONS – Continued

(b) Thermal cycles from aborted tunnel runs

Test	Time at 1089 K (1960° R), sec	Peak substructure temperature		False tunnel starts	Test chamber evacuations[a]	Time between 148 dB and 157 dB,[b] sec	Time between 159 dB and 168 dB,[c] sec
		K	°R				
3	195	---	---	1	1	---	
5	295	---	---	1	1	40	
6	603	---	---	1	0	57	
7	94	---	---	1	1	27	
8	87	---	---	1	1	18	17
9	90	---	---	1	1	29	
14	237	---	---	1	1	25	
15	483	375	675	2	1	333	
16	857	404	727	3	0	32	
18	815	409	736	2	1	100	[d]180
29	786	404	728	3	1	42	
30	345	361	650	1	1	30	
[e]31	378	---	---	1	0	13	
32	301	346	622	2	1	39	

[a]Static pressure in test chamber between 0.7 and 2.1 kPa (0.1 and 0.3 psia).

[b]Panel covered during subsonic flow periods of tunnel operation.

[c]Panel uncovered during subsonic flow periods of tunnel operation.

[d]Panel exposed to subsonic flow during air storage depletion.

[e]Aerothermal test followed the false tunnel start.

TABLE III. - TEST CONDITIONS – Concluded

(c) Aerothermal tests

Test	Preheat time at 1089 K (1960° R), sec	Time between 148 dB and 157 dB, sec (a)	Time in hypersonic stream, sec	Peak substructure temperature		α, deg (b)	Time at α, sec	Δp		p_b		p_l		q_l		M_l	M_∞	p_∞		p_t		T_t		R	
				K	°R			kPa	psi	kPa	psia	kPa	psia	kPa	psi			kPa	psia	MPa	psia	K	°R	Per meter	Per foot
4	73	35	24	---	---	-8.7	20	1.2	0.17	0.8	0.11	---	---	---	----	5.56	7.03	1.0	0.14	6.8	993	1897	3414	2.07×10^6	0.63×10^6
10	113	29	32	---	---	-9.6	27	4.6	.66	2.3	.33	---	---	---	----	5.10	6.59	1.9	.28	18.22	2643	1765	3177	5.09	1.55
11	52	27	47	---	---	-9.3	42	1.1	.16	.8	.11	---	---	---	----	5.26	6.86	.8	.12	7.01	1017	1796	3232	1.97	.60
12	642	27	37	---	---	-9.3	32	4.1	.60	2.3	.33	---	---	---	----	5.10	6.58	1.9	.28	18.23	2644	1769	3184	4.99	1.52
19	322	27	61	382	688	-9.3	55	4.9	.71	2.3	.34	8.0	1.16	146	21.12	5.10	6.52	2.1	.31	18.17	2635	1723	3102	5.09	1.55
20	1201	28	2	438	788	-5.3	2	3.0	.44	--	---	5.8	.84	---	----	---	---	2.1	.30	----	----	----	----	---------	---------
24	1289	38	34	444	800	-9.3	30	4.7	[c].68	2.1	.30	8.9	1.29	162	23.49	5.10	6.52	2.1	.31	18.13	2630	1716	3089	5.45	1.66
26	317	29	18	358	644	-9.3	5	5.4	.78	3.4	.49	8.6	1.25	157	22.76	5.10	6.53	2.2	.32	18.45	2676	1718	3092	4.92	1.50
						-7.3	3	4.0	.58	2.9	.42	6.7	.97	131	19.07	5.30	6.56	2.2	.32	18.33	2659	1741	3133	5.18	1.58
31	378	27	43	376	676	-9.3	4.5, 4.5	[c]4.3, 5.2	[c]0.63, 0.75	2.4	.35	8.3	1.20	157	22.71	5.20	6.71	2.3	.33	18.23	2644	1831	3295	5.02	1.53
						-7.5	4	4.8	.54	1.7	.25	6.4	.93	130	18.84	5.38	6.63	2.3	.33	18.20	2640	1783	3210	4.79	1.46
						-5.5	3	2.6	.38	1.2	.18	4.8	.70	112	16.20	5.75	6.63	2.3	.33	18.20	2640	1780	3204	4.95	1.51
						-3.1	2	1.5	.22	1.2	.18	3.6	.52	95	13.77	6.15	6.64	2.3	.33	18.15	2632	1711	3080	5.54	1.69
						-5.5	7	2.6	.38	1.2	.18	4.8	.69	108	15.69	5.70	6.58	2.3	.33	18.20	2640	1749	3148	5.41	1.65
34	60	28	50	342	616	-9.3	19.3	.1	[c].02	2.3	.33	7.9	1.15	147	21.35	5.15	6.67	2.1	.31	18.18	2637	1802	3243	5.05	1.54
						-11.0	8	.6	[c].09	2.1	.30	9.9	1.44	157	22.74	4.75	6.52	2.2	.32	18.14	2631	1728	3111	5.15	1.57
						-12.3	8	.6	[c].09	7.4	1.07	11.7	1.69	158	22.90	4.40	6.29	2.6	.38	18.12	2628	1596	2873	5.25	1.60
						-9.3	3	-.6	[c]-.08	2.1	.31	8.1	1.17	136	19.66	4.90	6.25	2.2	.32	18.12	2628	1574	2833	5.28	1.61
35	0	36+	46	319	574	-9.5	6	4.4	[c].64	2.1	.31	8.5	1.23	156	22.66	5.13	6.68	1.9	.29	18.24	2646	1806	3251	5.05	1.54
						-10.5	7	5.4	[c].78	2.2	.32	9.7	1.41	170	24.68	5.00	6.70	1.9	.29	18.22	2642	1834	3302	5.02	1.53
						-11.6	7	6.2	[c].90	1.8	.26	11.0	1.60	178	25.80	4.80	6.70	1.9	.29	18.20	2640	1840	3312	4.99	1.52
						-9.5	15	4.6	[c].66	2.1	.31	8.3	1.21	158	22.90	5.20	6.76	1.9	.29	18.20	2639	1856	3340	4.95	1.51

[a]Panel covered during subsonic flow periods of tunnel operation.

[b]Includes model inclination relative to panel holder.

[c]Vent doors locked closed.

TABLE IV.- PANEL FREQUENCIES AFTER SPECIFIED TEST EVENTS

Test	f, Hz				Number of accumulated test events		
	m = 1, n = 1	m = 1, n = 2	m = 1, n = 6	m = 1, n = 9	Static loading	Thermal cycle	Aerothermal
Static load-deflection test	222	232	291	376	4		
2	222	233	288	372		2	
3	221	229	291	374		3	
6	221	231	289	373		6	1
8	219	231	292	373		8	
10	218	229	286	374		10	2
12	218	232	289	372		12	4
15	218	231	285	369		13	
18	218	231	281	371		18	
19	219	232	283	371		19	5
21	220	231	286	372		21	
25	222	233	286	375		25	6
28	221	232	285	374		28	7
29	221	234	284	373		29	
32	221	233	284	375	7	35	8
35	222	234	286	375		37	10

TABLE V.- DENSITY AND EMITTANCE OF PANEL MATERIALS

Material	Emittance	Density	
		kg/m^3	lb/ft^3
René 41 (oxidized)	0.75	8250	515
René 41 foil	.55	8250	515
347 stainless steel	.4	7690	480
Silica fibrous insulation (Micro-Quartz)	.5	67	4.2

TABLE VI.- MEASURED AND CALCULATED FREQUENCIES OF PANEL BEFORE THERMAL TESTS

Modes		f, Hz	
m	n	Experiment	Calculated
1	1	222	221
1	2	232	235
1	3	245	252
1	4	258	271
1	5	272	287
1	6	291	302
1	7	---	314
1	8	355	326
1	9	376	337
1	10	---	348

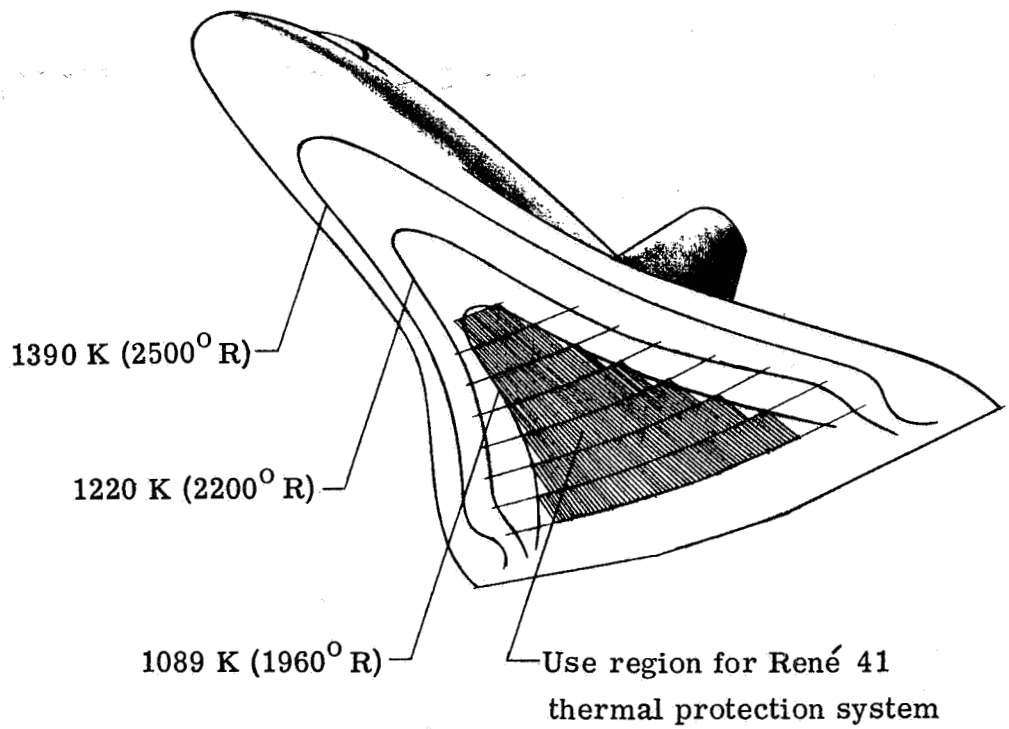

Figure 1.- Isotherms on reentry surface.

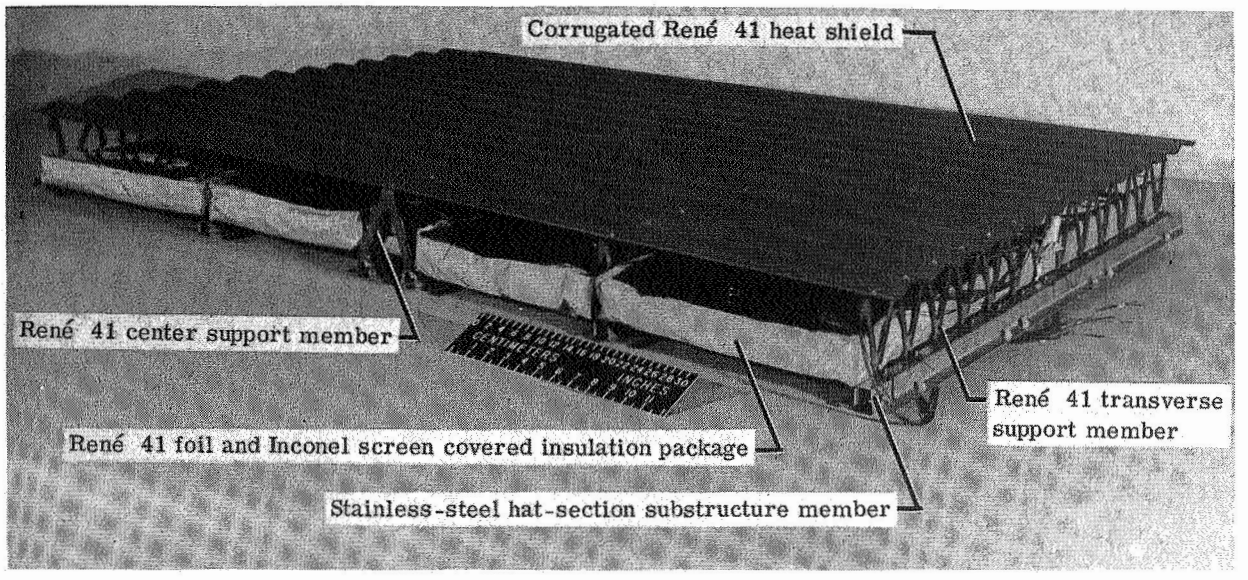

(a) Heat-shield surface view.

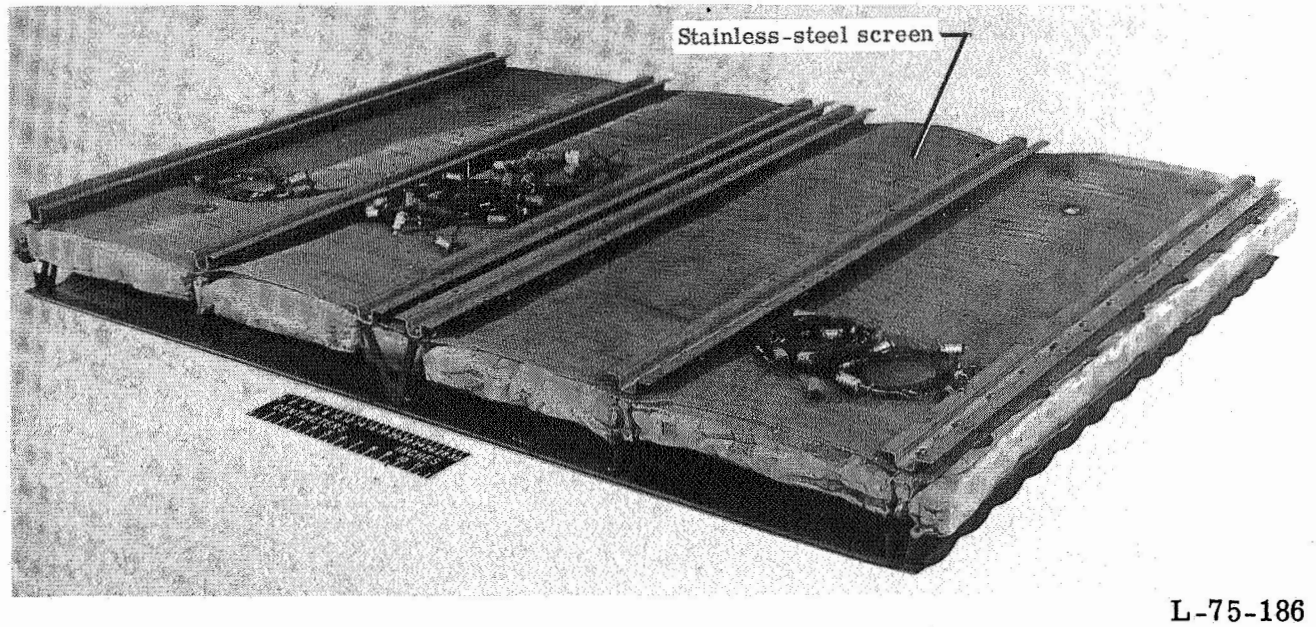

(b) Back surface view.

Figure 2.- René 41 thermal-protection-system model.

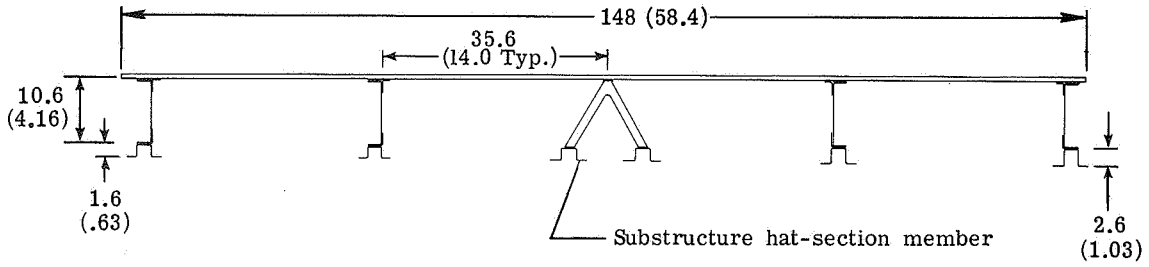

(a) Heat-shield support member arrangement.

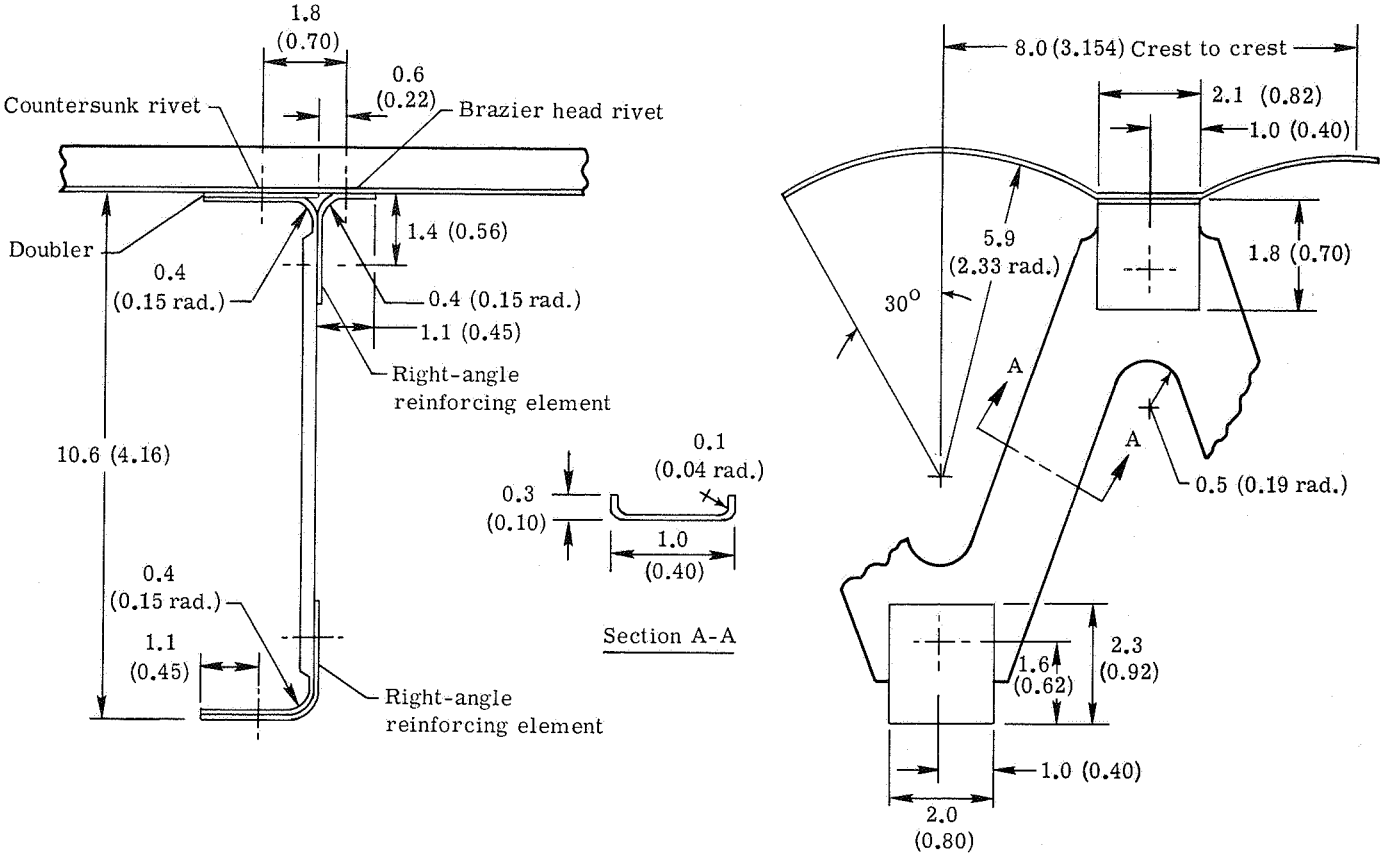

(b) Transverse support member.

Figure 3.- Details of René 41 heat shield. Dimensions in cm (in.).

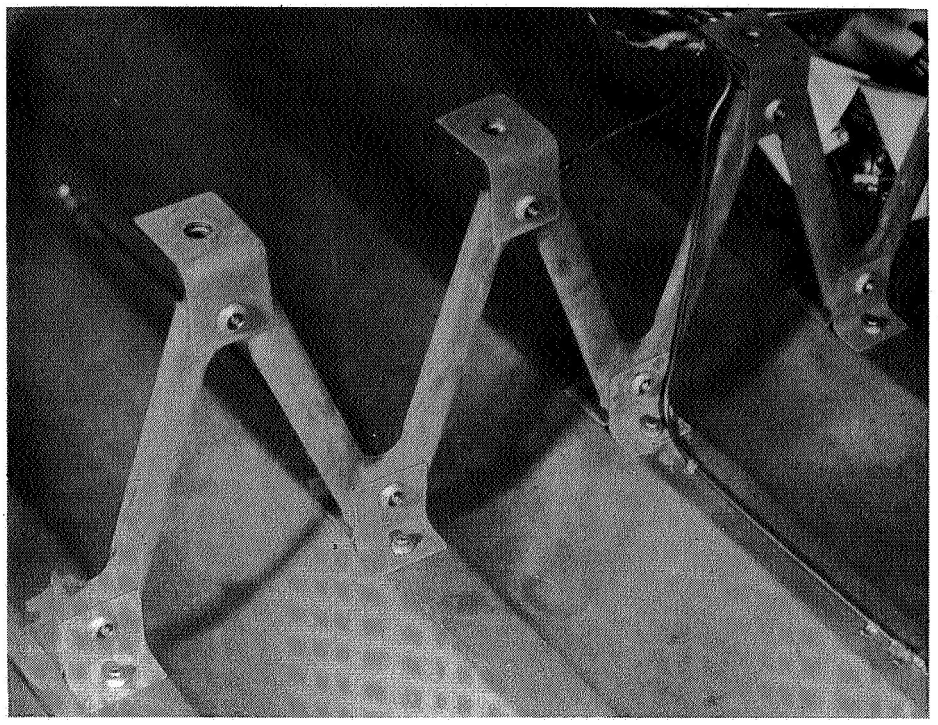

(a) Transverse support member.

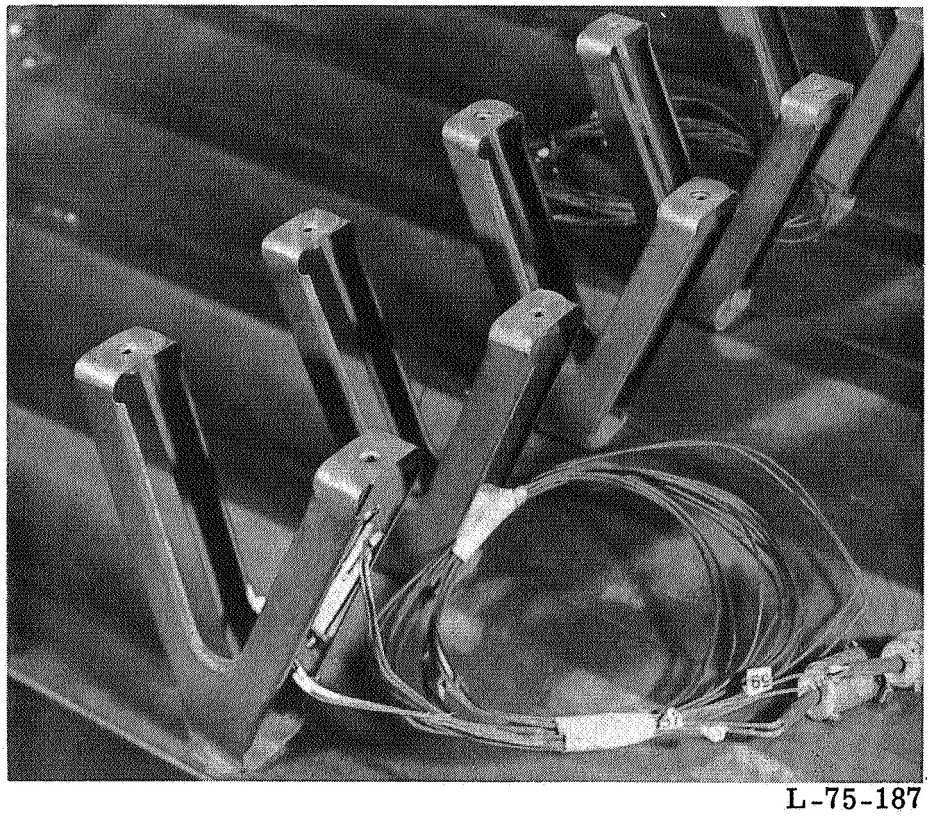

L-75-187

(b) Center support members.

Figure 4.- Heat-shield support members.

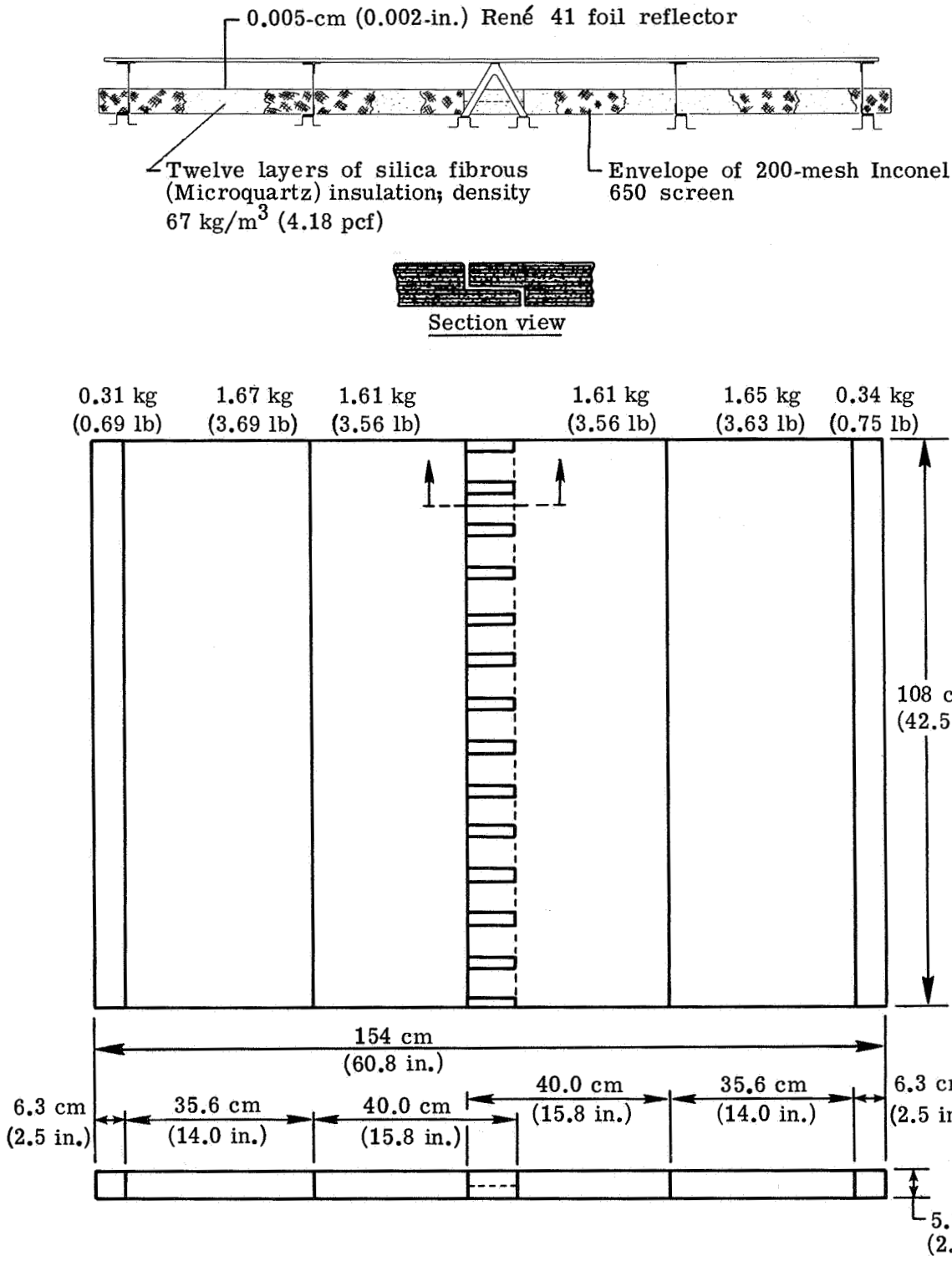

Figure 5.- Insulation-package configuration. Package weight, 4.3 kg/m^2 (0.88 lb/ft^2).

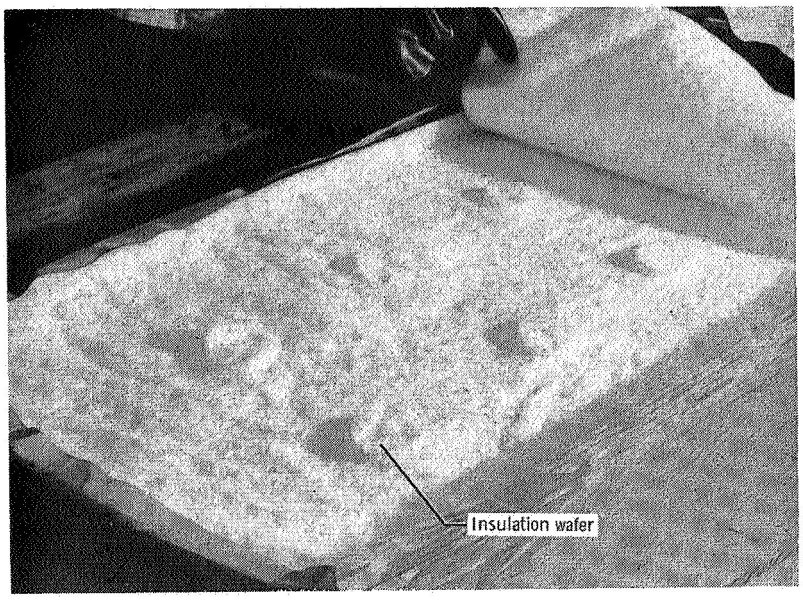

(a) Fabrication.

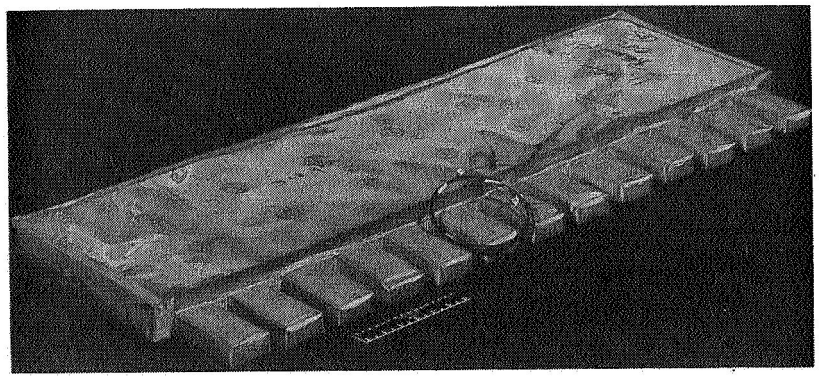

(b) Fabricated center section.

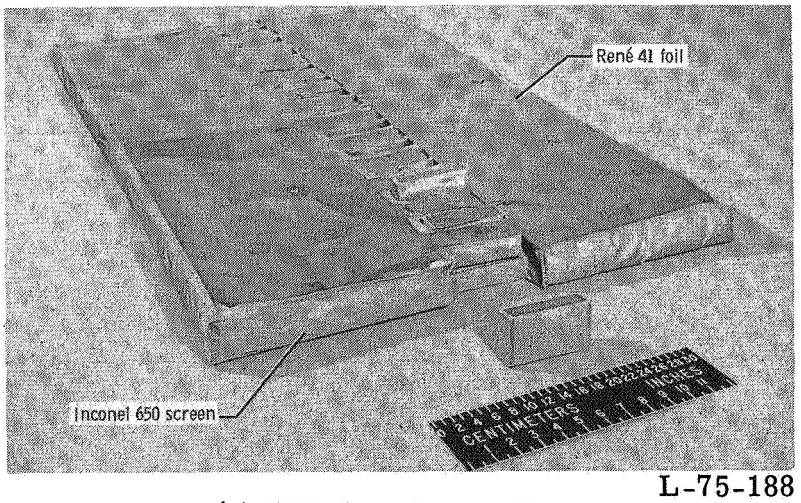

L-75-188

(c) Fitted center sections.

Figure 6.- Insulation packages.

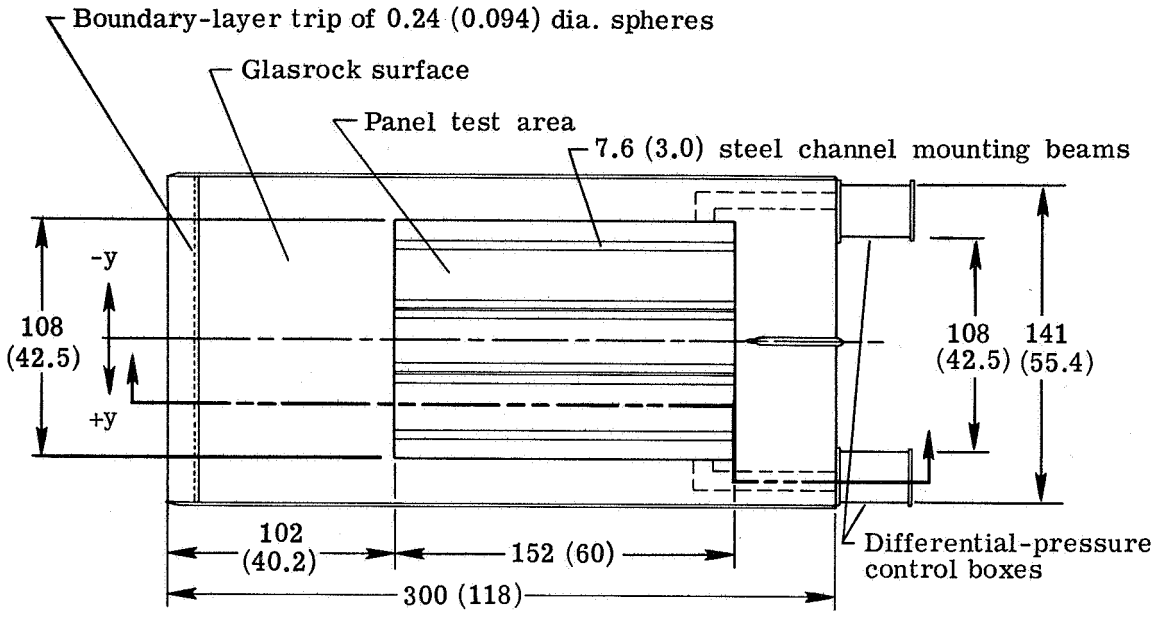

(a) Planview without panel.

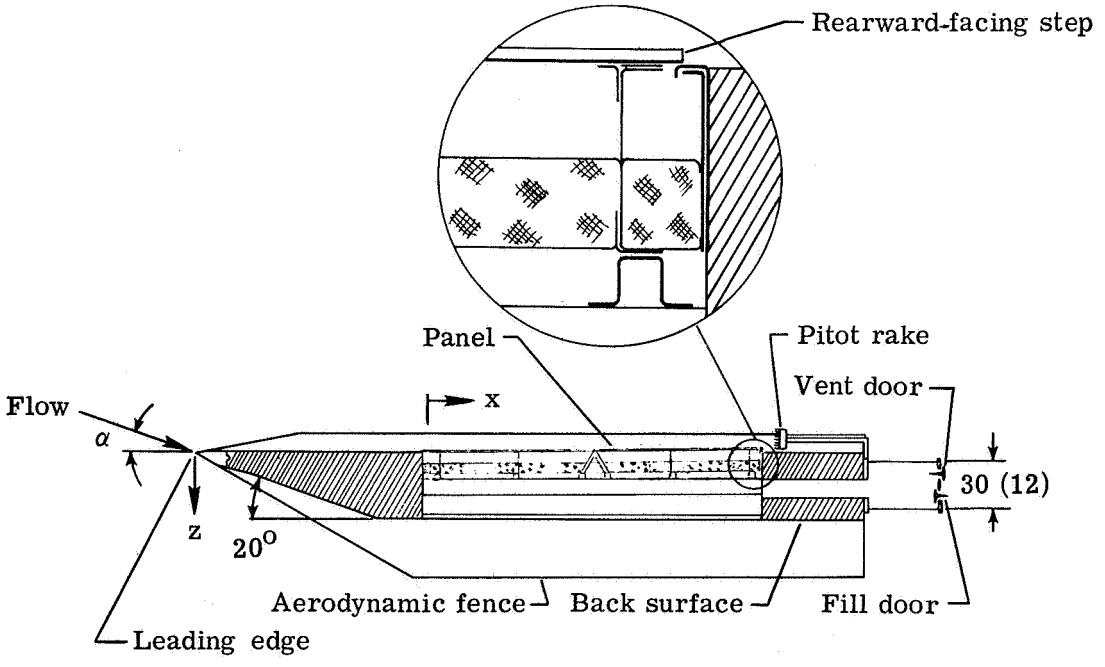

(b) Longitudinal cross section with panel in place.

Figure 7.- Details of panel holder. Dimensions are in cm (in.).

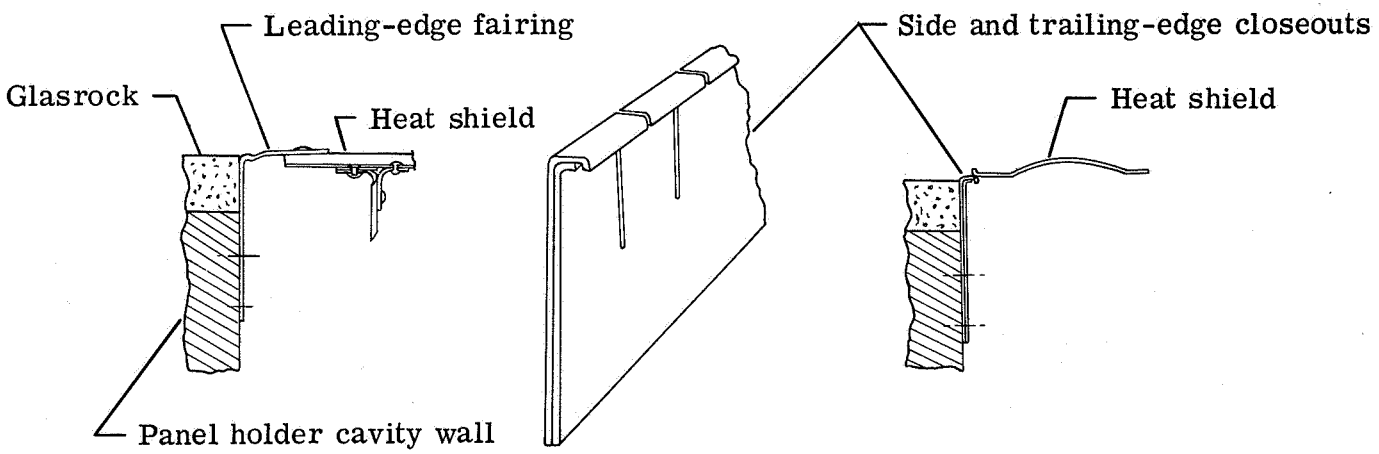

(a) Heat-shield edge closeouts.

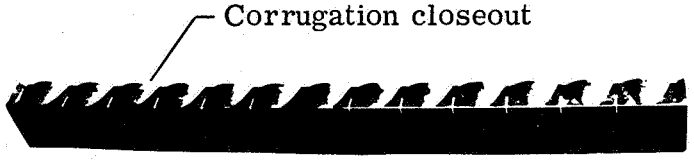

(b) Leading-edge fairing.

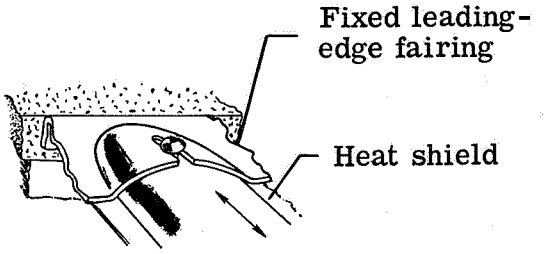

(c) Thermal expansion guide at heat-shield leading edge.

Figure 8.- Edge closeouts.

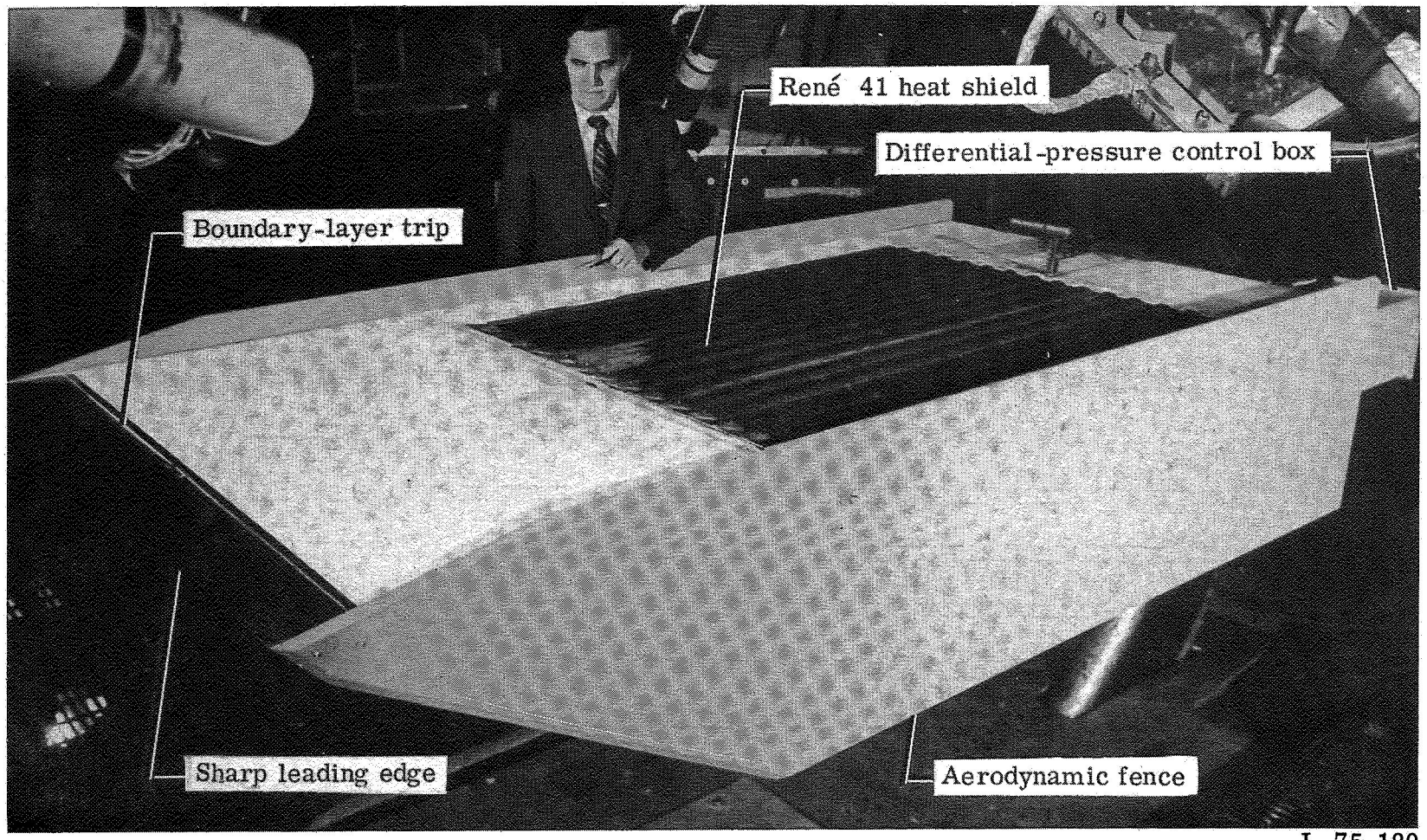

L-75-189

Figure 9.- René 41 thermal protection panel in test section.

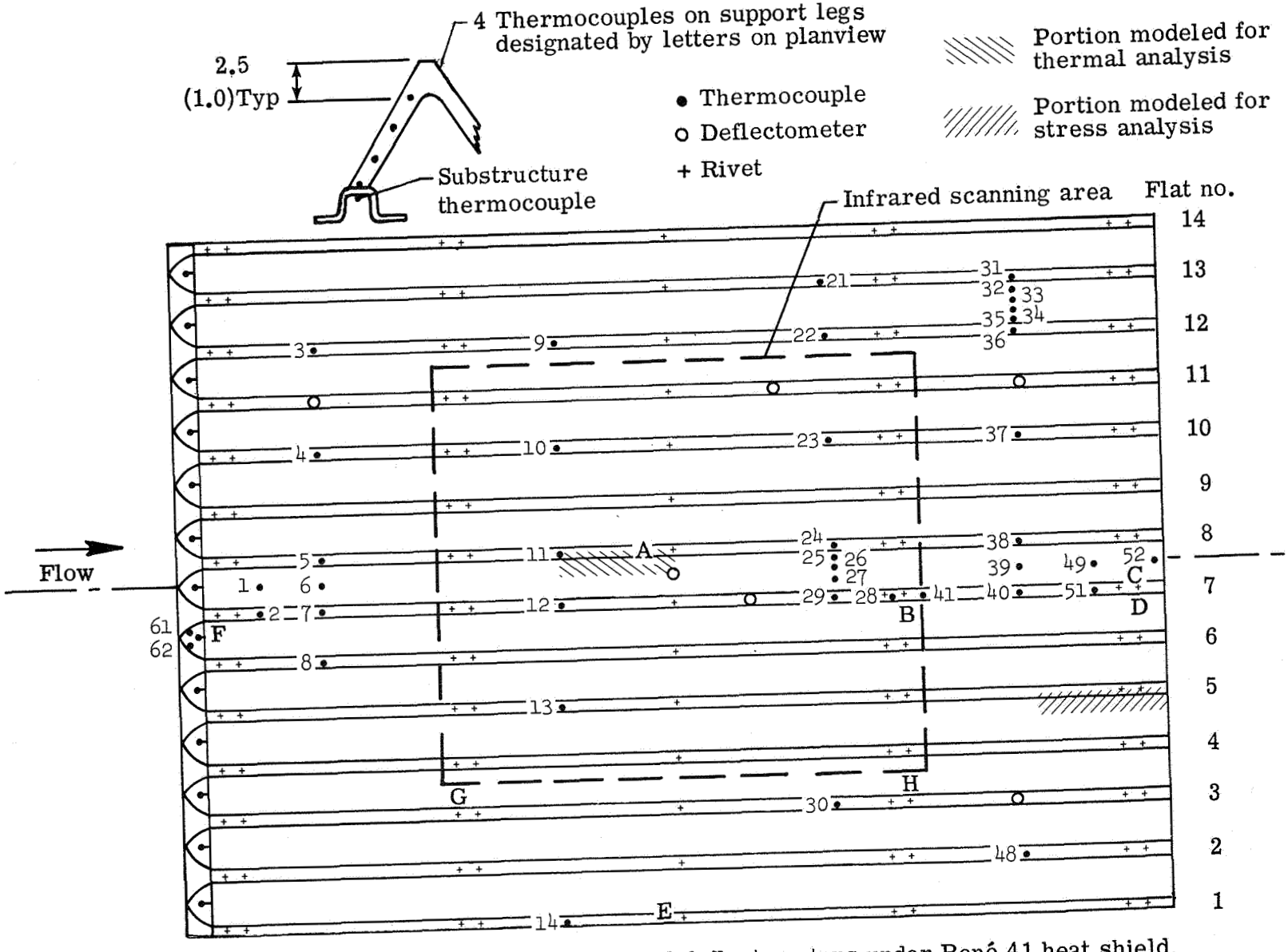

Figure 10.- Distribution of thermocouples and deflectometers under René 41 heat shield.

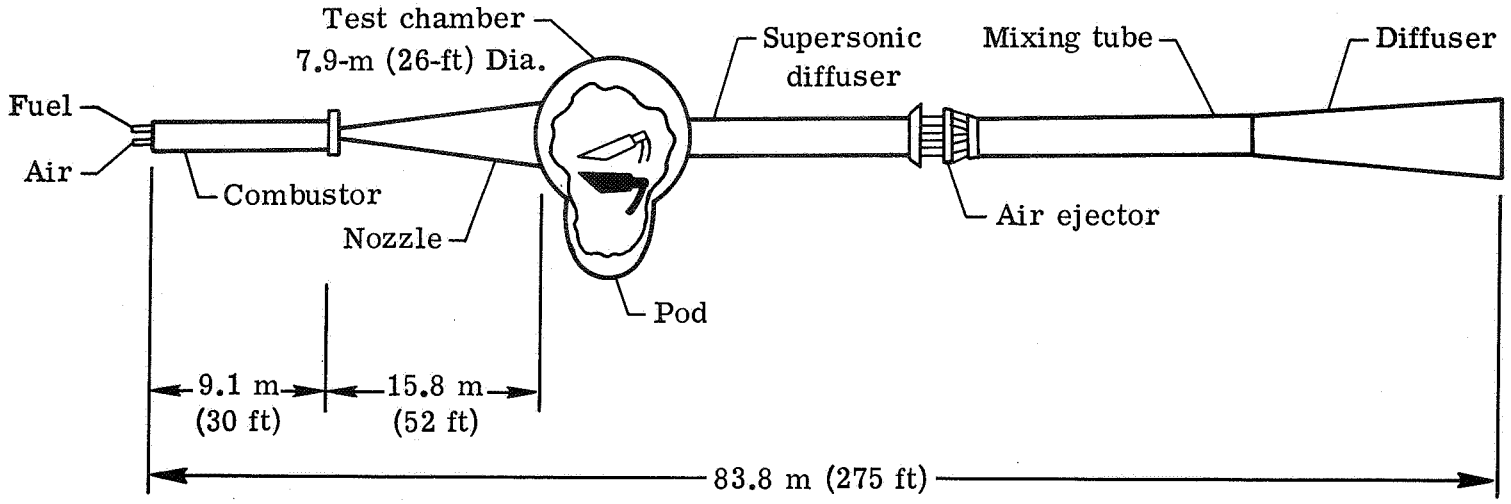

Figure 11.- Langley 8-foot high-temperature structures tunnel.

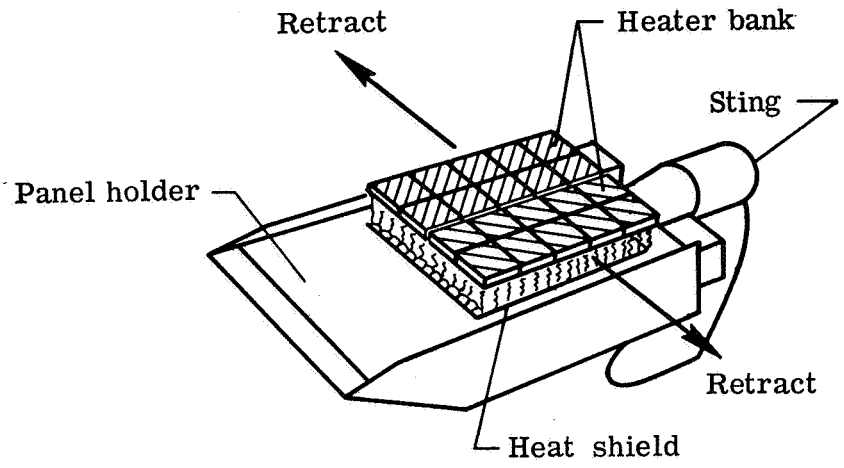

Figure 12.- Retractable quartz-lamp radiant heaters.

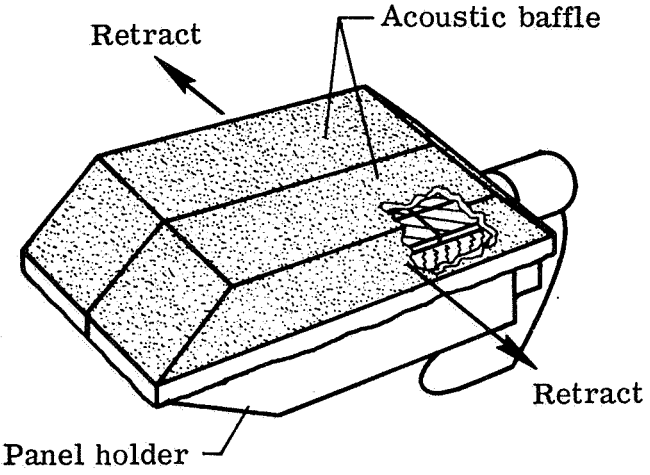

Figure 13.- Retractable acoustic baffles extended over panel holder.

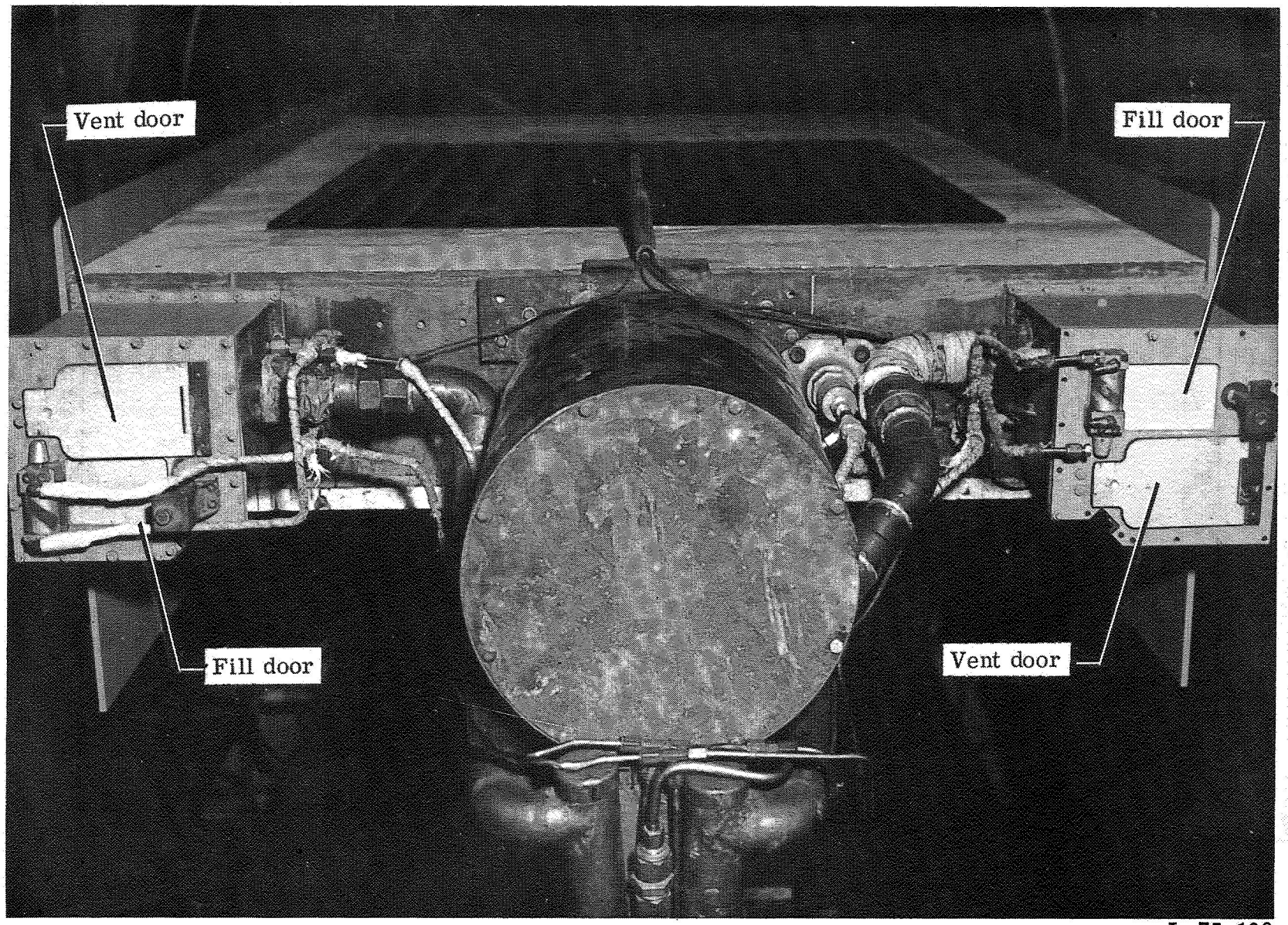

L-75-190

Figure 14.- Differential-pressure apparatus of panel holder.

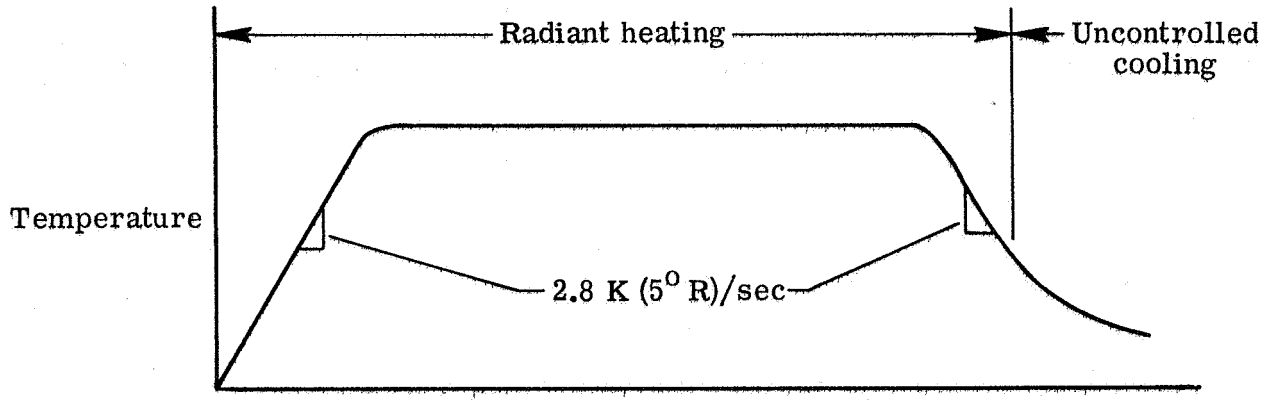

(a) Thermal cycle by radiant heating.

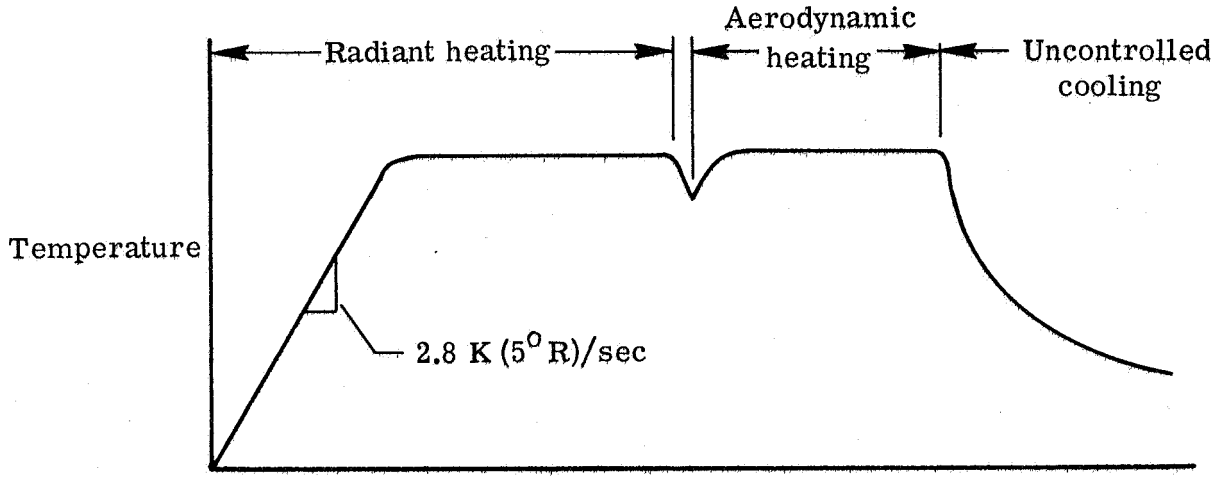

(b) Radiant-preheat—aerothermal exposure.

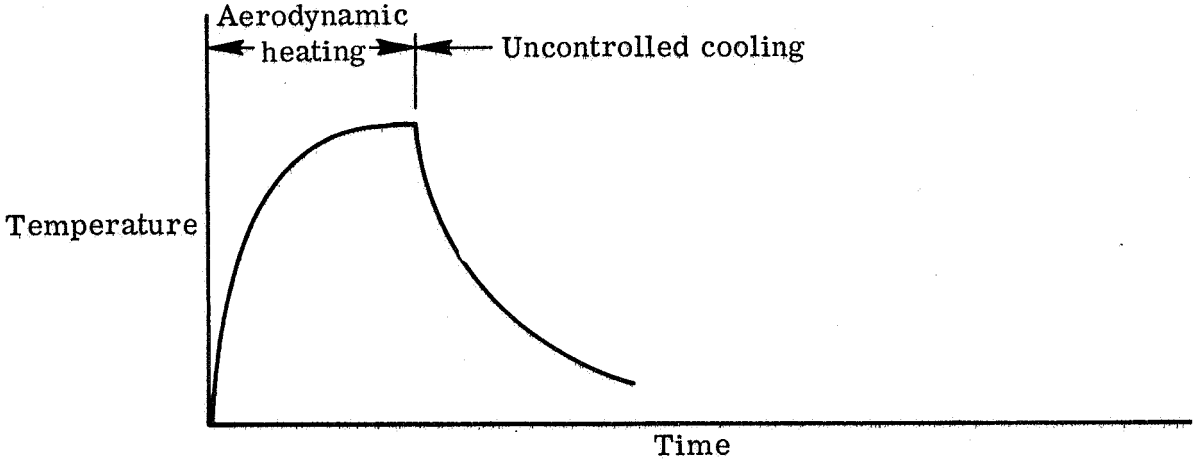

(c) Aerothermal shock.

Figure 15.- Typical surface temperature histories.

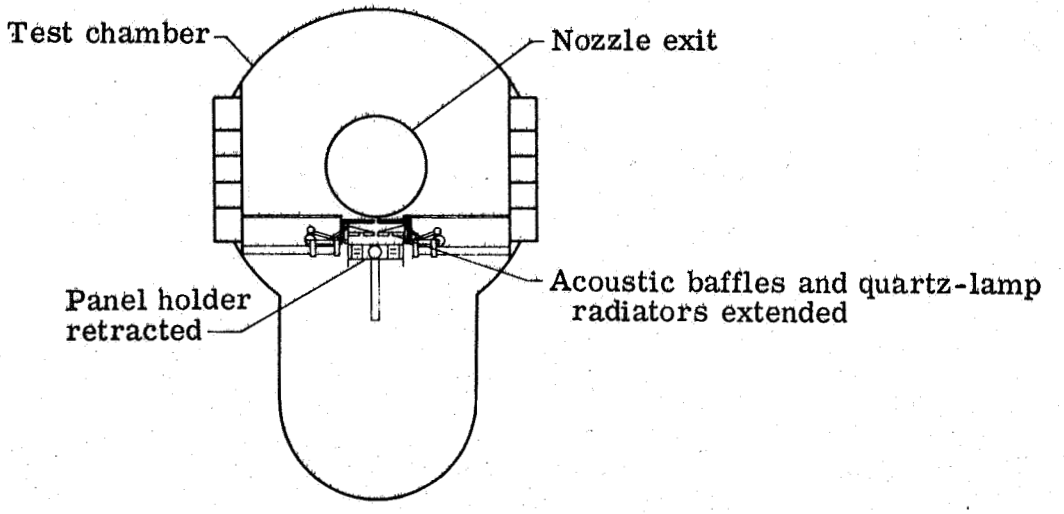

(a) Preheat and posttest.

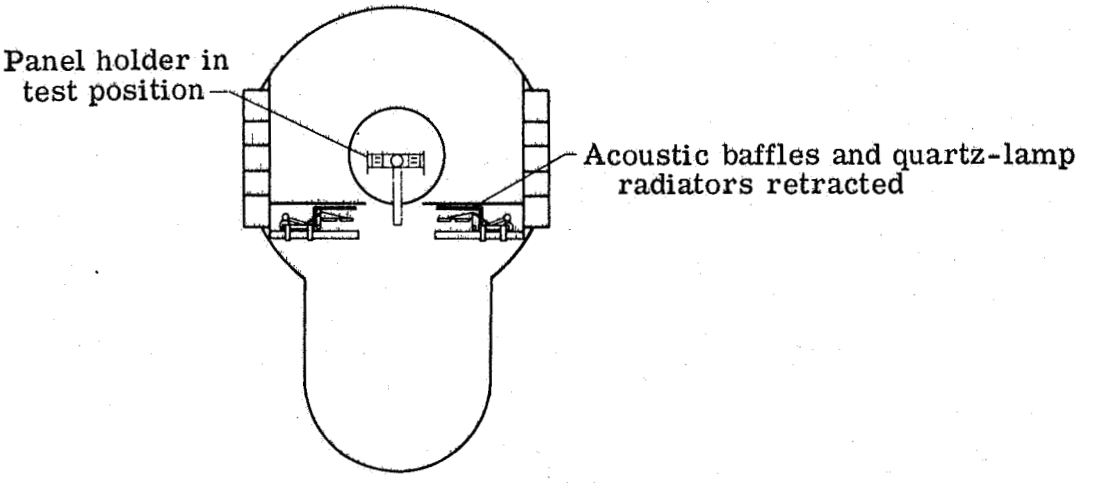

(b) During test.

Figure 16.- Panel holder and radiator positions during radiant-preheat—aerothermal test.

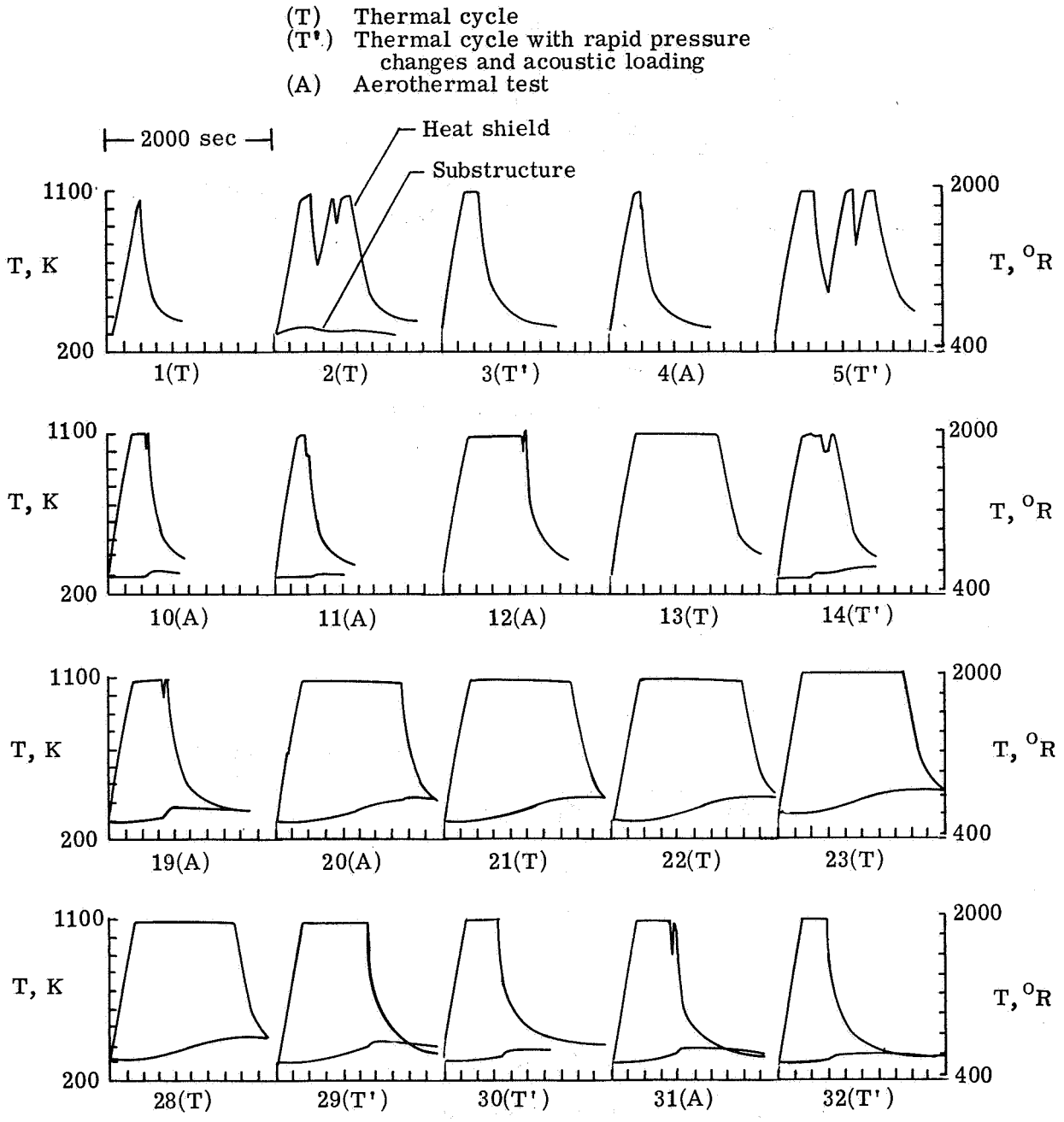

Figure 17.- Summary of heat-shield and substructure temperature responses.

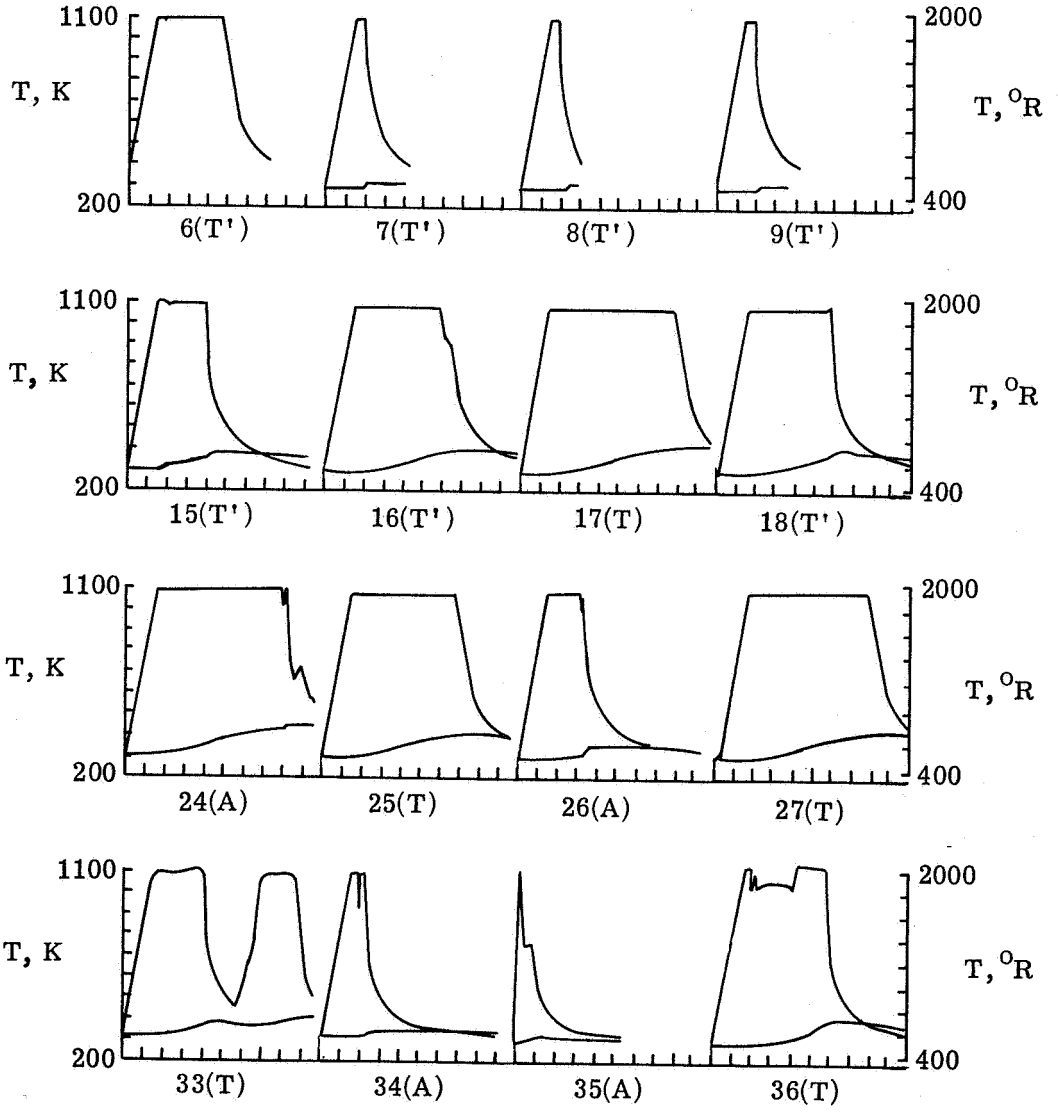

Figure 17.- Concluded.

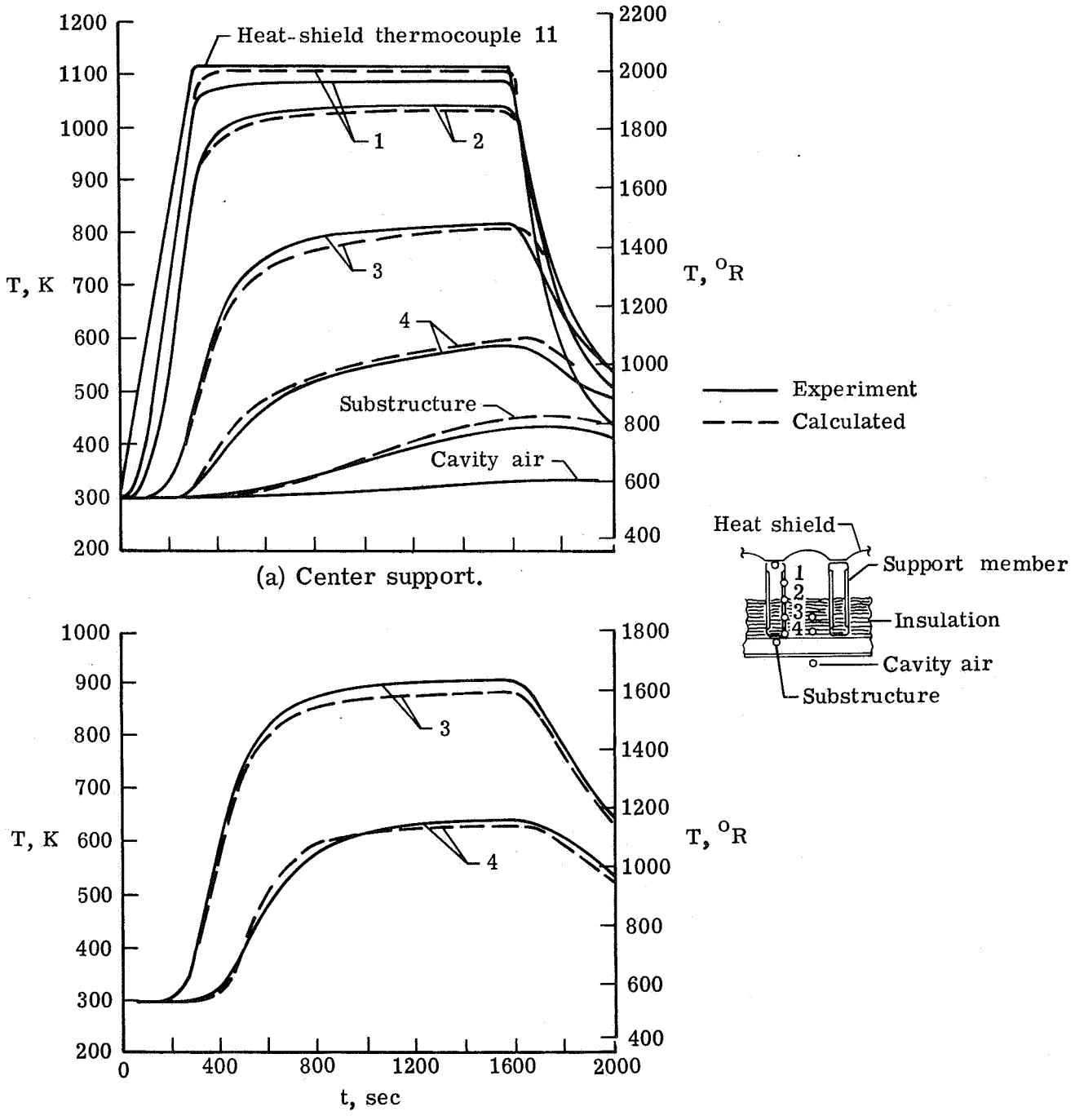

(a) Center support.

(b) Insulation.

Figure 18.- Response of panel to radiant heating (test 17).

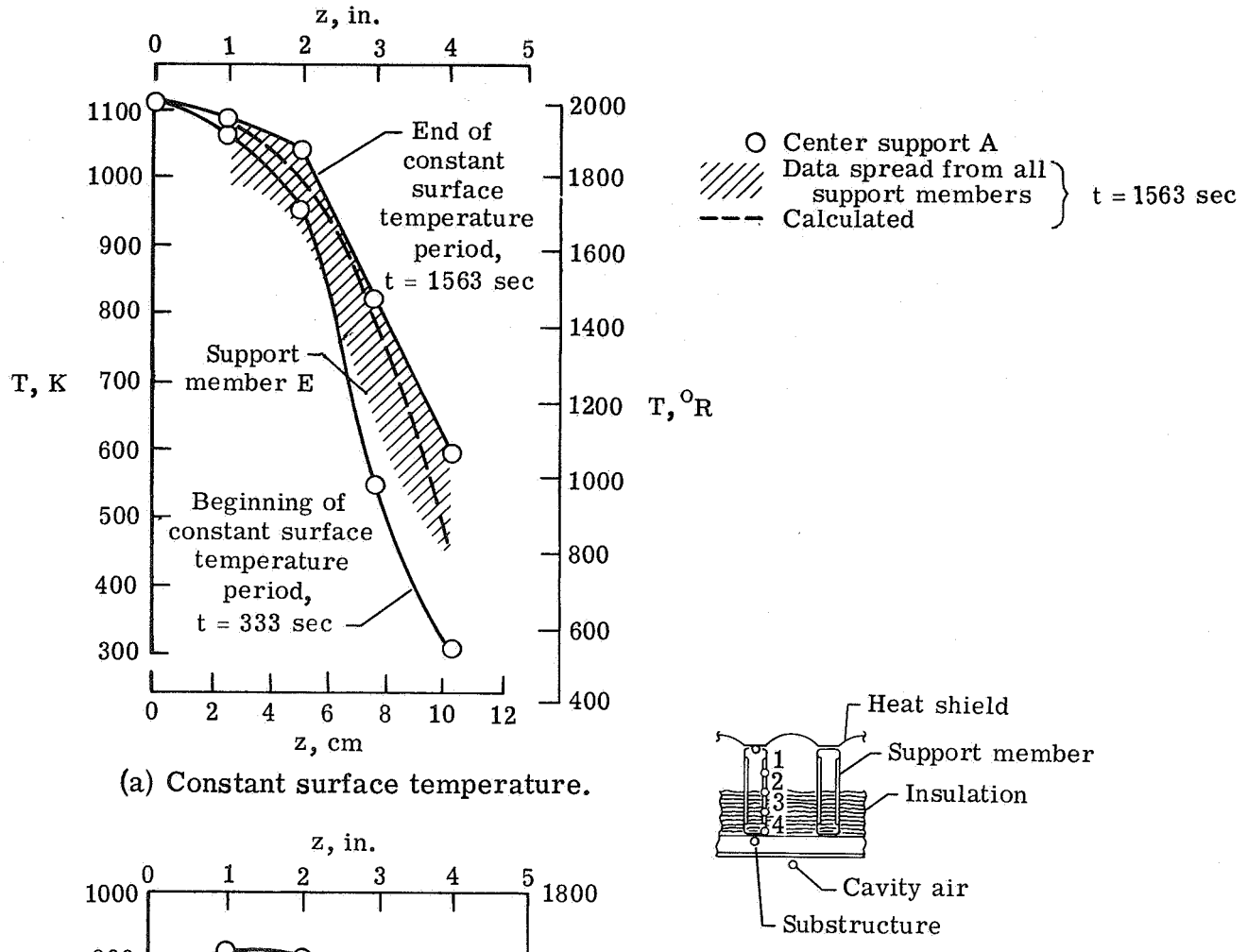

(a) Constant surface temperature.

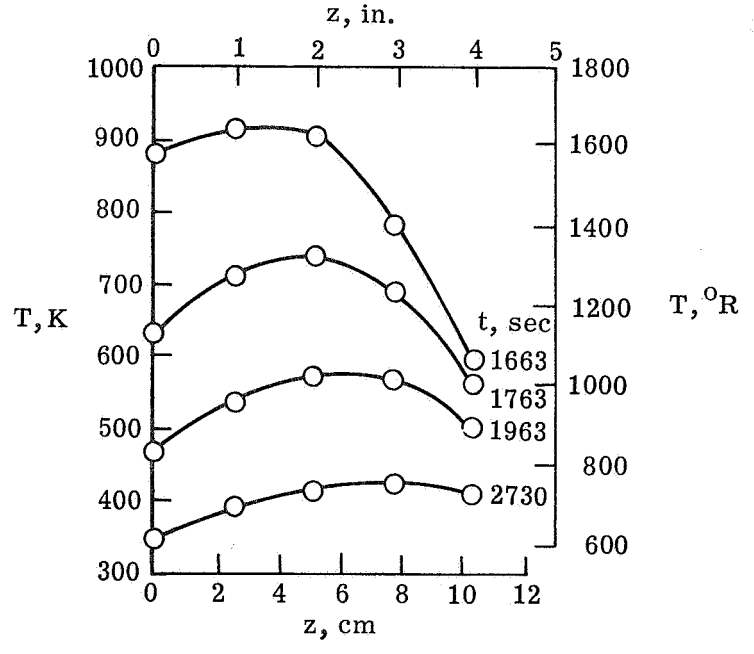

(b) Cooldown.

Figure 19.- Comparison of support-member temperatures during heating and cooling.

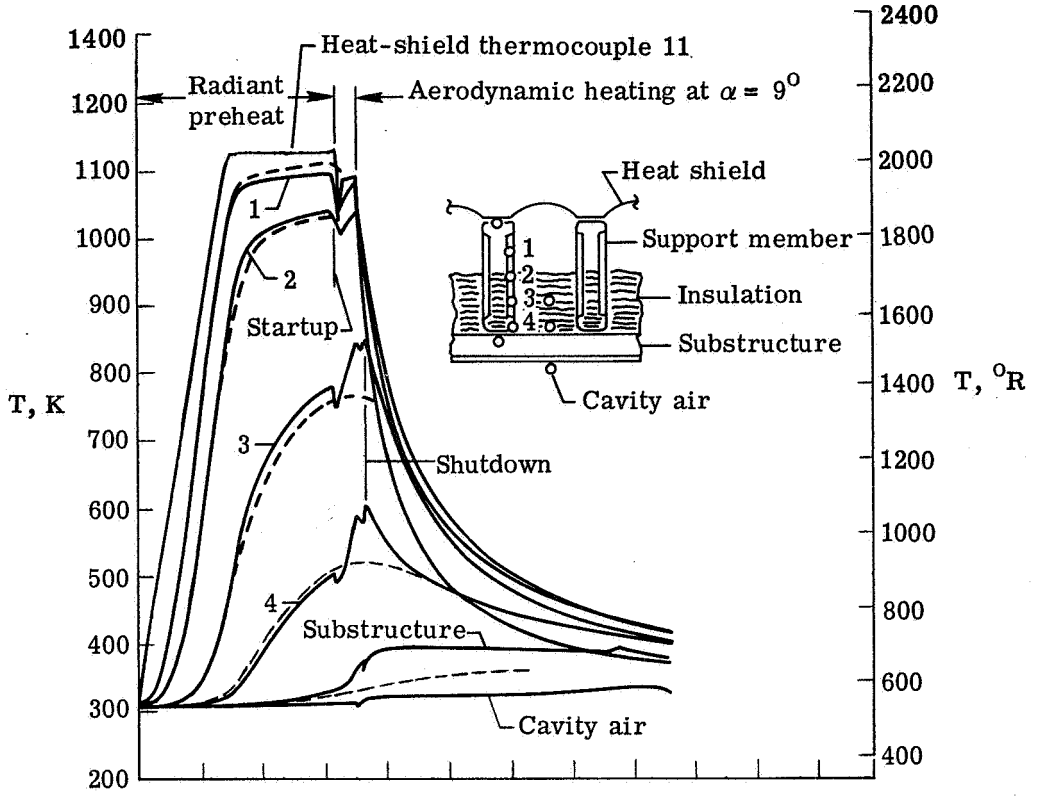

(a) Center support.

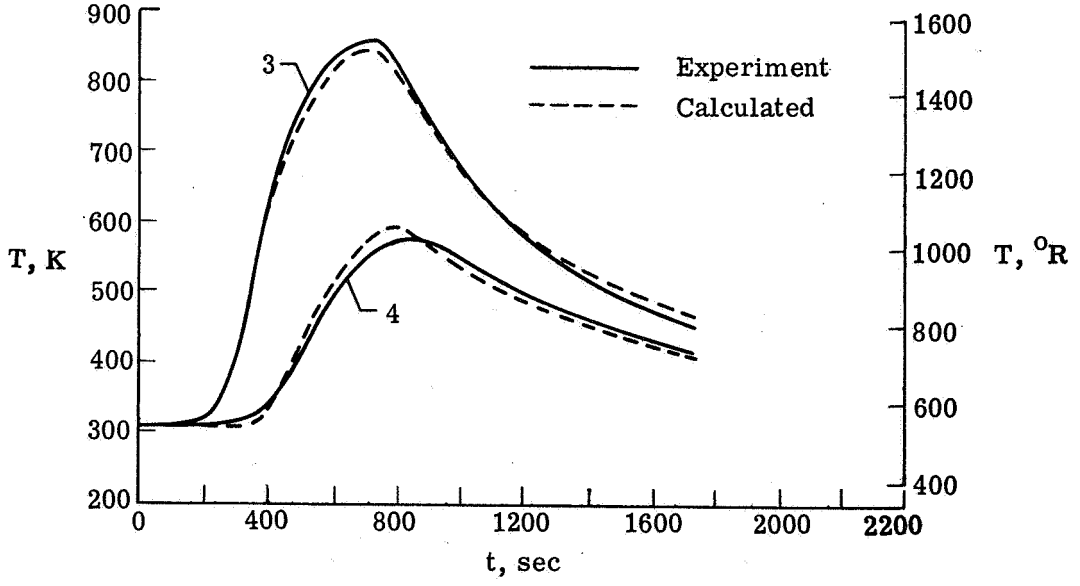

(b) Insulation.

Figure 20.- Response of panel to radiant preheating followed by exposure to aerodynamic heating; vent doors open (test 19).

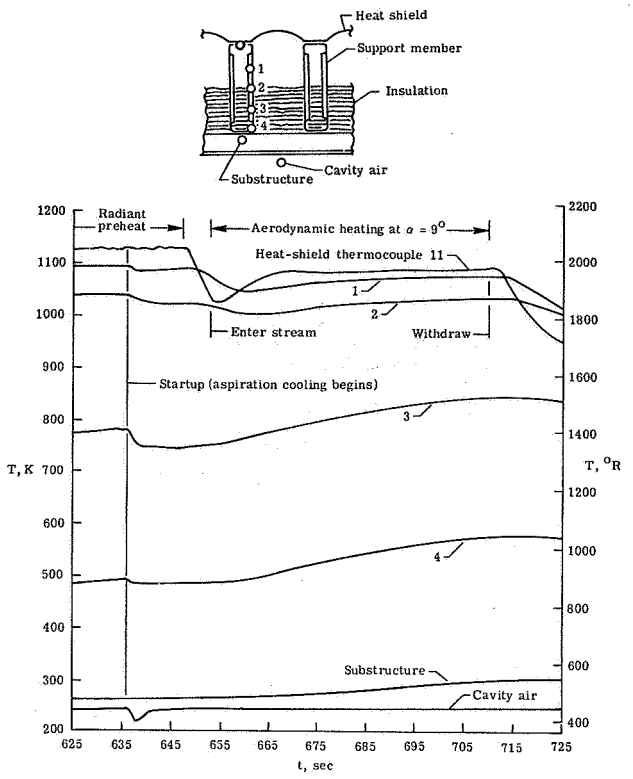

Figure 21.- Thermal response of panel to aerodynamic heating; vent doors open (test 19).

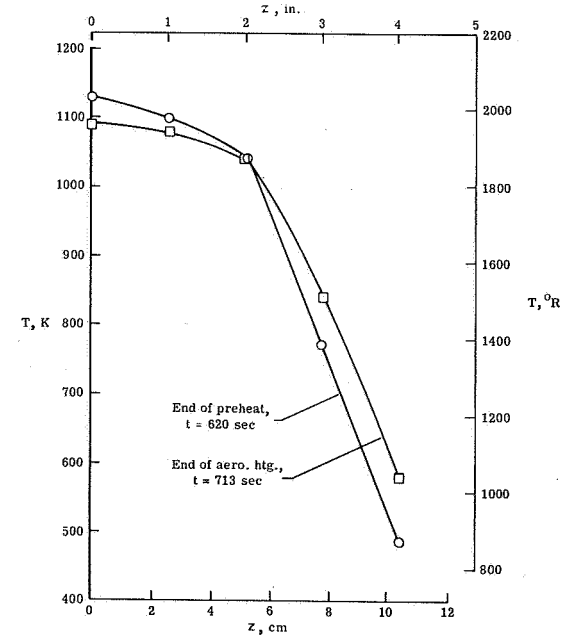

Figure 22.- Temperature distributions on center support during radiant-preheat—aerothermal test; vent doors open (test 19).

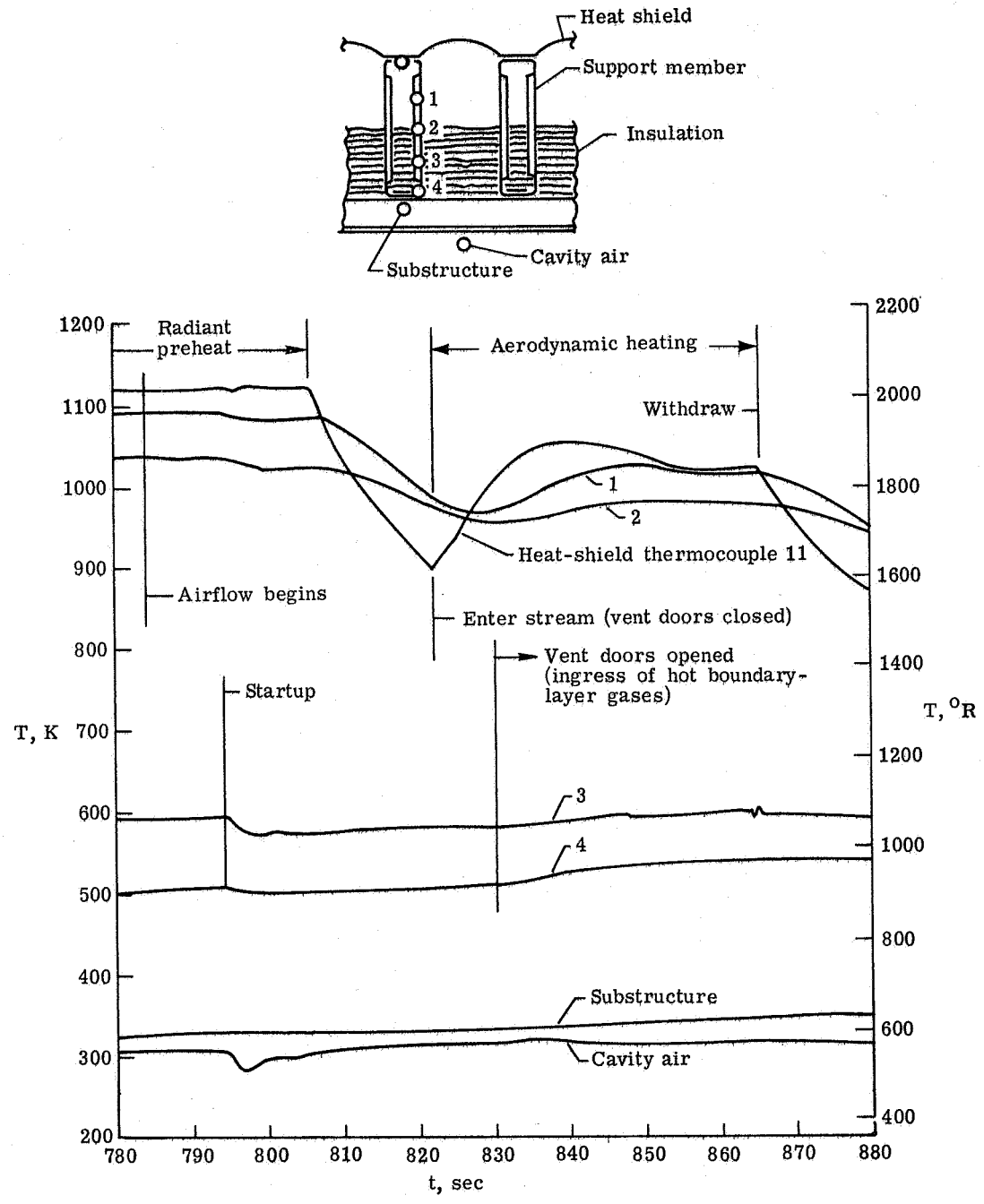

Figure 23.- Thermal response of panel during test 31 showing effect of vent door position.

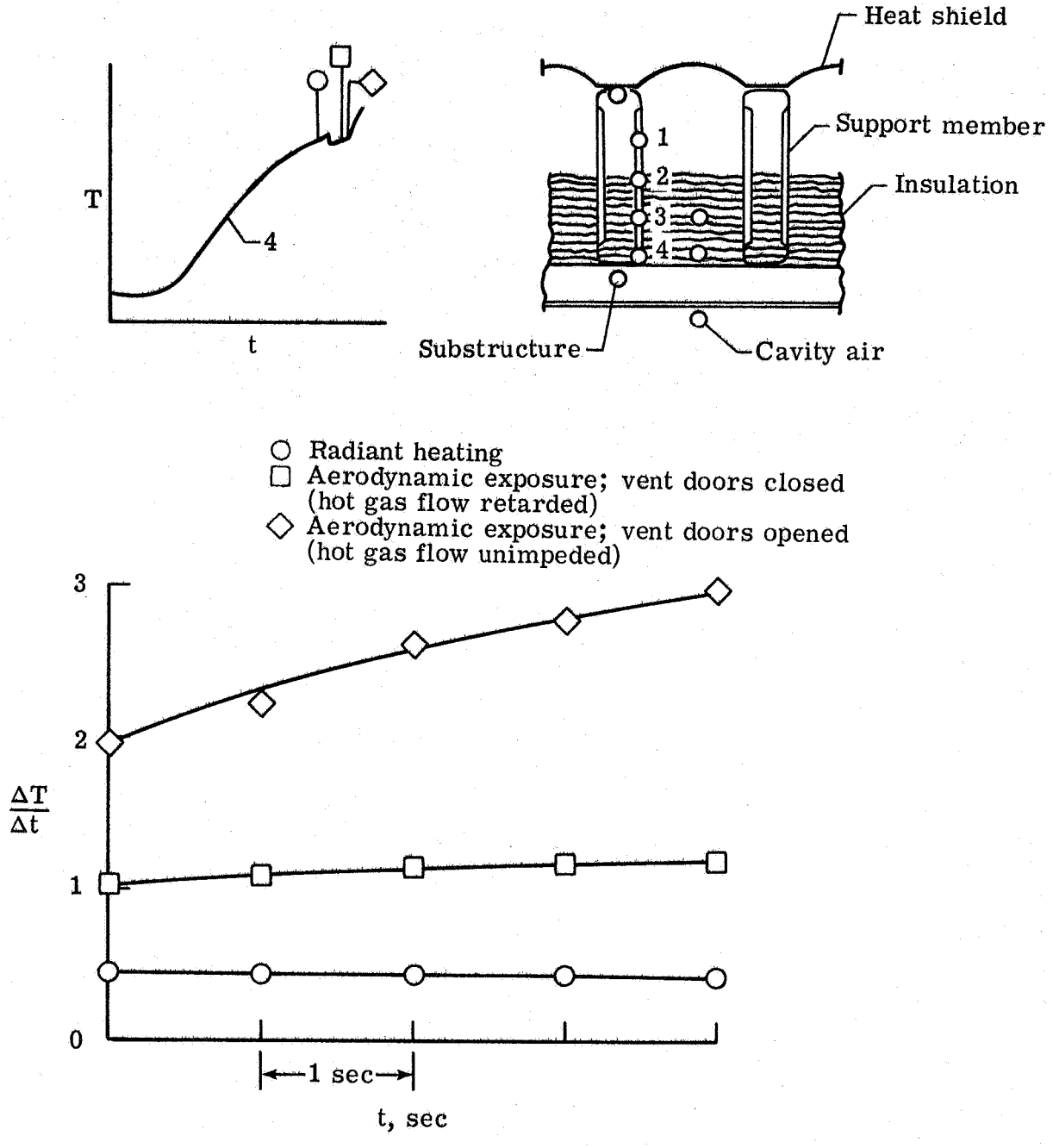

Figure 24.- Effect of hot-gas flow on thermal response at bottom of support member (location 4), test 31.

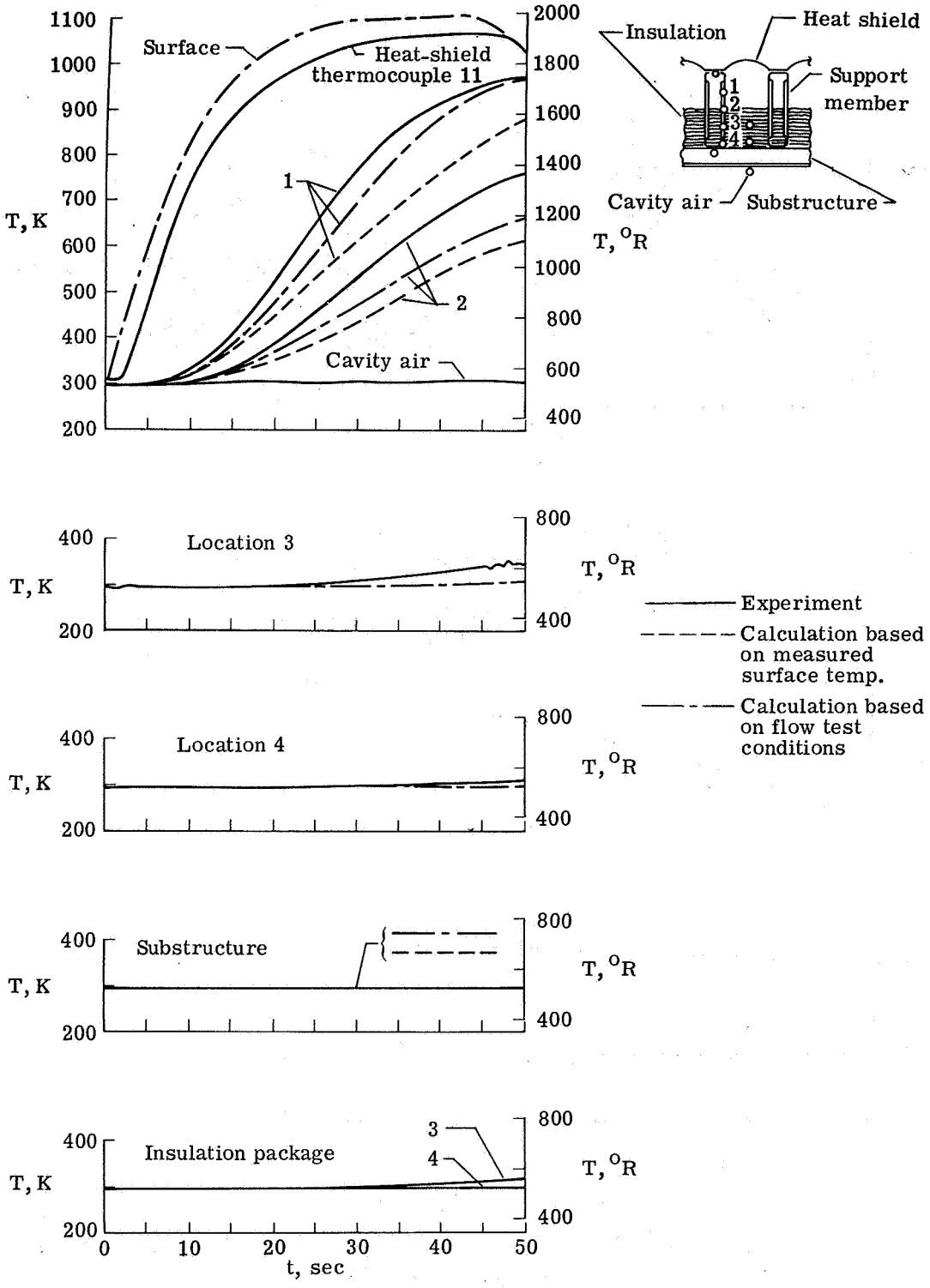

Figure 25.- Response of panel to aerothermal shock at $M_\infty \approx 7$; vent doors closed (test 35).

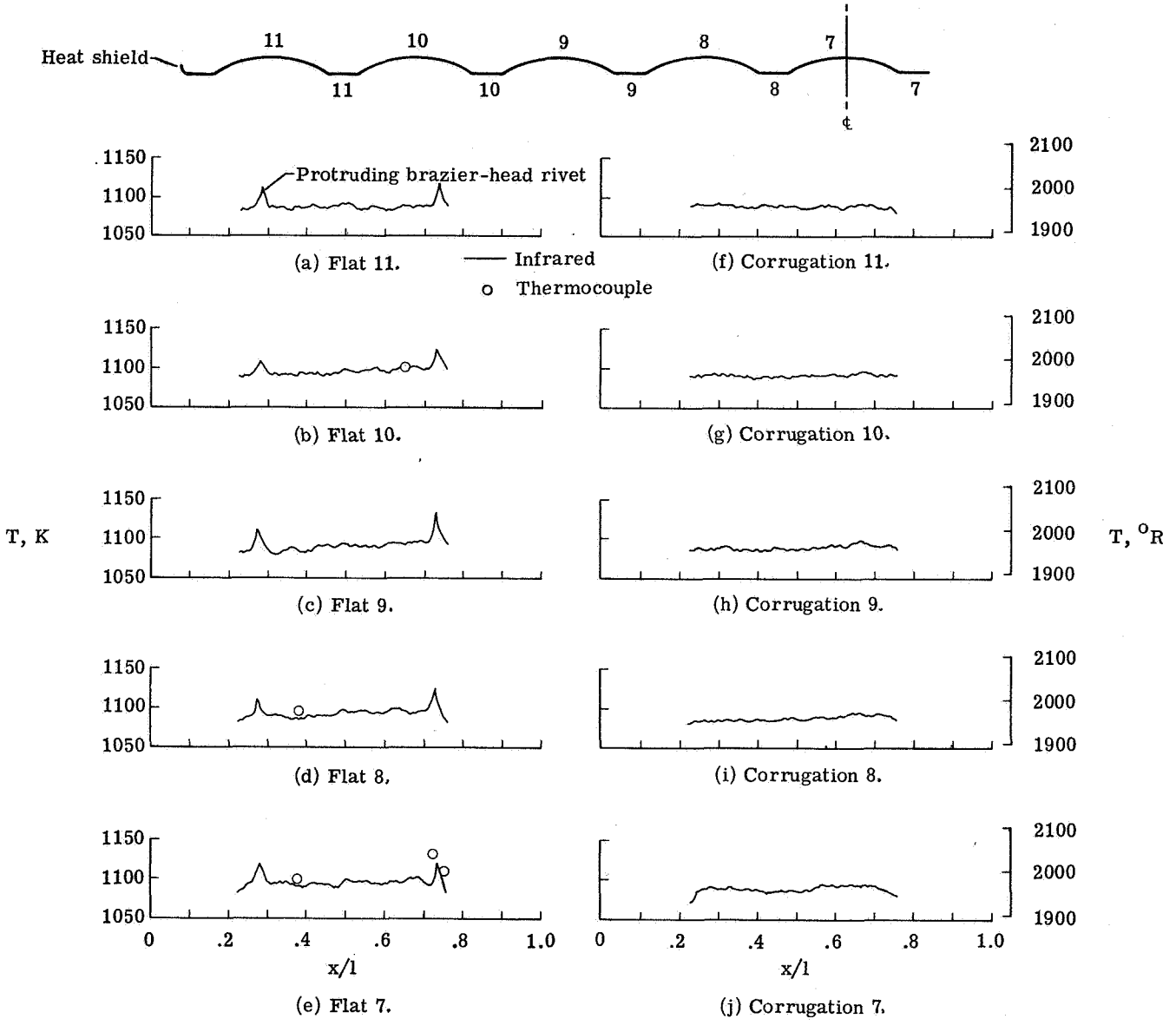

Figure 26. - Infrared scanlines of René 41 heat-shield surface temperatures after approximately 55 sec of aerodynamic heating following radiant preheating (test 19).

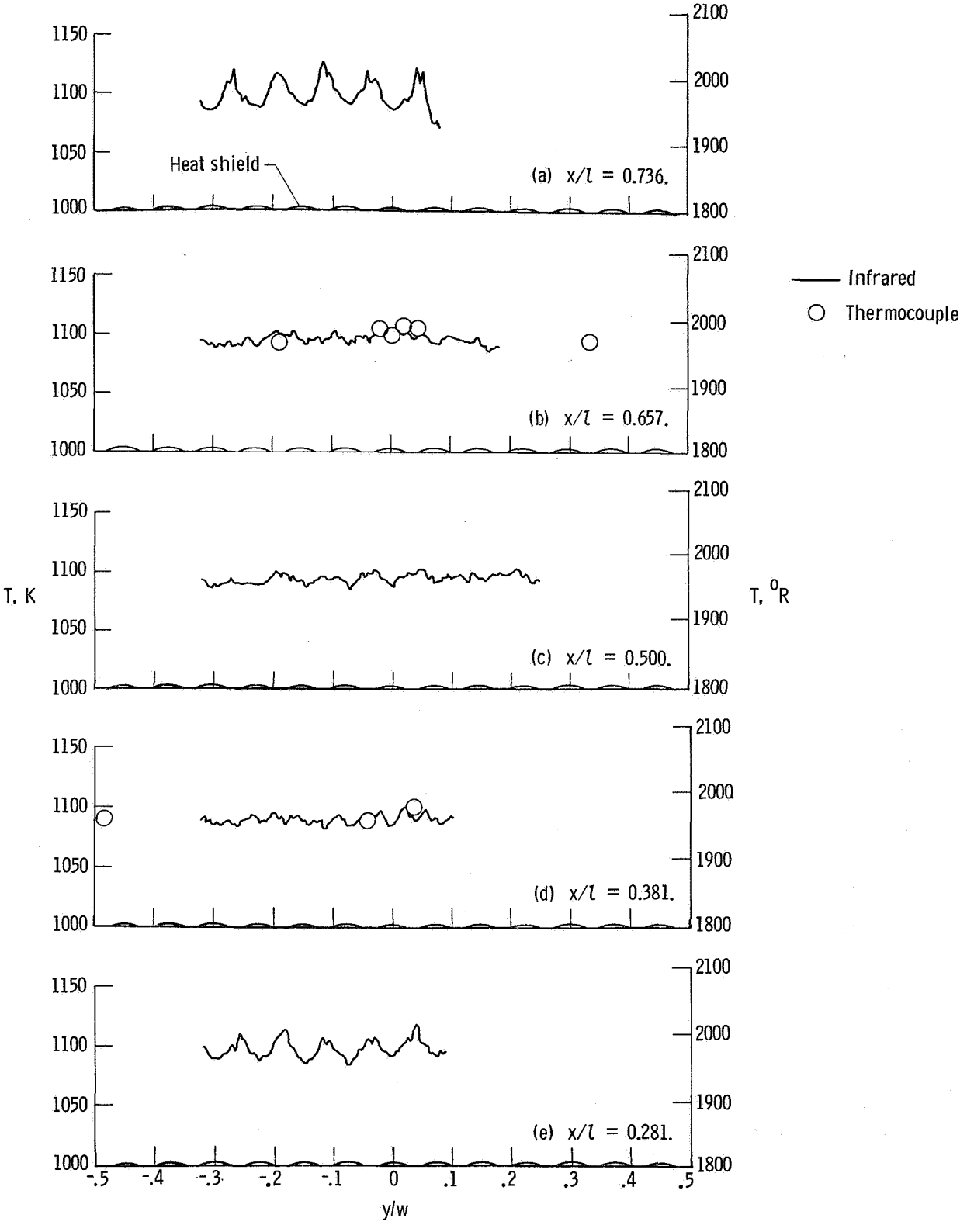

Figure 27.- Spanwise surface temperature distributions of René 41 heat shield by infrared radiometry after approximately 55 sec of aerodynamic heating following radiant preheating (test 19).

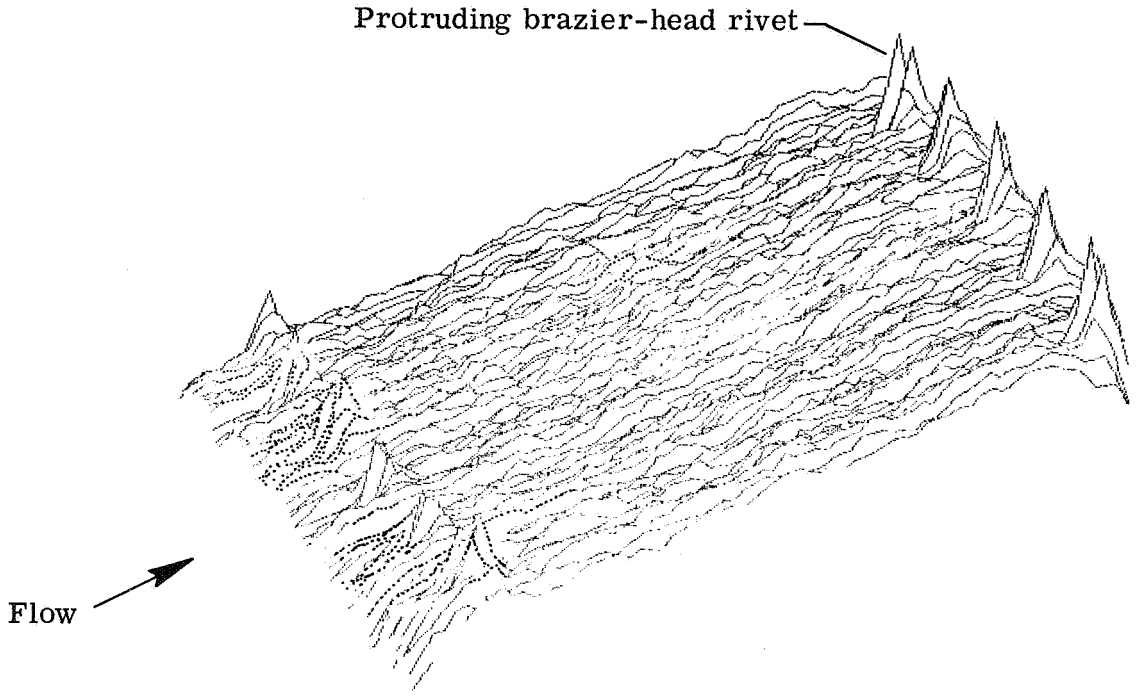

Figure 28.- Pictorial representation of aerodynamically heated René 41 heat-shield surface from infrared radiometry.

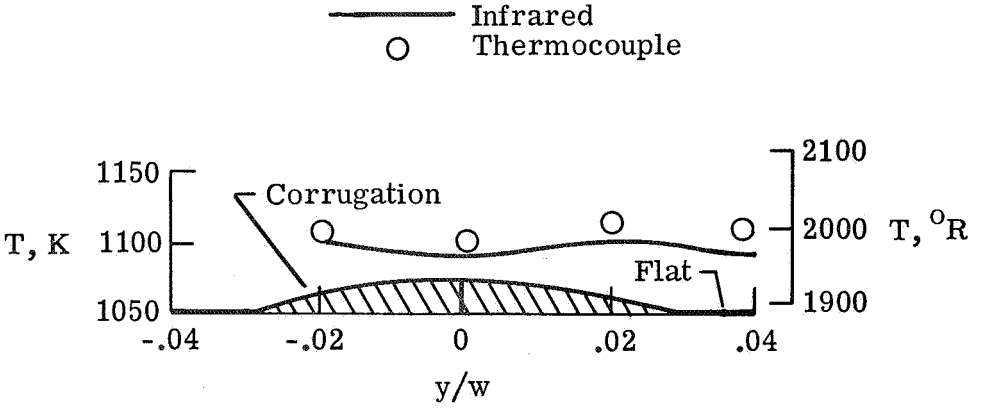

Figure 29.- Temperature distribution across center-line corrugation of René 41 heat shield during aerodynamic heating.

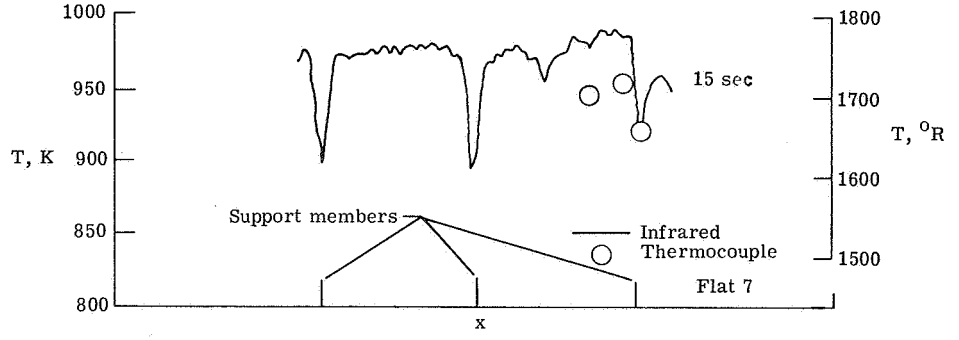

Figure 30.- Infrared scanline of René 41 heat shield during transient aerodynamic heating (test 35).

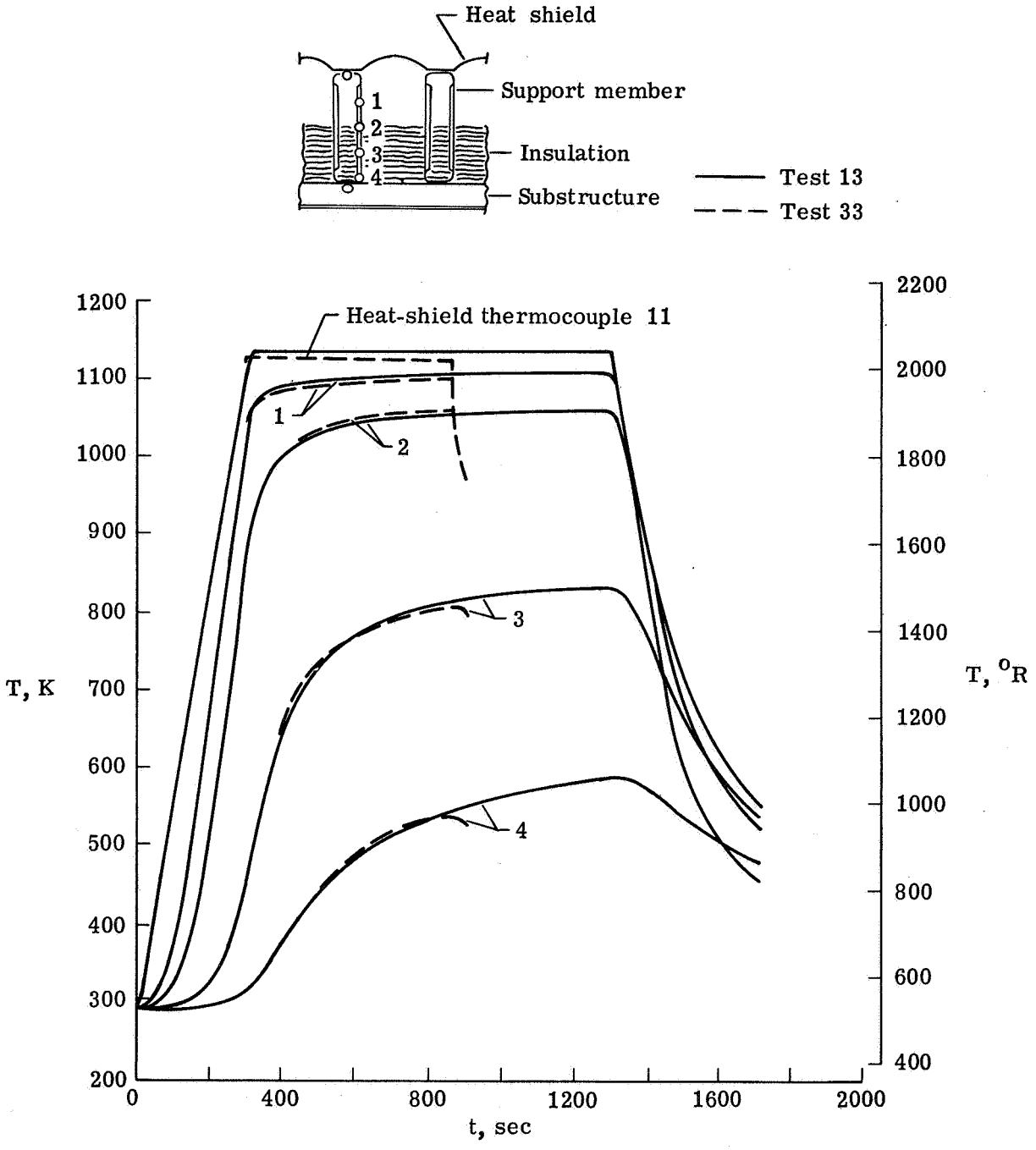

Figure 31.- Comparison of temperatures obtained early and late in heating-test series on René 41 heat shield and support members.

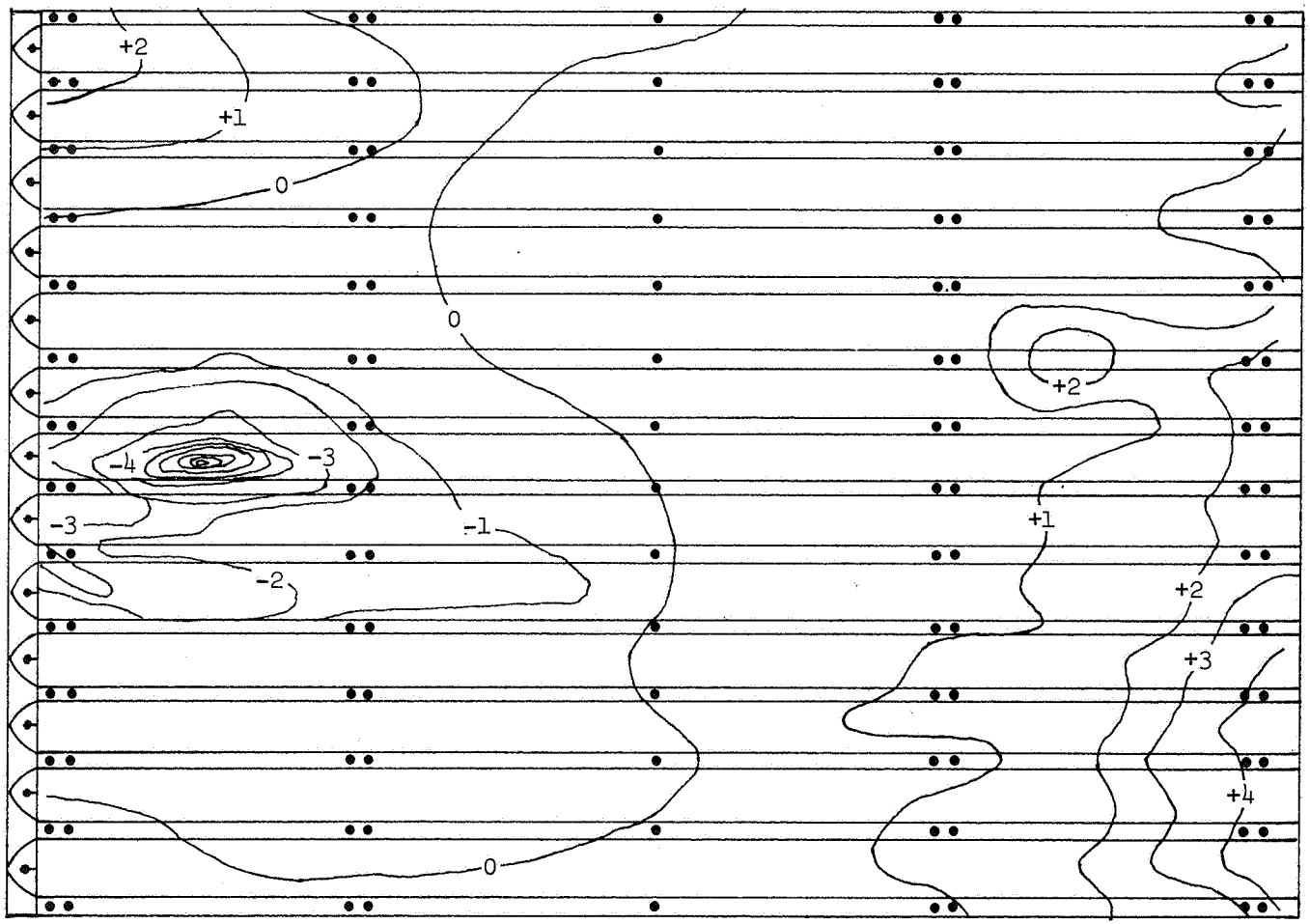

Figure 32.- Map of changes in surface deformations of René 41 heat shield at end of heating test series. Each contour represents 0.025-cm (0.010-in.) change.

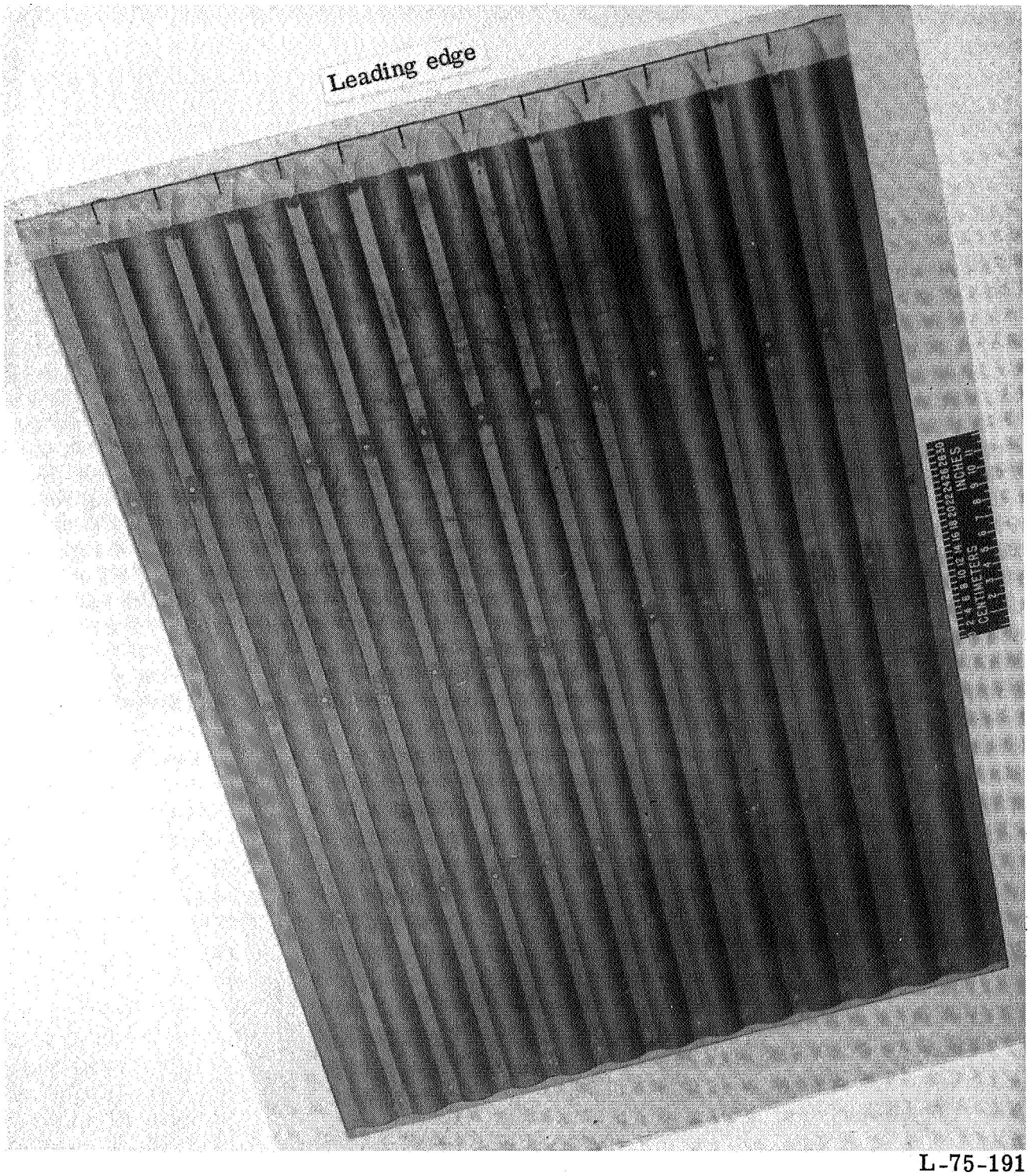

L-75-191

(a) Before testing.

Figure 33.- René 41 heat-shield surface before and after testing.

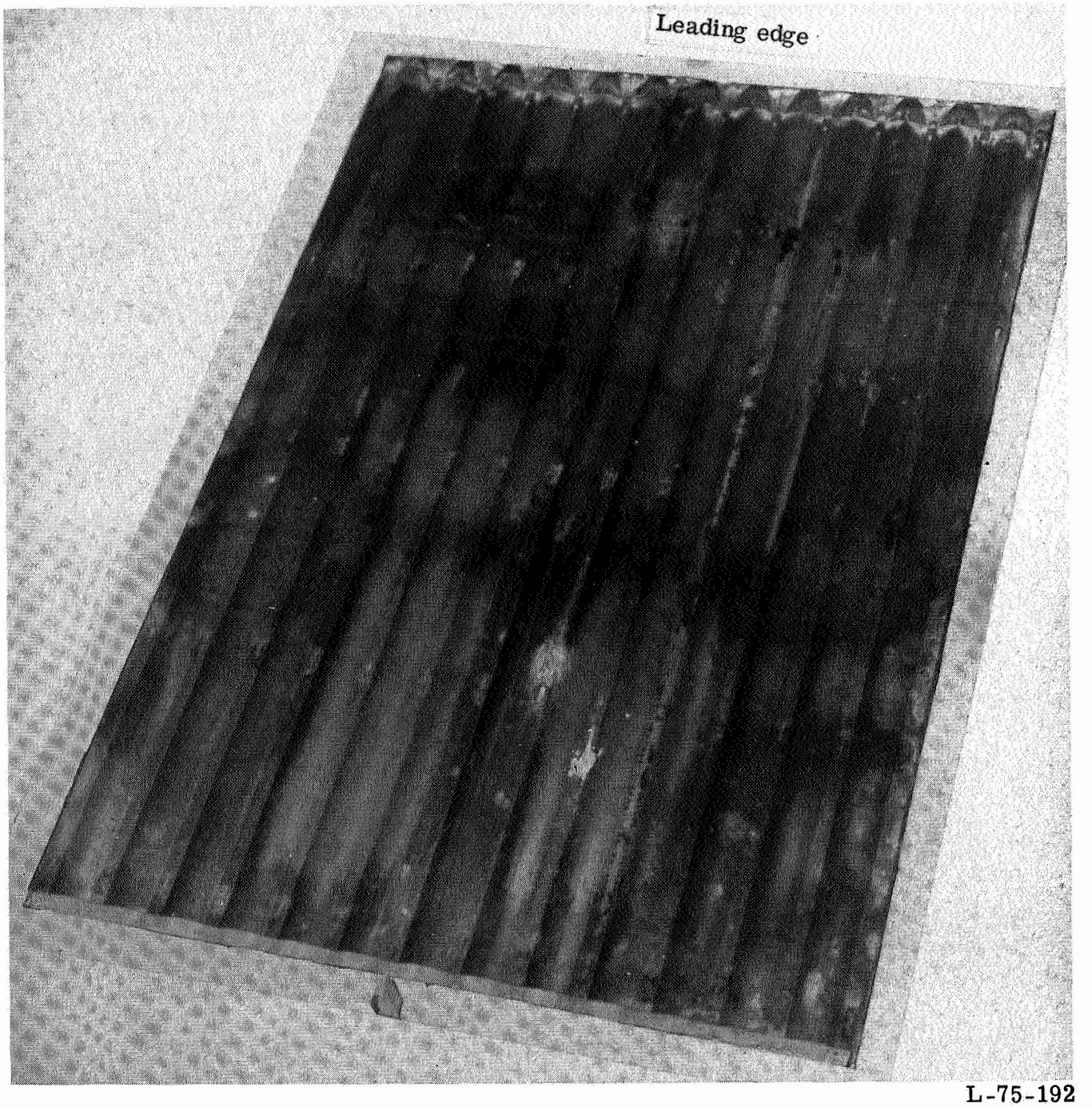

L-75-192

(b) After testing.

Figure 33.- Concluded.

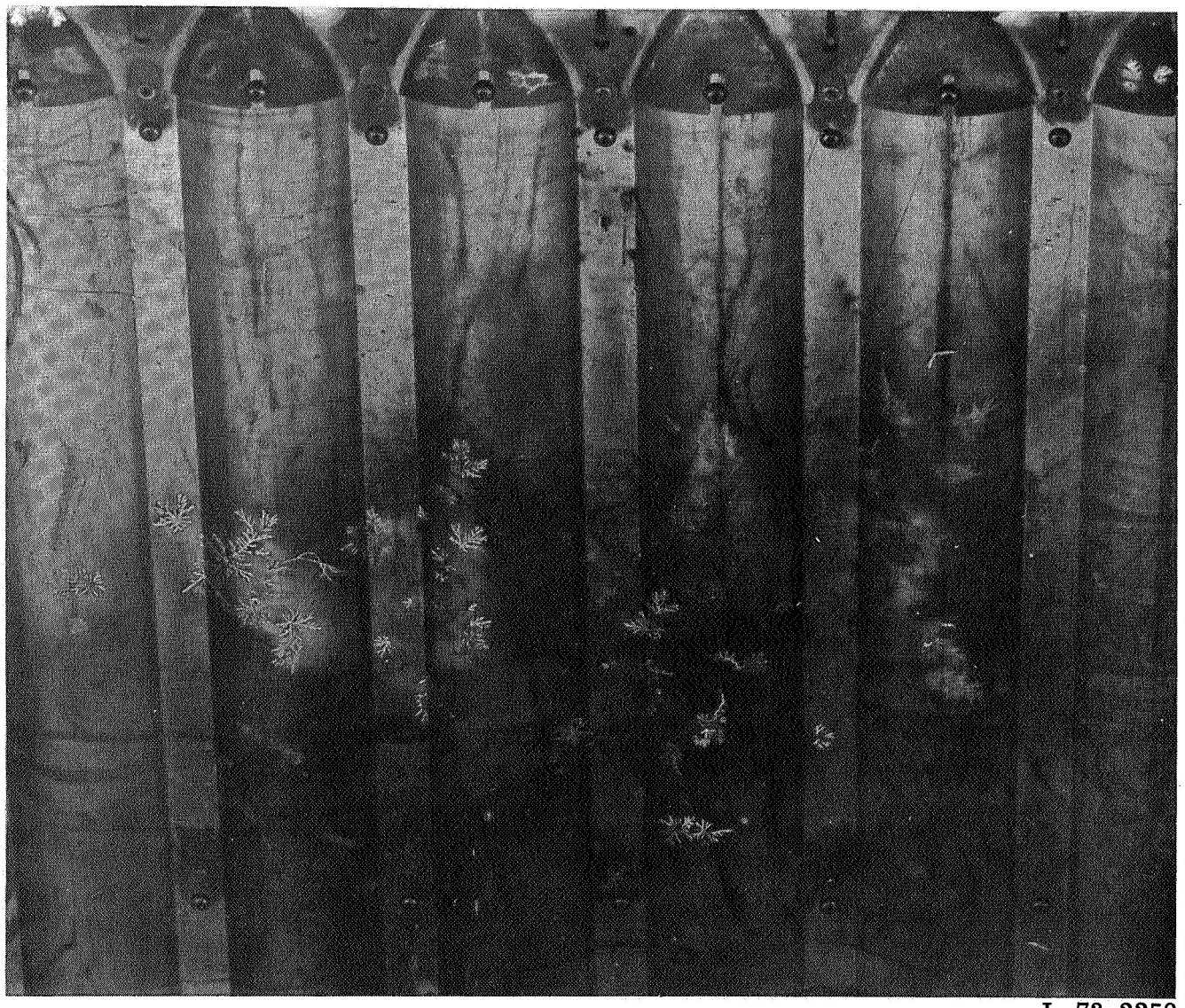

L-73-2258

Figure 34.- Electrical arcing patterns on René 41 heat-shield surface.

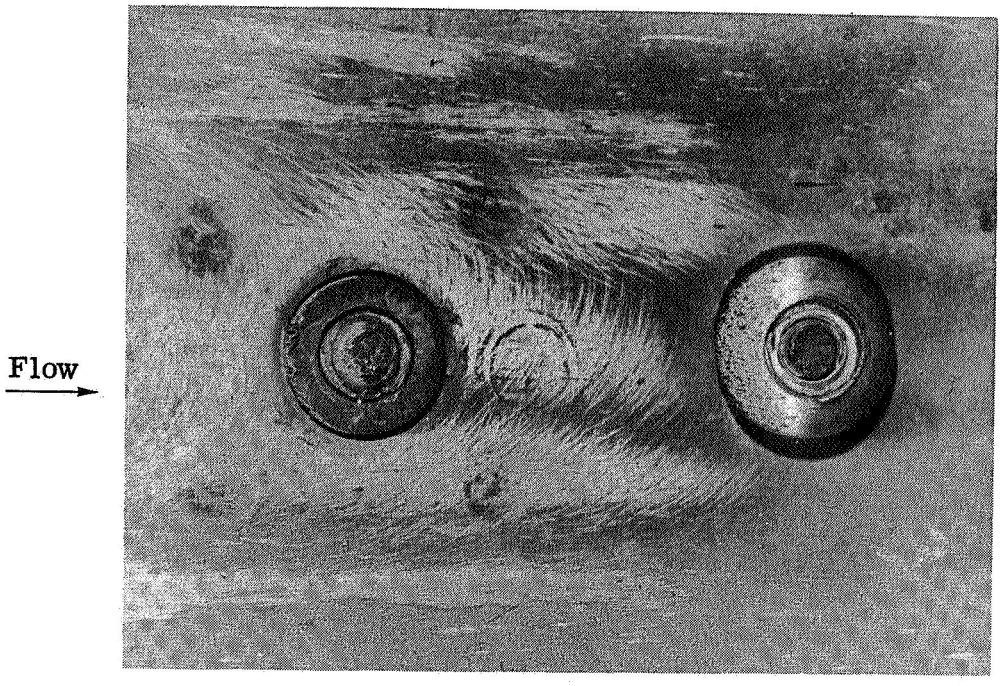

(a) At upstream support member.

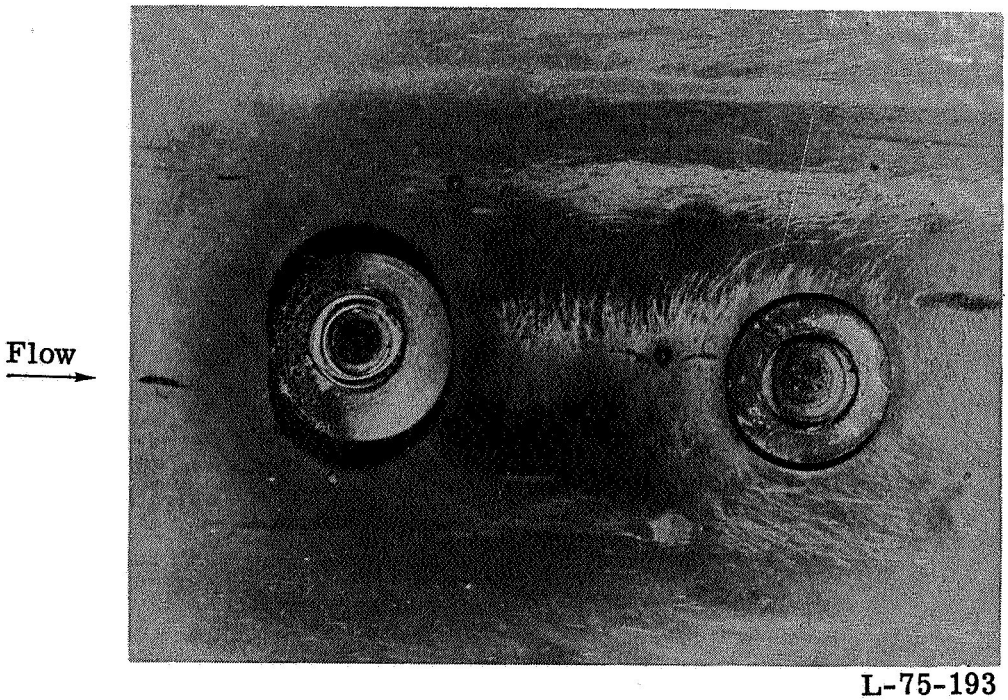

(b) At downstream support member.

Figure 35.- Eroded rivets after exposure to aerodynamic heating at $M_\infty = 6.7$ and $T_t \approx 1722$ K (3100° R); maximum rivet-head diameter, 0.8 cm (0.3 in.).

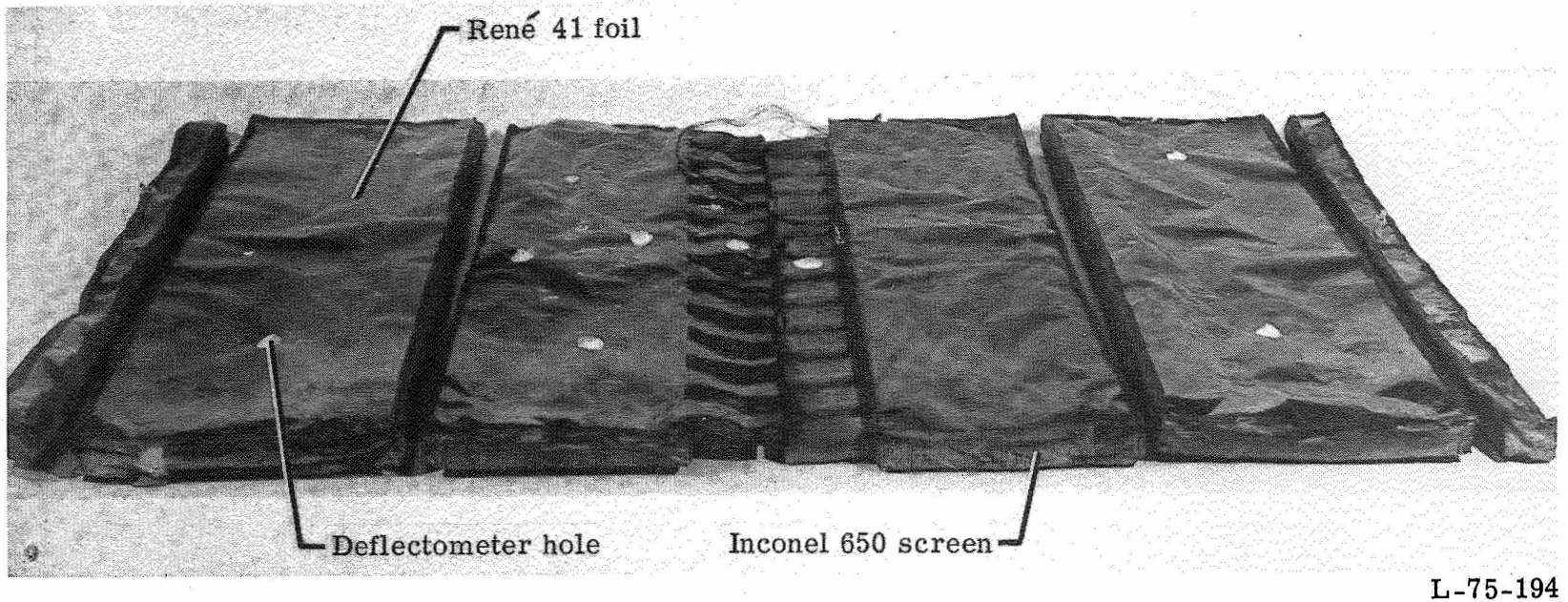

L-75-194

Figure 36.- Oxidized surfaces of René 41 foil and Inconel 650 screen envelopes of insulation packages after exposure to radiant heating.

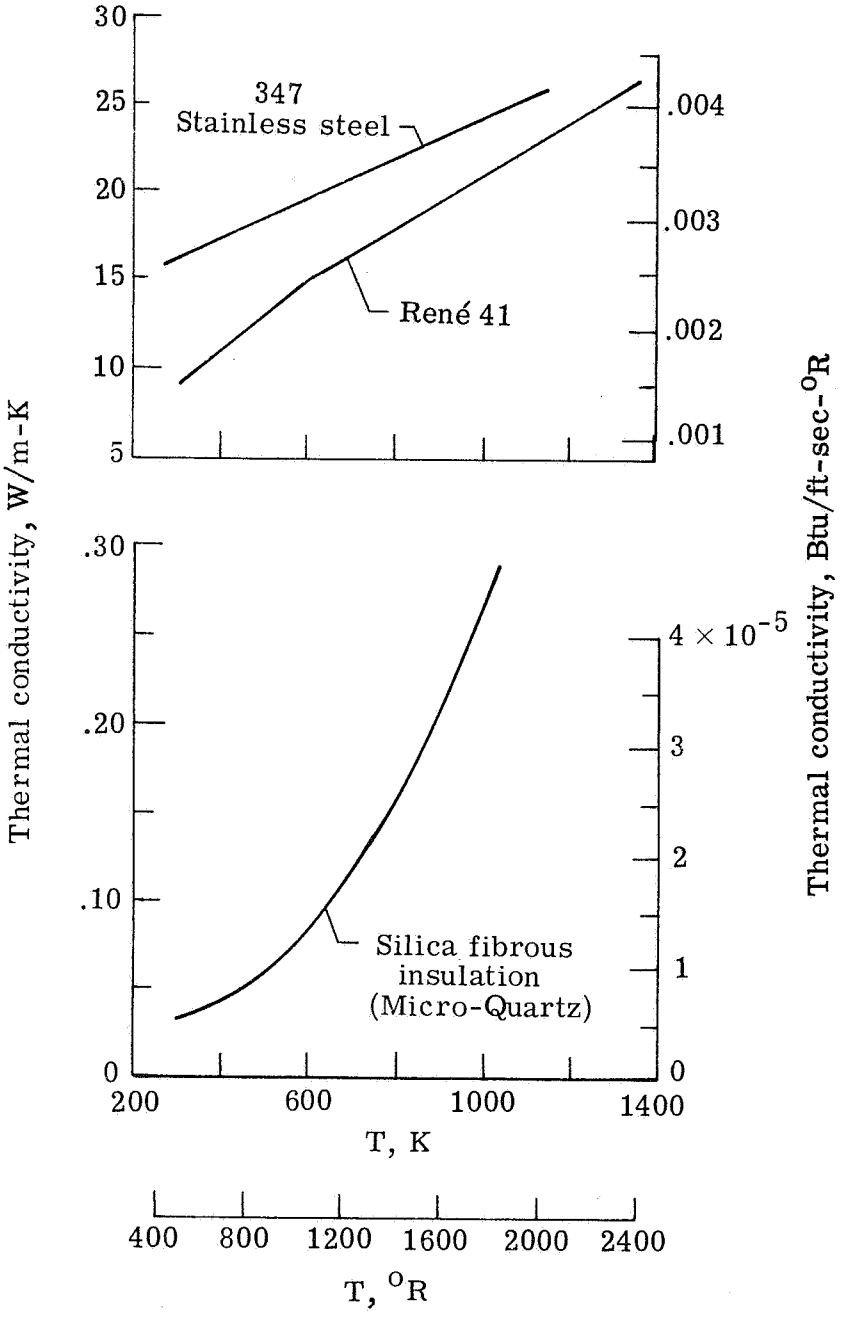

(a) Thermal conductivity.

Figure 37.- Temperature-dependent properties of panel materials.

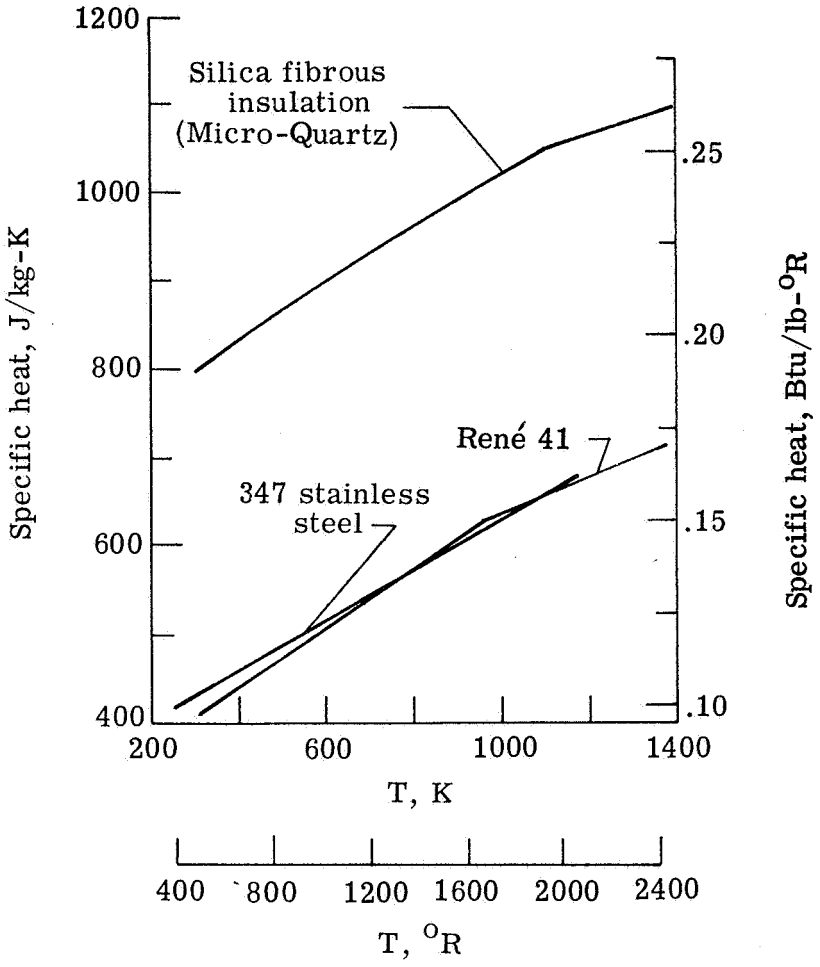

(b) Specific heat.

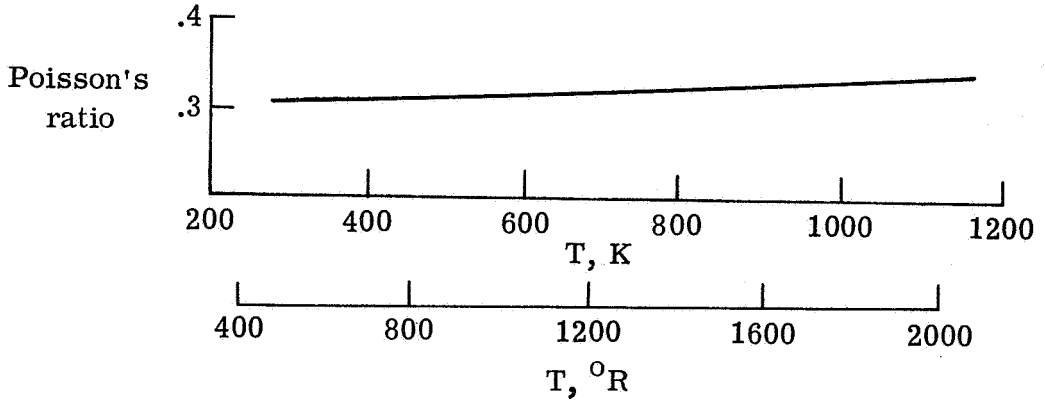

(c) Poisson's ratio for René 41.

Figure 37.- Continued.

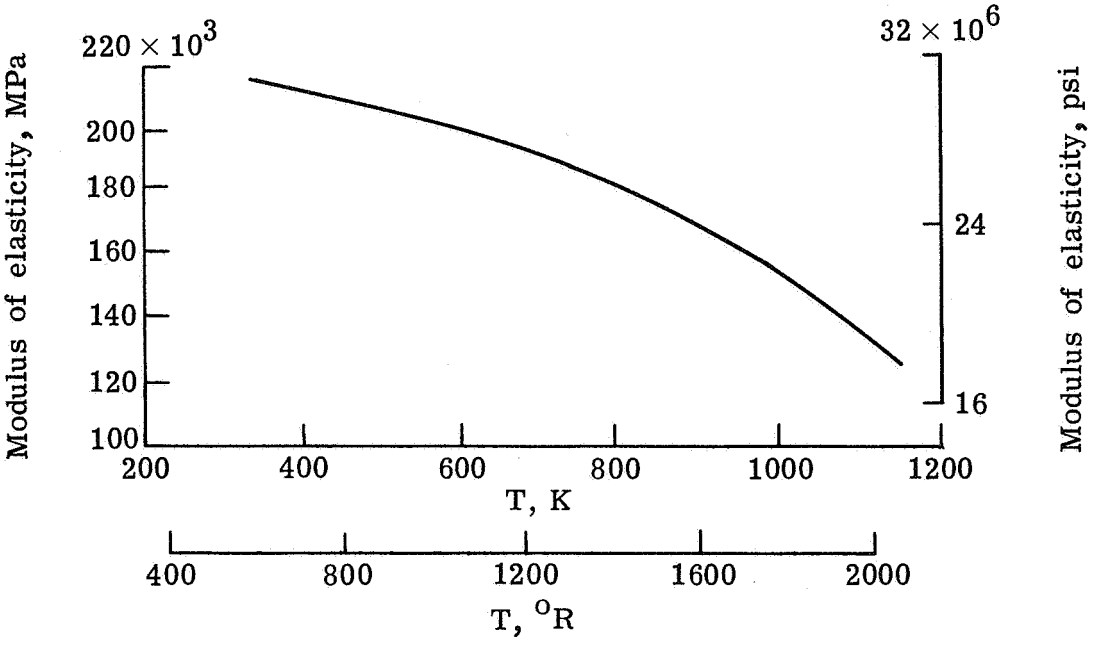

(d) Modulus of elasticity for René 41.

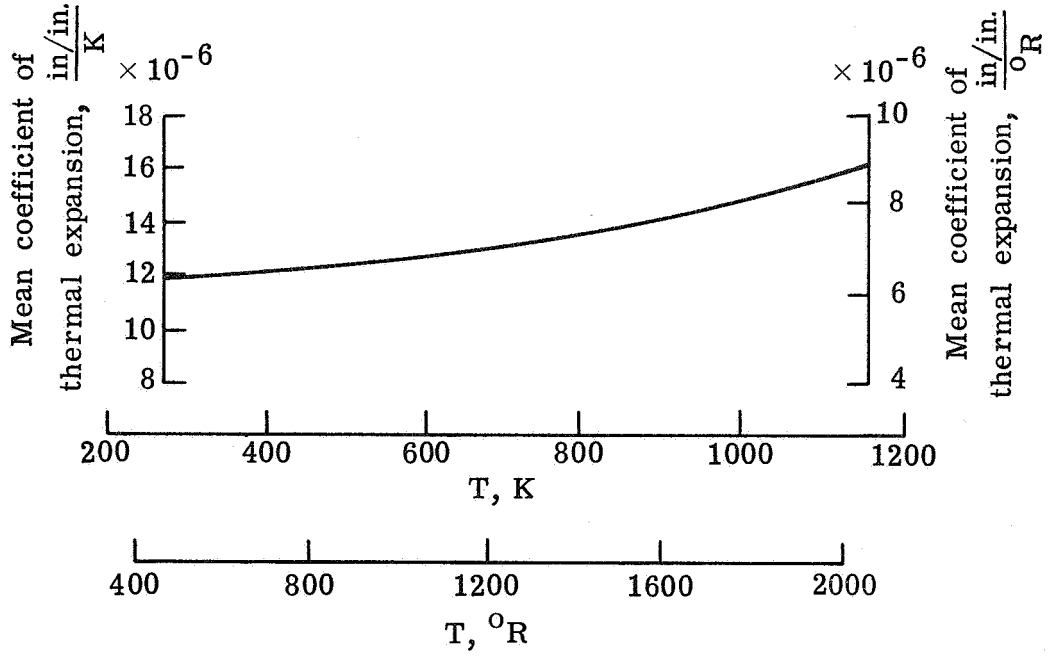

(e) Mean coefficient of thermal expansion from 294 K (530° R) for René 41.

Figure 37.- Continued.

Ni-19Cr-11Co-10Mo-3Ti-1.5Al
Sheet and plate 0.013 to 0.79 (0.005 to 0.312 in.)
1353 to 1450 K (2435 to 2610° R)
30 min to 4 hr at 1172 K (2110° R), 4 hr air cooled

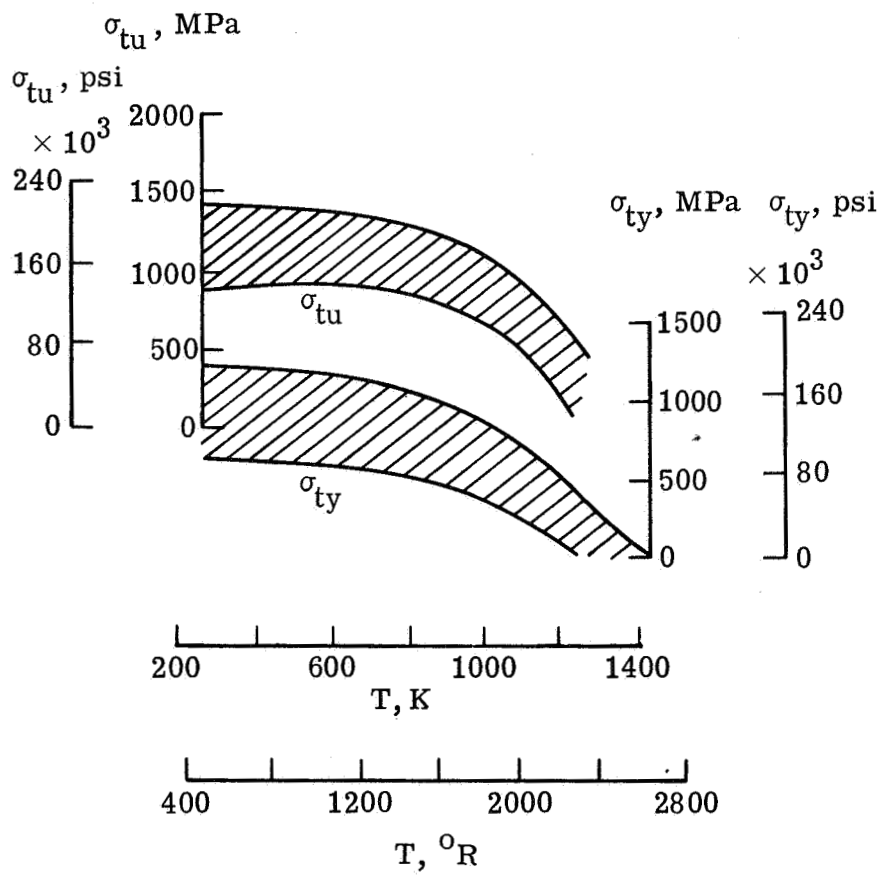

(f) Tensile properties for René 41.

Figure 37.- Concluded.

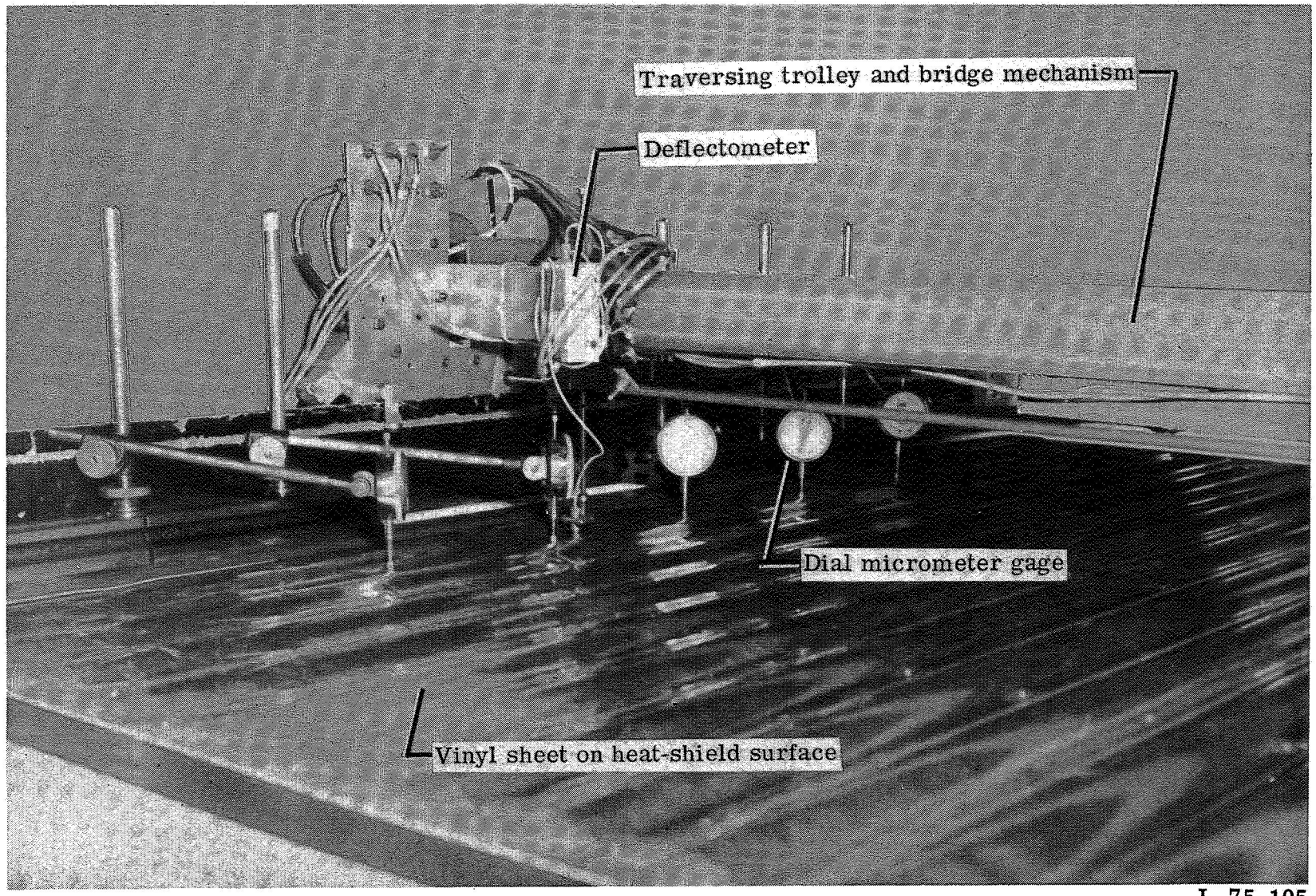

L-75-195

Figure 38.- Apparatus for measuring heat-shield deflections under differential-pressure loading.

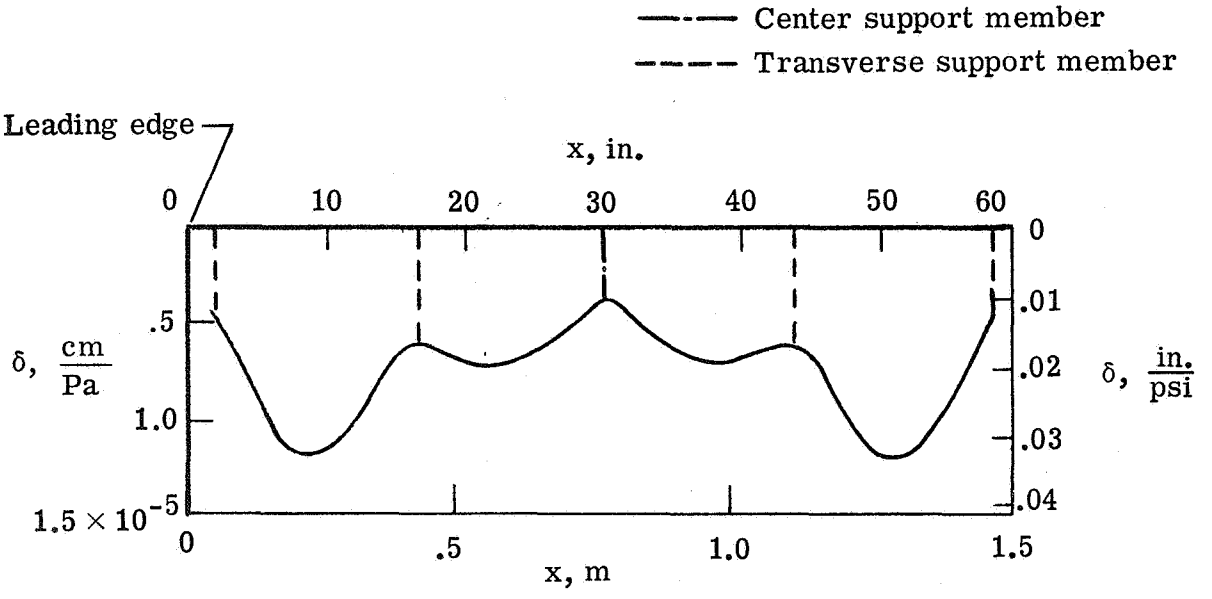

Figure 39.- Measured deflections of the heat shield and support members for a differential pressure of 6.9 kPa (1.0 psi).

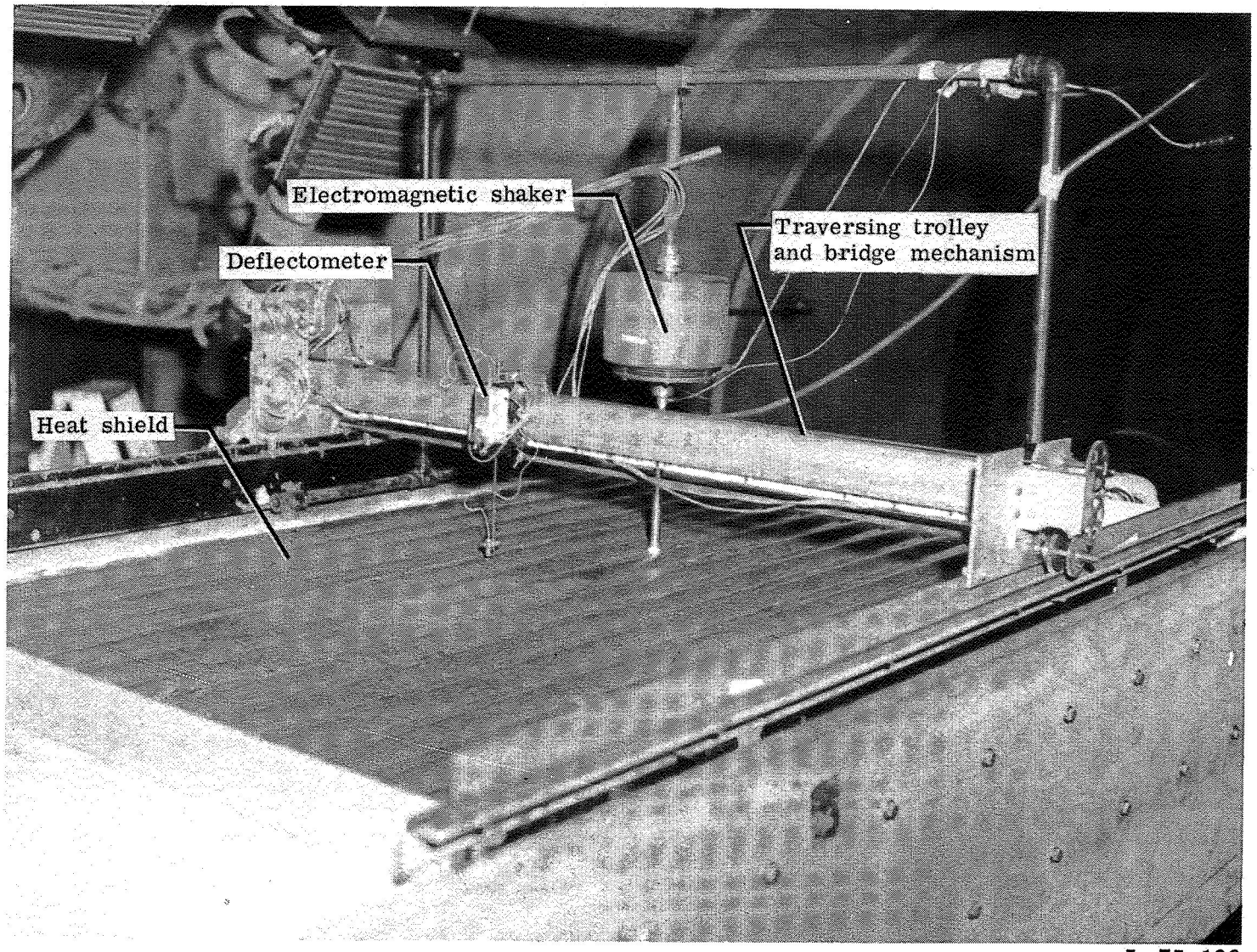

L-75-196

Figure 40.- Apparatus for surveying vibration modes and frequencies.

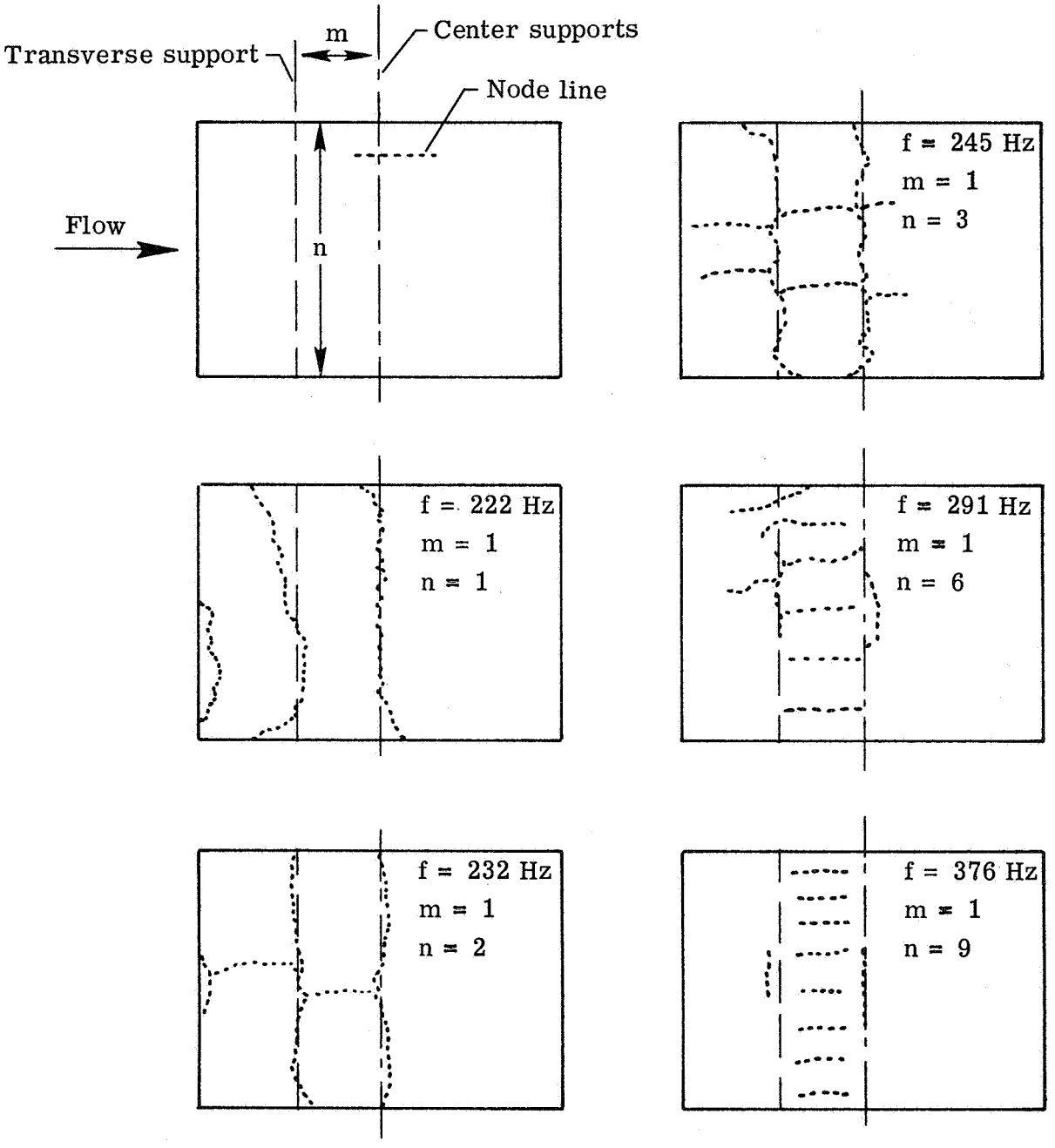

Figure 41.- Some of the experimentally observed nodal patterns and associated frequencies of the René 41 heat shield obtained prior to the heating tests.

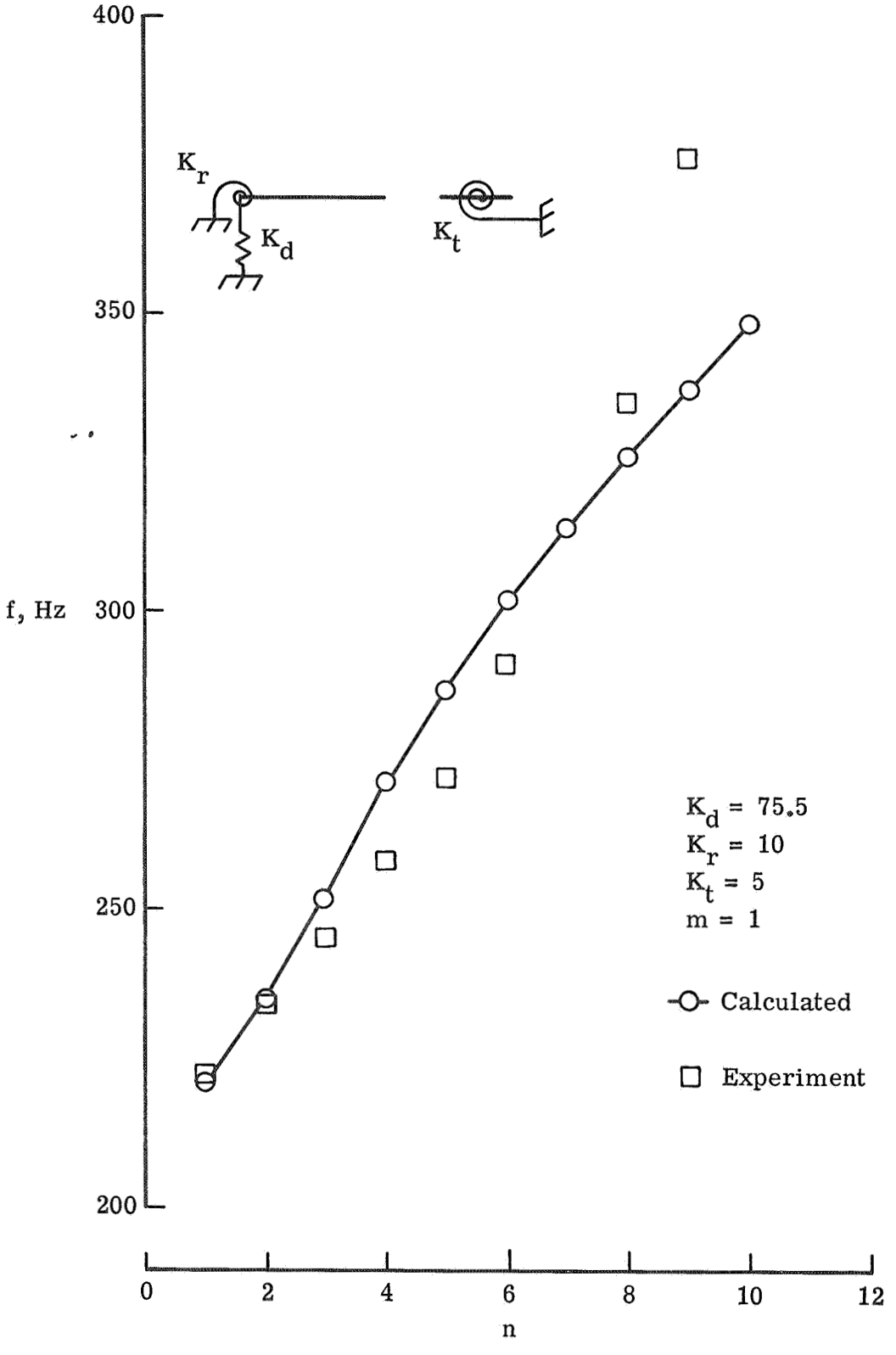

Figure 42.- Calculated and experimental frequencies for different modes in a single bay of the René 41 heat shield.

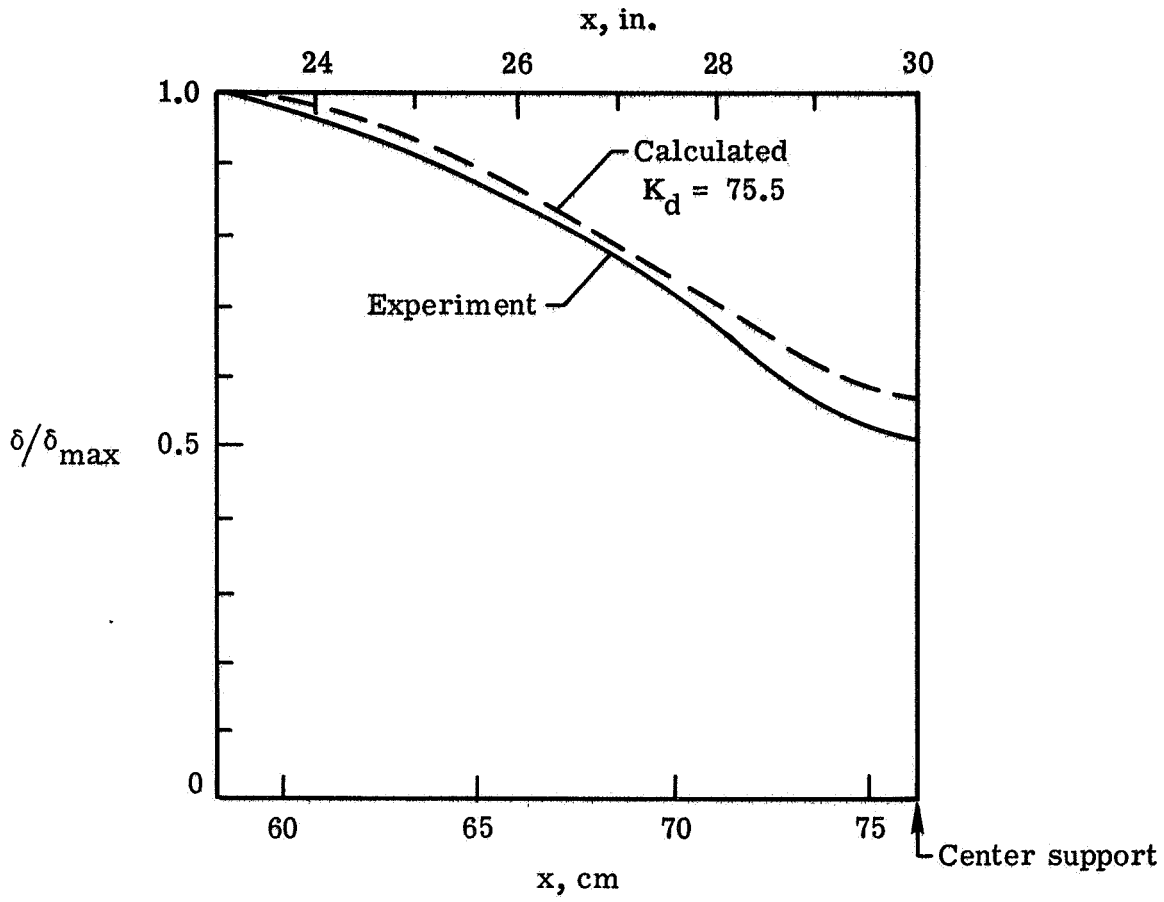

Figure 43.- Normalized static deflections of one-half of the second bay of the René 41 heat shield.

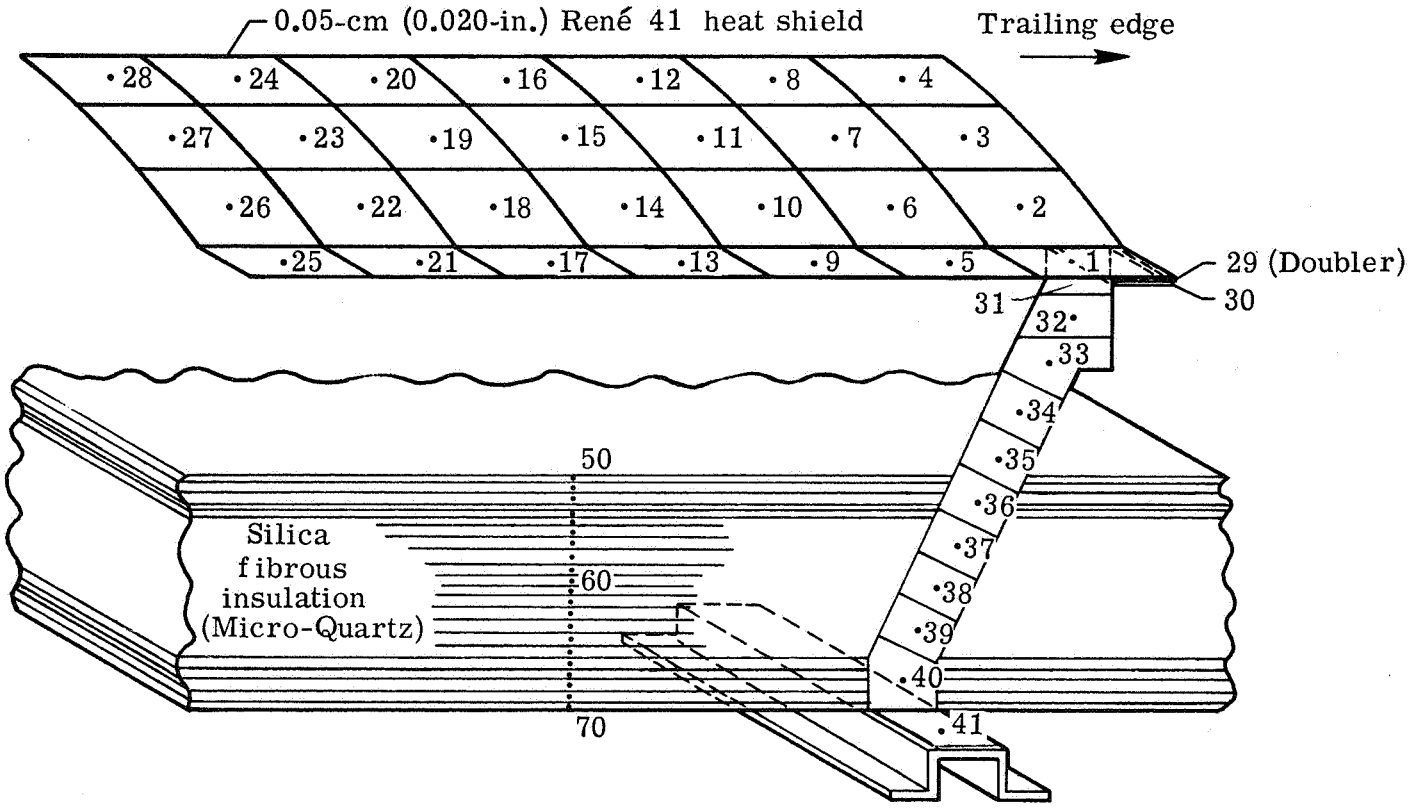

Figure 44.- Nodal representation for thermal analysis of René 41 thermal protection system.

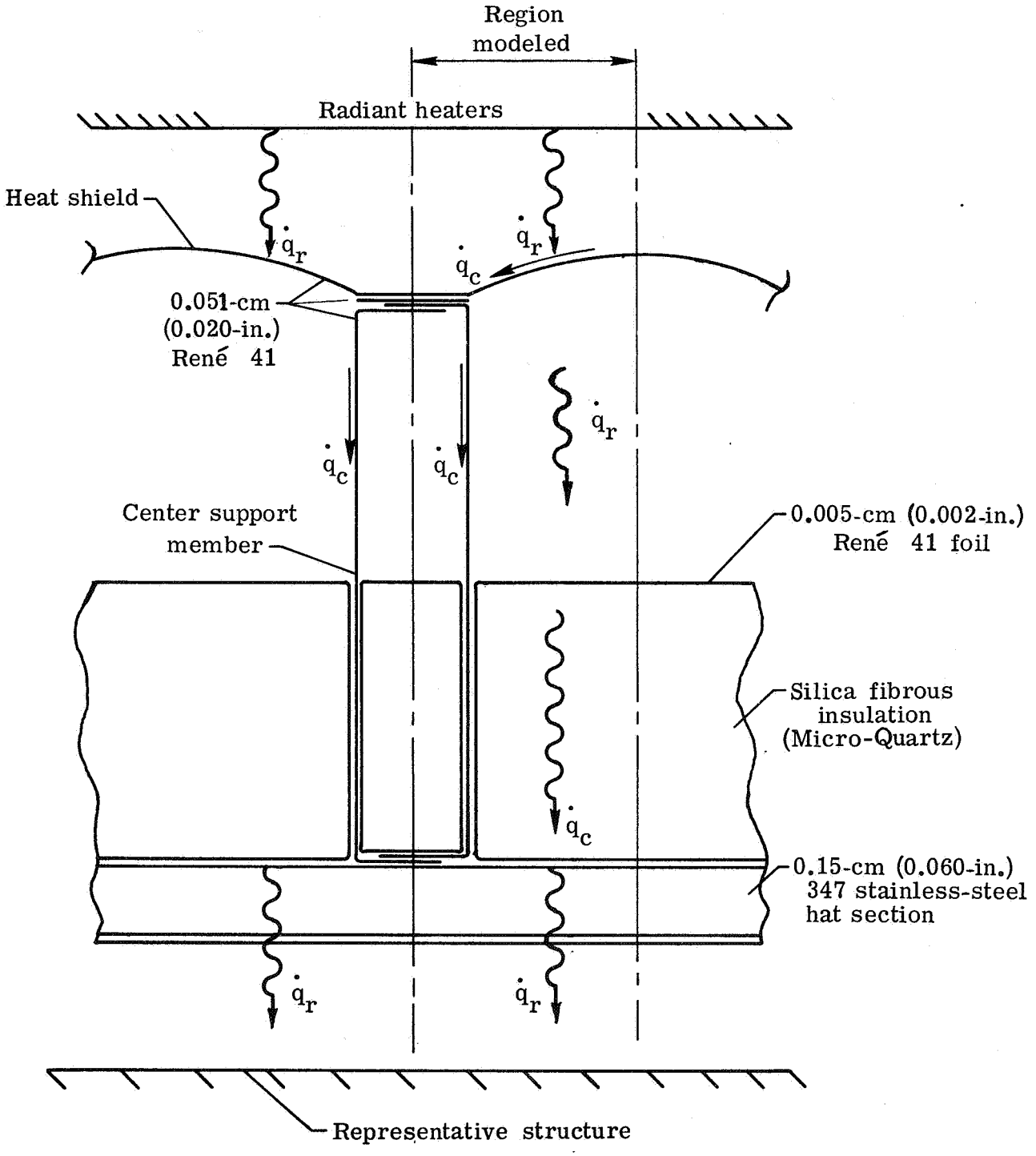

Figure 45.- Section identifying panel components and heating modes used for thermal analysis. ($\dot{q}_r$ is radiative heating rate; $\dot{q}_c$ is convective heating rate.)

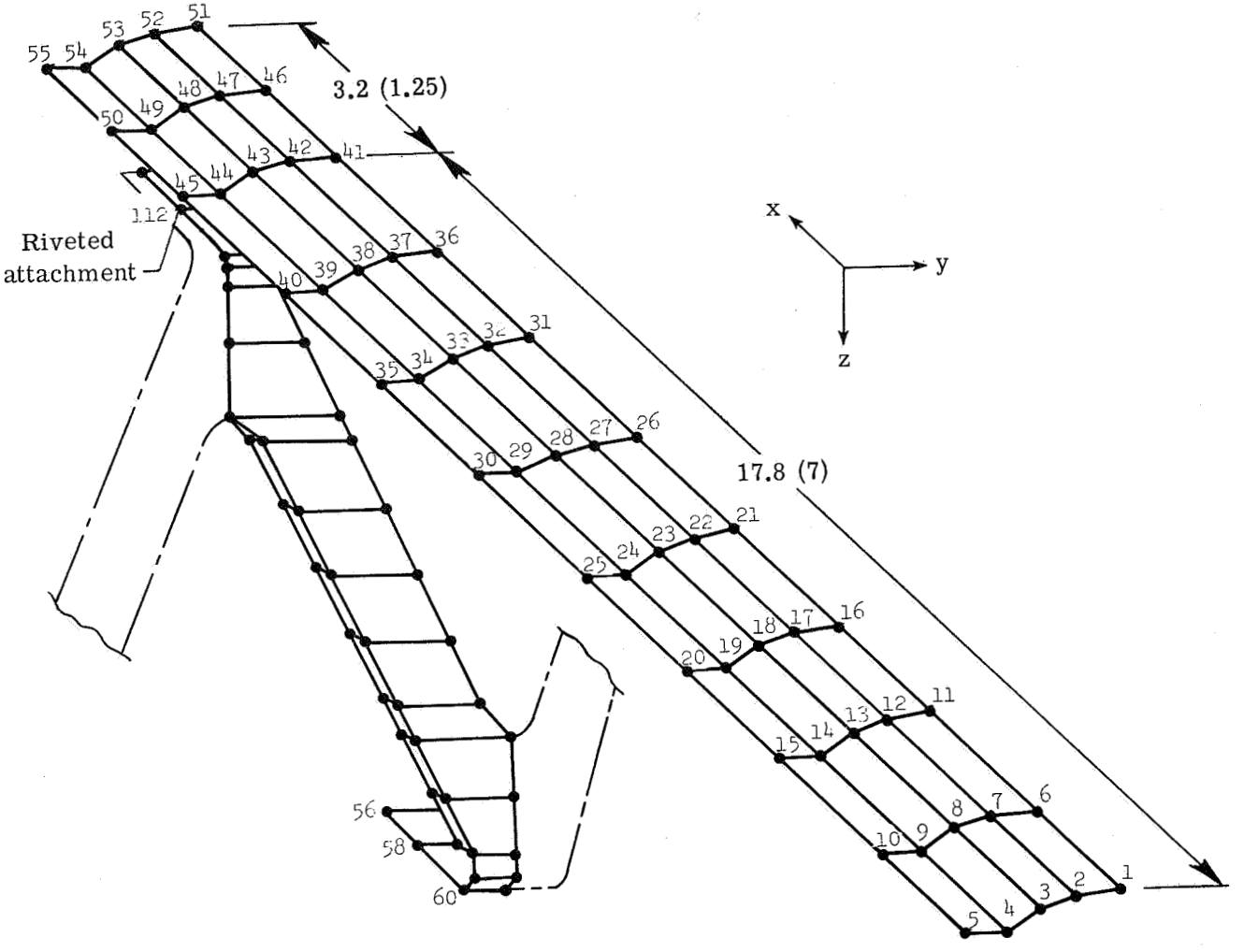

(a) Heat-shield elements.

Figure 46.- Finite element grid used for stress analysis of René 41 heat shield and support member.

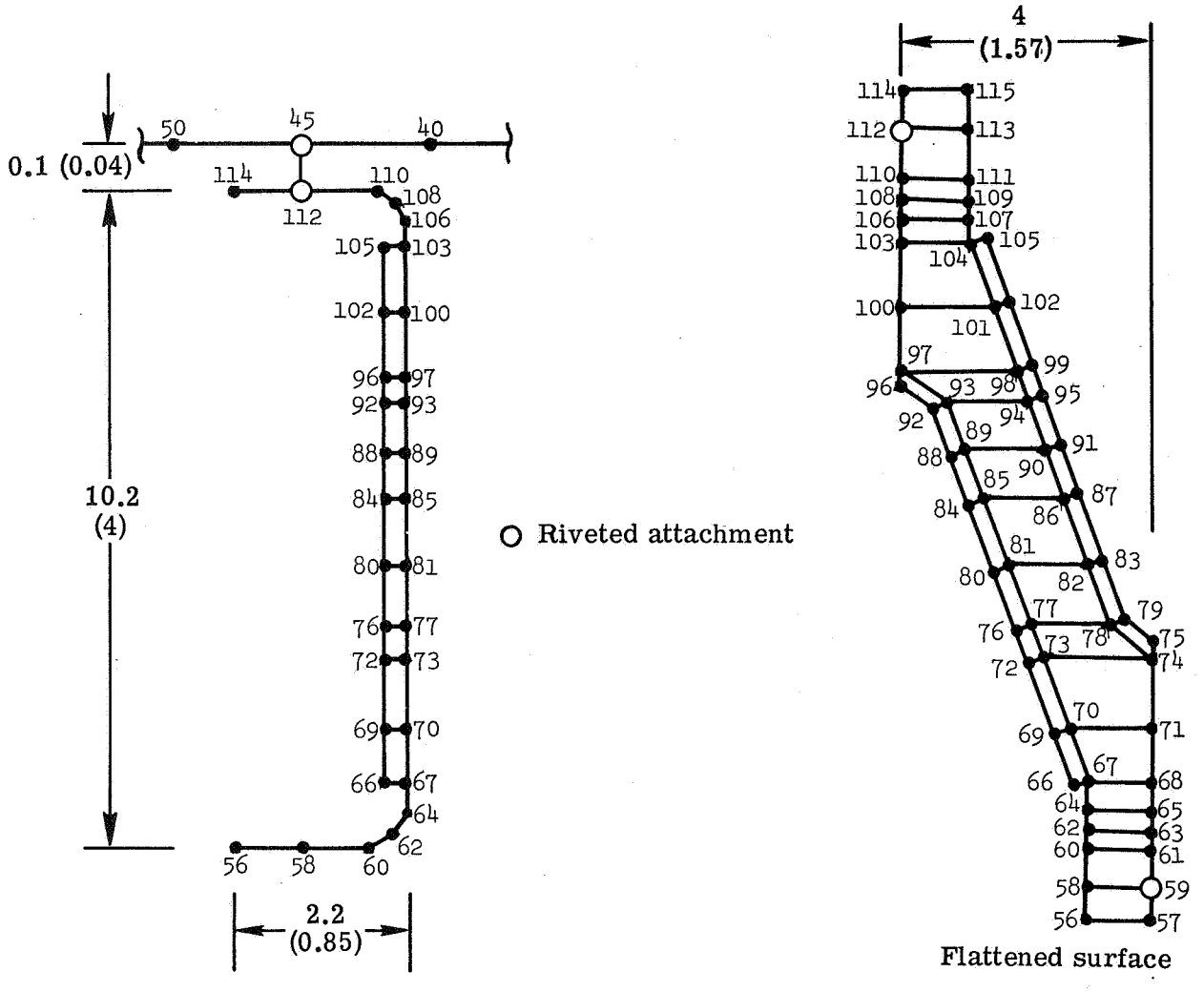

(b) Support-member elements.

Figure 46.- Concluded.

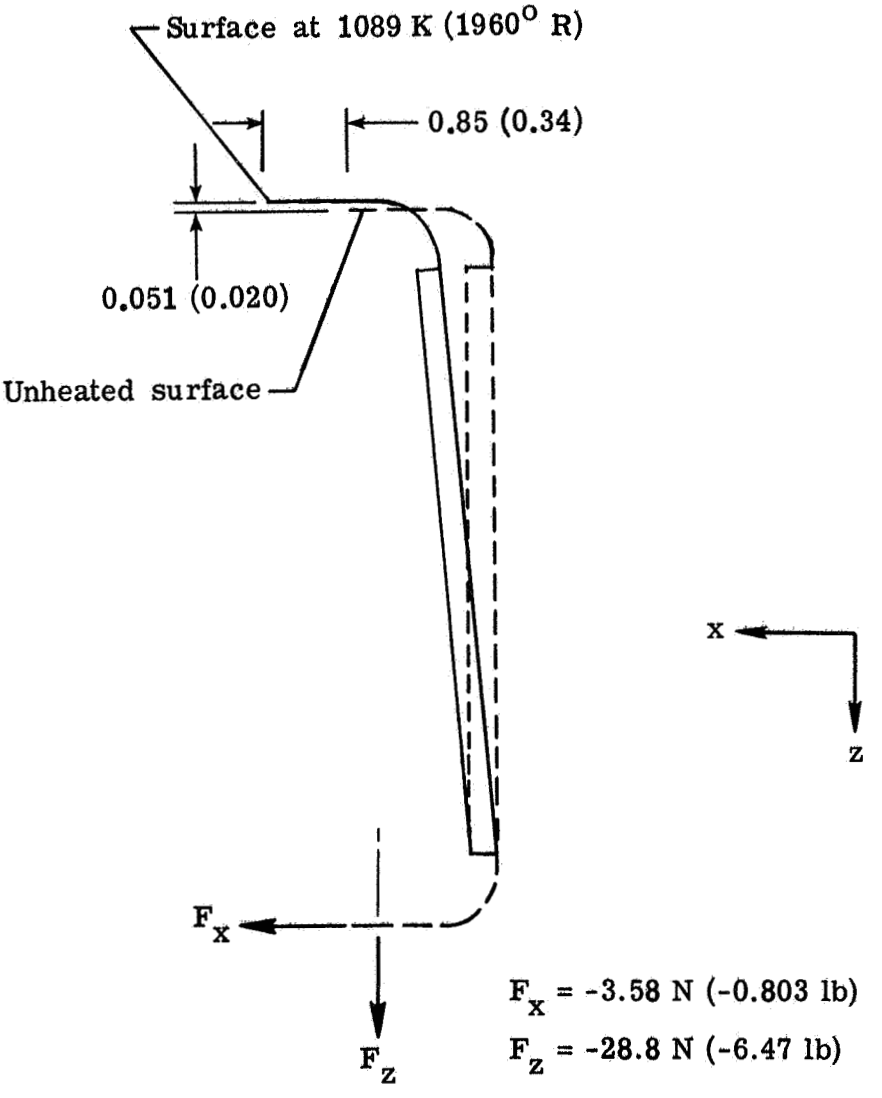

Figure 47.- Support-member reaction forces and displacements.

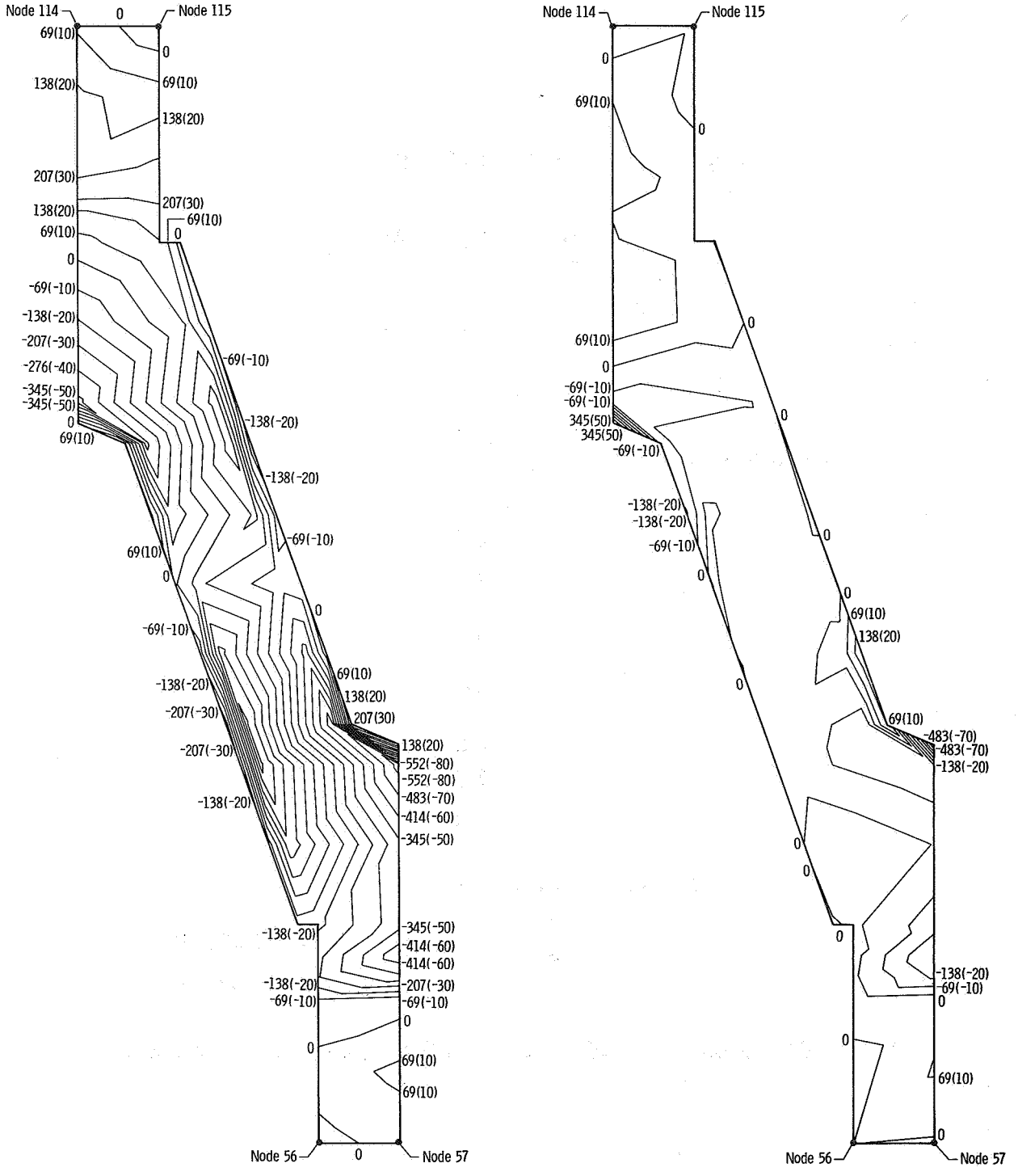

(a) Support-member stress in z-direction for σ_{max} = -583 MPa (-84.6 ksi).

(b) Support-member stress in y-direction for σ_{max} = -539 MPa (-78.1 ksi).

Figure 48.- Stress contours for René 41 support member.

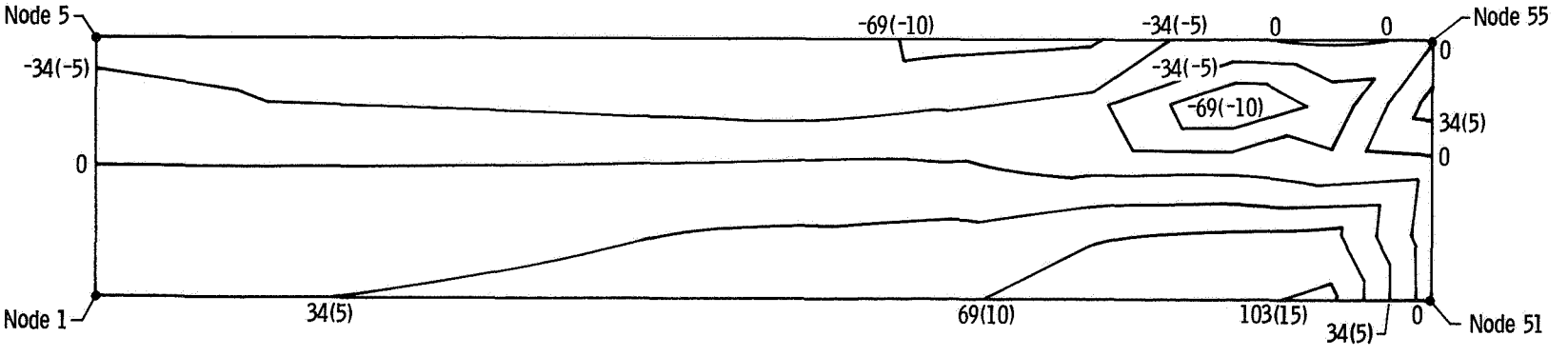

(a) Heat-shield stress in x-direction for σ_{max} = 113 MPa (16.3 ksi).

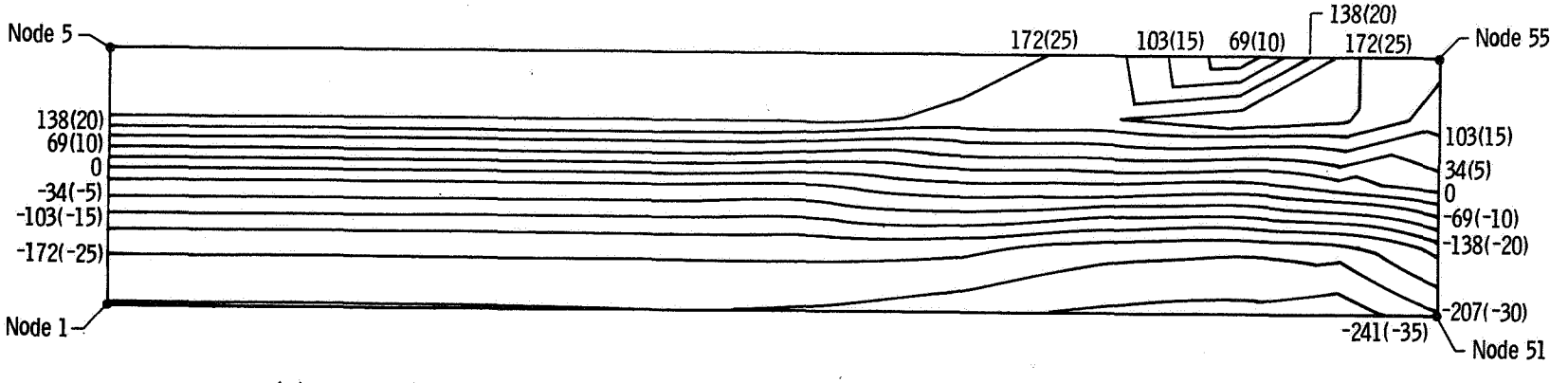

(b) Heat-shield stress in y-direction for σ_{max} = -267 MPa (-38.7 ksi).

Figure 49.- Stress contours for René 41 heat shield.